EPIGENETIC SILENCING OF THE GLUCOCORTICOID RECEPTOR IN SMALL CELL LUNG CANCER CELLS

BY

KERRYN HOUSTON

Submitted in fulfilment of the academic requirements for the degree of

Master of Science in the School of Life Sciences,

University of KwaZulu-Natal

Durban

January 2013

As the candidate's supervisor I have approved this dissertation for submission.

Signed: _____ Name: Dr Paula Sommer Date: _____

ABSTRACT

Small cell lung cancer (SCLC) is an aggressive neuroendocrine tumour which secretes ACTH and other related peptides. Contrary to normal production by the pituitary, ACTH production is not inhibited by glucocorticoids (Gcs) in SCLC. This insensitivity to Gc action can be attributed to impaired Gc receptor (GR) expression in these cells. Over-expression of the GR induces apoptosis both *in vitro* and *in vivo*. Evasion of GR signalling thus confers a significant survival advantage to SCLC cells. Re-expression of endogenous GR in SCLC cells may provoke the same effect. Many tumours silence the expression of tumour suppresser genes by epigenetic mechanisms. Recent evidence suggests that the GR in SCLC cells is epigenetically silenced by hypermethylation of its promoter.

The overall aim of this study was to determine whether endogenous GR re-expression induces apoptosis of SCLC cells. The DMS 79 SCLC cell line, and the control HEK and non-SCLC A549 cell lines were treated with the DNA methyltransferase inhibitor (DNMTi), 5-aza-2'-deoxycytidine (5-aza), to determine whether treatment with 5-aza results in re-expression of endogenous GR. Conflicting results were thought to result from the use of possibly degraded 5-aza. However, a quantitative real-time PCR analysis using newly purchased, freshly prepared 5-aza indicated that 5-aza treatment up-regulated GR mRNA expression in the DMS 79 cells (p<0.0005). No significant changes in GR expression were seen in the HEK and/or A549 cells, suggesting that the GR in these cell lines is not methylated. Contrary to expectations and possibly due to the use of degraded stock, Western blot analysis revealed that 5-aza had no effect on GR protein expression in DMS 79 cells, yet affected GR protein expression in HEK and A549 cells (p=0.003 and p=0.042, respectively).

Cell viability assays indicated that treatment with varying concentrations of 5-aza had no effect on the viability of DMS 79 and A549 cells, but had a minimal effect on HEK cell (p<0.0005) viability. These data reinforce the hypothesis that stock 5-aza had degraded as 5-aza is known to exert cytotoxic effects at higher concentrations.

Using newly purchased, freshly prepared 5-aza, flow cytometry and/or microscopy were performed to establish whether endogenous GR re-expression was sufficient to kill the SCLC cells by apoptosis. FITC Annexin V staining and nuclear morphology showed that significant

proportions of the 1 µM (p=0.010 and p=0.027) and 5 µM (p=0.002 and p=0.018) 5-aza treated DMS 79 cells were apoptosing, with little apoptosis seen in HEK cells. 5-Aza induced negligible HEK cell death, as determined by microscopic analyses.

The effect of dexamethasone (Dex; a synthetic Gc) on HEK and DMS 79 cells was examined to determine whether Gc treatment could enhance apoptosis. Treatment with Dex alone, and in combination with 5-aza, resulted in significant HEK cell death (p=0.046 and p=0.005 respectively), but not apoptosis. This was unexpected as HEK cells express very little unmethylated GR, and may be due to excessive drug exposure or combined drug toxicity. The same effect was observed with DMS 79 cells (p=0.003 and p<0.0005 respectively), with 5-aza appearing to enhance cell death induced by Dex. No effects on apoptosis were seen confirming earlier reports that GR-mediated apoptosis is ligand-independent.

As 5-aza does not selectively demethylate the GR, cells were exposed to the GR antagonist, RU486, to establish whether apoptosis associated with 5-aza treatment is specifically due to demethylation and subsequent expression of the GR. Treatment with RU486 in conjunction with 5-aza induced cell death (p=0.014), but not apoptosis, of HEK cells. Again, this may have been due to excessive drug exposure or combined drug toxicity. Flow cytometric data showed that DMS 79 cell death was induced by both RU486 (p=0.004), and RU486 in combination with 5-aza (p=0.003). Furthermore, although not significant, RU486 treatment appeared to inhibit apoptosis induced by 5-aza in the DMS 79 cells. The data suggest that re-expression of the GR may be responsible for apoptotic induction. Our findings, although not significant, hint that endogenous re-expression of the GR leads to apoptosis.

Unlike mutations, epigenetic marks are reversible and clinical trials with DNMTis have shown promising results. The identification of a novel endogenous mechanism that specifically induces apoptosis of SCLC cells offers great promise for the development of targeted therapeutics for the treatment of this deadly disease.

PREFACE

The experimental work described in this dissertation was carried out in the School of Life Sciences, University of KwaZulu-Natal, Durban, from January 2011 to December 2012, under the supervision of Doctor Paula Sommer.

These studies represent original work by the author and have not otherwise been submitted in any form for any degree or diploma to any tertiary institution. Where use has been made of the work of others it is duly acknowledged in the text.

Kerryn Houston (Candidate)

Dr Paula Sommer (Supervisor)

DECLARATION OF PLAGIARISM

I, Kerryn Houston, declare that

1. The research reported in this thesis, except where otherwise indicated, is my original research.

2. This thesis has not been submitted for any degree or examination at any other university.

3. This thesis does not contain other persons' data, pictures, graphs or other information, unless specifically acknowledged as being sourced from other persons.

4. This thesis does not contain other persons' writing, unless specifically acknowledged as being sourced from other researchers. Where other written sources have been quoted, then:
   a. Their words have been re-written but the general information attributed to them has been referenced
   b. Where their exact words have been used, then their writing has been placed in italics and inside quotation marks, and referenced.

5. This thesis does not contain text, graphics or tables copied and pasted from the Internet, unless specifically acknowledged, and the source being detailed in the thesis and in the References sections.

Signed: ……

TABLE OF CONTENTS

LIST OF TABLES

LIST OF FIGURES

ABBREVIATIONS

ACTH	Adrenocorticotrophin hormone
ANOVA	Analysis of variance
AP	Activator protein
5-Aza	5-Aza-2'-deoxycytidine
B(a)P	Benzol-a-pyrene
BCA	Bicinchoninic acid
BPDE	Benzol-a-pyrene diol-epoxide
BSA	Bovine serum albumin
cPR	Chicken progesterone receptor
DABCO	1,4-diazabicyclo[2.2.2]octane
DAPI	4',6-diamidino-2-phenylindole
Dex	Dexamethasone
DIC	Differential interference contrast
Di.H_2O	Deionised water
DISC	Death inducing signalling complex
DMEM	Dulbecco's modified eagle medium
DNMT	DNA methyltransferase
DNMTi	DNA methyltransferase inhibitor
DMSO	Dimethyl sulfoxide
EDTA	Ethylenediaminetetraacetic acid
FADD	Fas-associated death domain
FBS	Foetal bovine serum
FHIT	Fragile histidine triad gene
FITC	Fluorescein isothiocyanate
GAPDH	Glyceraldehyde-3-phosphate dehydrogenase
Gc	Glucocorticoid
GR	Glucocorticoid receptor
GRE	Glucocorticoid-responsive element
h	hour(s)
HDAC	Histone deacetylase
HEK	Human embryonic kidney

HEPES	4-(2-Hydroxyethyl)-1-piperazineethane-sulfonic acid
HPA	Hypothalamic-pituitary-adrenal
HRP	Horse radish peroxidase
Hsp	Heat shock protein
MBD	Methyl-CpG binding domain protein
m^5C	5-methylcytosine
MDS	Myelodysplastic syndrome
MeCP2	Methyl-CpG binding protein 2
min	minute(s)
MR	Mineralocorticoid receptor
MWM	Molecular weight marker
NF	Nuclear factor
NSCLC	Non-small cell lung cancer
NTC	No-template control
P	Passage
PBS	Phosphate-buffered saline
PcG	Polycomb group protein
PCR	Polymerase chain reaction
PI	Propidium iodide
PMSF	Phenylmethylsulfonyl fluoride
POMC	Proopiomelanocortin
PRC	Polycomb-repressive complex
PS	Phosphatidylserine
qPCR	Quantitative real-time polymerase chain reaction
RIPA	Radio-immunoprecipitation assay
RT	Reverse transcriptase
RU486	Mifepristone
s	second(s)
SCLC	Small cell lung cancer
SEM	Standard error of the mean
TBST	Tris-buffered saline-tween
TMS	Target of methylation-induced silencing
TNF	Tumour necrosis factor

TRAIL	TNF-related apoptosis-inducing ligand
TSG	Tumour suppressor gene
WR	Working reagent

ACKNOWLEDGEMENTS

Foremost, I would like to thank my supervisor Dr Paula Sommer for her unwavering encouragement, and guidance with instruction in the lab, and the writing of this dissertation. You always reminded me of my goals and kept me motivated.

Nimisha Singh, thank you for your continuous counsel and assistance with lab work. Your help has been invaluable, and I could not have made it through this degree without you.

To Roxanne Wheeler, thank you for patiently teaching me how to do Western blots, and for being so entertaining! You always brightened the atmosphere of the lab with your contagious happiness, strange noises and animated dance moves.

Thanks also to Zenzi for your help with microscopy, and for being such a good commiserator.

The inhabitants of office 05-074: Ellisha, Ashlin, Natasha and Kashmira, thank you for the gossip and funny stories that kept me amused for hours, when I should have been doing work!

To my fiancé Russell Taylor, thank you for always supporting me, encouraging me, and telling me to “do my work!” when I was being lazy. The pride you take in your work has been an example to me.

Thank you to my parents for the encouragement and support, and for always urging me to be the best person that I can be.

And finally, thanks to the National Research Foundation (NRF) for the financial support towards this research.

1. INTRODUCTION AND LITERATURE REVIEW

1.1. Lung cancer

Lung cancer is the most common cause of cancer and cancer deaths in the world. It is the most prevalent cancer in men, with lower incidence rates in women (Parkin, 2001). Lung cancer is the fourth leading cause of death in South Africa. Mortality due to lung cancer has declined for South African men, but is on the increase in women, which is synonymous with the latest global trends and is closely associated with cigarette smoking (Bello *et al.*, 2011).

Carcinogenesis is a multi-step process. A premalignant lesion, such as hyperplasia, metaplasia or dysplasia of bronchial epithelial cells precedes carcinogenesis from a normal, healthy cell, to an invasive carcinoma (Panani and Roussos, 2006). Lung cancers predominantly originate within the epithelium of the bronchi and spread into the surrounding lung tissue (Young *et al.*, 2006). Only a small number of premalignant lesions progress to invasive cancer, with the bulk of them remaining unchanged or regressing (Panani and Roussos, 2006).

Lung cancer development can be attributed to both genetic and environmental factors (Risch and Plass, 2008). HIV/AIDS has recently been linked to the development of lung cancer. Antiretroviral treatment is related to an increased risk of cancers not previously associated with suppressed immunity, such as cancers of the neck, head, liver, anus and including lung cancer (Bello *et al.*, 2011). Cigarette smoking and occupational exposures to agents such as asbestos and radon, have strong causal relationships with lung carcinoma (Rom *et al.*, 2000; Risch and Plass, 2008). Approximately 80-90% of lung carcinomas are caused by cigarette smoking, whereas only about 20% are attributable to a combination of environmental and genetic factors (Risch and Plass, 2008).

Lung cancer is divided into two main histological groups – small cell lung cancer (SCLC) and non-small cell lung cancer (NSCLC) (Toyooka *et al.*, 2001). The vast majority (80%) of lung tumours are NSCLCs, which include adenocarcinomas, squamous cell, large cell and bronchoalveolar carcinomas (Rom *et al.*, 2000; Risch and Plass, 2008). SCLC accounts for the remaining 20% of lung cancers (Kim *et al.*, 2006).

1.2. Small cell lung cancer

SCLC tumours develop in the peri-hilar region of the lung, and are accompanied by mediastinal lymphadenopathy and lobar collapse (Motadi *et al.*, 2007). SCLC represents a highly aggressive form of lung cancer, characterised by early and widespread metastases. Although it initially responds well to chemotherapy, SCLC disseminates rapidly and develops resistance to anti-cancer drugs. Due to recurrent tumours, only 5% of SCLC sufferers survive past 5 years (Jackman and Johnson, 2005).

1.2.1. Smoking and SCLC

In more than 95% of cases, SCLC is cigarette smoke induced (Jackman and Johnson, 2005). Trends in lung cancer mirror the maturity of the smoking epidemic in different countries (Parkin, 2001). Tobacco smoke contains a mixture of highly mutagenic compounds such as polycyclic aromatic hydrocarbons, specifically benzo(a)pyrene (B(a)P). B(a)P is a powerful carcinogen and major constituent of tobacco smoke (Sozzi *et al.*, 1997). Activated carcinogens in cigarette smoke interact with particular genes such as p53, K-RAS and the fragile histidine triad gene (FHIT) (Panani and Roussos, 2006).

The p53 tumour suppressor gene (TSG) is mutated in up to 70% of SCLCs. Epigenetic mutations of p53 in lung cancer are clustered in the centre of the gene at codons 157, 248 and 273, which contain cytosines preceding guanines (CpG), regions of high CpG content known as CpG islands (Baylin *et al.*, 2004). B(a)P diol-epoxide (BPDE), present in cigarette smoke, is the ultimate B(a)P carcinogen and the most reactive with DNA, specifically binding guanine-rich sequences. It forms BPDE-DNA adducts in the CpG islands of these codons. The formation of BPDE-DNA adducts is greatly enhanced by the presence of 5-methylcytosine (m^5C). *In vitro*, genetic mutations of p53 in lung cancers are guanine to thymine transversions, and occur at the CpG islands where the BPDE-DNA adducts are formed. Similarly, BPDE forms adducts with guanine in the CpG islands of K-RAS and FHIT (Sozzi *et al.*, 1997; Rom *et al.*, 2000; Mitsuuchi and Testa, 2002).

K-RAS belongs to the RAS family of proto-oncogenes. Expression of the RAS effector homologue, Ras association domain family 1 gene (RASSF1A), is absent from all SCLC cell lines (Mitsuuchi and Testa, 2002). RASSF1A encodes a microtubule-binding protein (Jackman and Johnson, 2005). In SCLC, expression of RASSF1A is lost as a result of methylation of promoter-

associated CpG islands (Mitsuuchi and Testa, 2002). This allows tumour cells to grow more rapidly (Jackman and Johnson, 2005).

FHIT is a TSG that spans the FRA3B common fragile site. The promoter region is frequently methylated in lung cancers (Kim *et al.*, 2004; Hsu *et al.*, 2007). Loss of FHIT expression by promoter hypermethylation is a very early event in lung cancer, suggesting that FHIT is involved in the initiation of lung tumourigenesis rather than in the progression of lung cancer (Kim *et al.*, 2004). Thus, chronic exposure to tobacco carcinogens may lead to the accumulation of both genetic and epigenetic alterations of these tumourigenesis related genes resulting in neoplastic bronchial lesions i.e. lung cancer (Panani and Roussos, 2006) (see Fig. 1.1).

a) b)

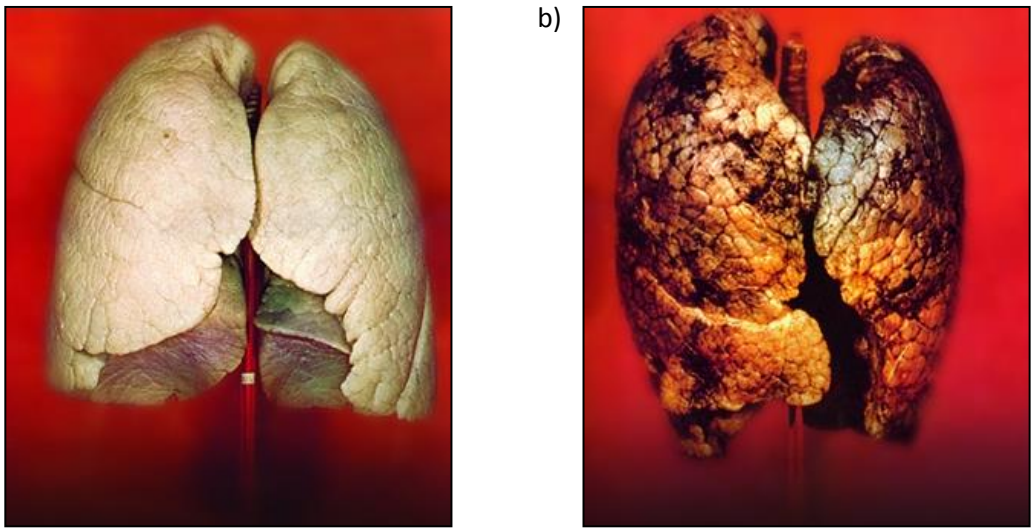

Figure 1.1. a) Normal, healthy lungs, contrasted with b) the lungs of a smoker. Image modified from cfrankdavis.wordpress.com.

1.2.2. The physiology of SCLC

SCLCs are derived from neuroendocrine cells of the bronchoepithelium (Hopkins-Donaldson *et al.*, 2003). These neuroendocrine tumours secrete ectopic neuropeptides such as the adrenocorticotrophin hormone (ACTH) precursor, proopiomelanocortin (POMC), gastrin-releasing peptide and neuromedin B (Jackman and Johnson, 2005).

Glucocorticoids (Gcs) normally inhibit ACTH secretion from the pituitary, however this does not occur with ectopic ACTH secretion by SCLC tumours and SCLC cell lines (Waters *et al.*,

2004). Here, the secretion of ACTH peptides is resistant to normal negative feedback of Gcs, leading to the development of ectopic ACTH syndrome (Ray *et al.*, 1996). Normally, the level of circulating POMC is under tight control by negative feedback regulation of Gcs via the hypothalamic-pituitary-adrenal (HPA) axis (Cole *et al.*, 1995). The hypothalamus signals to the anterior pituitary to release ACTH (Fig. 1.2). ACTH acts on the cells of the adrenal cortex through high-affinity receptor-binding, prompting the cells to secrete Gcs. Gcs then negatively feedback and inhibit pituitary ACTH production in proportion to the circulating Gc level (Ganong, 2005).

SCLC has a high incidence of associated endocrine disorders. Nearly half of all SCLC patients present with biochemical or clinical features of aberrant ACTH production at diagnosis (Waters *et al.*, 2004; Motadi *et al.*, 2007). SCLC is the most common cause of ectopic ACTH syndrome (Ray *et al.*, 1996). The ectopic secretion of ACTH by SCLC tumour cells is, in contrast to the pituitary, unresponsive to negative feedback by Gcs. This is evidence of Gc resistance in SCLC (Ray *et al.*, 1994; Sommer *et al.*, 2007).

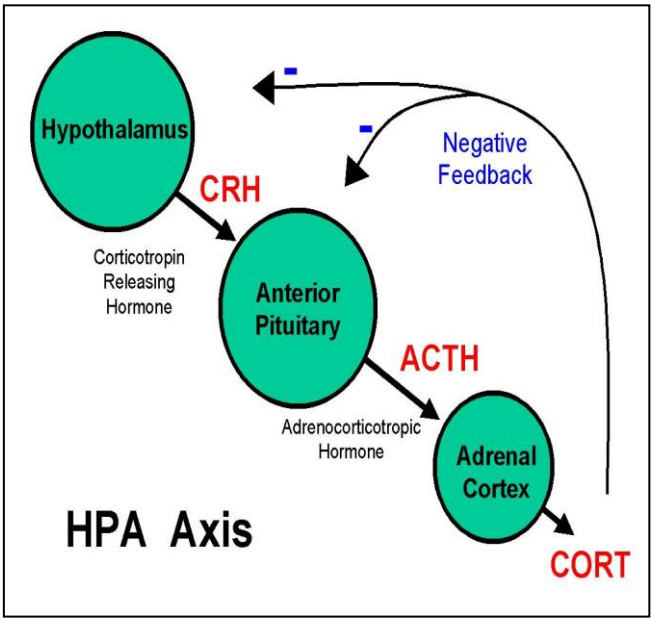

Figure 1.2. Normal ACTH regulation as seen in the HPA axis. CORT = corticotropin, a Gc. Image taken from www.biology.ucr.edu/.../Garland/HPA_axis.jpg.

1.3. The glucocorticoid receptor

The physiological effects of Gcs are mediated by the glucocorticoid receptor (GR). The GR is a steroid hormone receptor, a subset of receptors (including oestrogen, androgen and progesterone receptors) that belong to the nuclear receptor superfamily (Turner and Muller, 2005). The GR is encoded by a single copy gene on chromosome 5 which spans an area of 110 kb (Turner and Muller, 2005; Zhou and Cidlowski, 2005). Two highly homologous receptors able to bind Gcs have been described: the GR (type II GR) and the mineralocorticoid receptor (MR; type I GR) (Cole *et al.*, 1995). The majority of the physiological effects of Gcs are believed to be regulated by the GR, despite the fact that the MR has a greater affinity for Gcs than the GR. The GR is also expressed more ubiquitously and is a stronger activator of transcription (Cole *et al.*, 1995). In order to understand GR expression, it is important to first understand its gene structure.

1.3.1. The structure of the GR gene

Briefly, the GR gene (NR3C1; denoting nuclear receptor subfamily 3, group C, member 1) (Turner and Muller, 2005) consists of seven constant coding/translated exons (exons 2-8), two exon 9s encoding the α and β protein isoforms, and nine 5'-non-coding/untranslated alternative first exons (exon 1) (Schaaf and Cidlowski, 2002; Alt *et al.*, 2010). Each first exon has its own promoter associated with an alternative transcription start site. Seven of these promoters are clustered together in a 3.1 kb CpG island upstream of exon 2. Genuine, full-length GR protein is generated from transcription at any transcription start site, as the translation start site is in the common exon 2 (Turner *et al.*, 2006; Alt *et al.*, 2010).

1.3.2. Regulation of the GR

The effects of Gcs are exerted through the GR. Gcs are steroid hormones that affect virtually all cells and tissues influencing metabolism, growth, development and immunosuppression (Matthews *et al.*, 2008), and are essential for embryonic lung development. They stimulate surfactant synthesis in alveolar epithelial cells of the developing lung during the perinatal period. Thus, Gcs are administered in the treatment of respiratory distress syndrome of children born prematurely (Cole *et al.*, 1995). Gcs are potent anti-inflammatory agents, widely used in the treatment of inflammatory diseases such as asthma, rheumatoid arthritis and other auto-immune diseases (Eickelberg *et al.*, 1999; Schaaf and Cidlowski, 2002; Matthews *et al.*, 2008). They induce immense apoptosis in lymphoid cells, thus are used for the treatment

of many haematological malignancies (Lu *et al.*, 2005). Gcs are also used, primarily for their anti-inflammatory and anti-emetic effects, in the early treatment of lung cancer (Rice *et al.*, 2008). Co-administration of Gcs with anti-cancer drugs in the treatment of patients with solid tumours is common to avoid drug-induced allergic reactions or nausea/vomiting (Lu *et al.*, 2005). Gcs inhibit cell cycle progression and cell proliferation in some human lung cancer cell lines. They also display anti-tumourigenic effects in mouse models of lung cancer, probably by inhibiting cell proliferation as in human lung cancer cells, but possibly by affecting cell differentiation (Hofmann *et al.*, 2005).

Gcs act by binding to the GR, an intracellular ligand-activated transcription factor. Unliganded GR resides in the cytosol associated with a macromolecular complex (Schmidt *et al.*, 2004) of chaperone proteins including heat shock proteins Hsp90, Hsp70, and Hsp56 (Eickelberg *et al.*, 1999), as well as several other proteins (Weigel and Zhang, 1998) (see Fig. 1.3). Hsp90 plays an integral part in the complex as it associates with the ligand binding domain of the receptor, ensuring the receptor remains transcriptionally silent, yet still able to bind Gcs. Furthermore, Hsp40, Hsp70, p23 and p60 are necessary to keep the GR-Hsp90 complex in a stable formation (Schaaf and Cidlowski, 2002).

Upon ligand binding, the GR which is phosphorylated in the absence of ligand, becomes hyperphosphorylated (Schaaf and Cidlowski, 2002). Gc binding also causes conformational changes in the GR resulting in dissociation of the receptor from the inactive, cytoplasmic multiprotein complex (Weigel and Zhang, 1998) (Fig. 1.3). The hyperphosphorylated receptor subsequently dimerizes and migrates to the nucleus where it binds to specific, palindromic DNA sequences in regulatory sequences of target genes named Gc-responsive elements (GREs) (Schaaf and Cidlowski, 2002; Herr *et al.*, 2003). Once bound to the GRE, the complex recruits either co-activators or co-repressors. For example, recruitment of co-activator proteins such as histone acetyltranferases, opens the chromatin structure to allow up-regulation of gene transcription. Alternatively, recruitment of co-repressor proteins such as histone deacetylases, compacts the chromatin to form a structure that does not permit transcription (Schlossmacher *et al.*, 2011). GR-signalling is thus able to modify chromatin to stimulate or suppress the expression of a plethora of target genes (Ray *et al.*, 1996; Schmidt *et al.*, 2004).

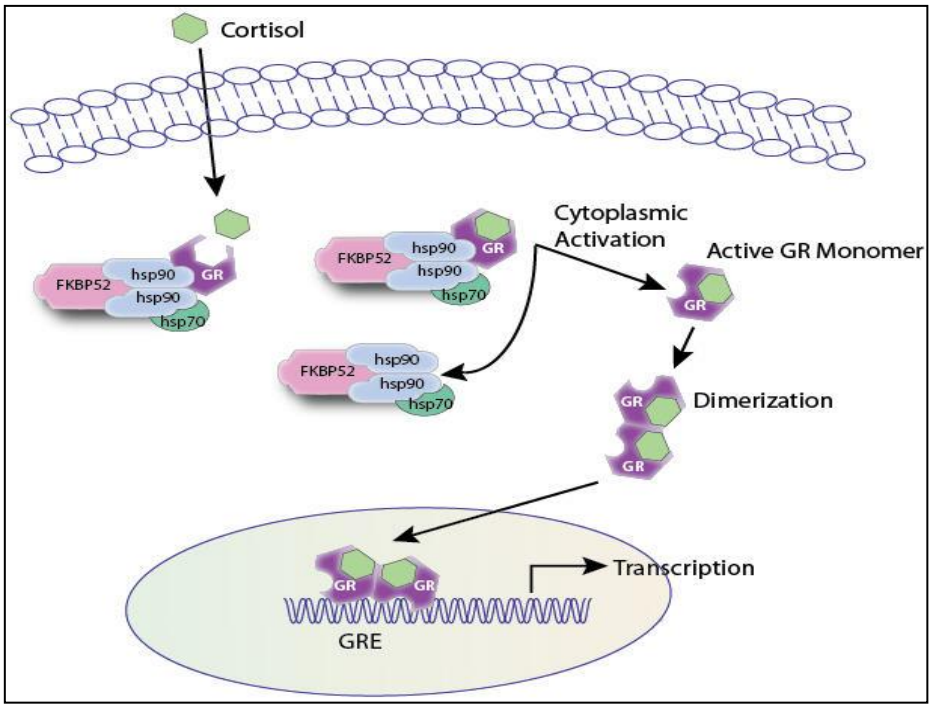

Figure 1.3. The principal mechanism of Gc action. Cortisol (a Gc) diffuses across the plasma membrane and binds to the GR. The GR then dissociates from its multiprotein complex, dimerizes and translocates to the nucleus. In the nucleus it binds GREs and acts as a transcription factor to induce or suppress the expression of target genes. Image taken from www.panomics.com/index /index.php?id=product 94.

Alternatively, GRs can modulate the activity of other transcription factors such as activator protein (AP)-1, nuclear factor (NF)-AT and NF-κB (Herr *et al.*, 2003). Schmidt *et al.* (2004) and Sommer *et al.* (2007) believe that the insensitivity of ACTH production by SCLC cells to Gc action can be attributed to impaired and/or reduced expression of the GR in these cells.

1.3.3. Effects of a synthetic Gc and anti-Gc

Gcs are commonly used as co-treatment during cancer therapy. Besides reducing nausea, hyperemesis and acute toxicity on normal tissue, Gcs have pro-apoptotic effects on lymphoid cells and osteoblasts. Dexamethasone (Dex) is a synthetic anti-inflammatory Gc with a range of effects on cell survival, cell signalling and gene expression. It is therefore frequently used to study apoptosis, cell signalling pathways and Gc effects on gene expression. Dex has been found to regulate survival, growth, and differentiation of T cells, and to inhibit the induction of nitric oxide synthase (Herr *et al.*, 2003; Herr *et al.*, 2007).

Hofmann *et al.* (1995) discovered that exposure to Dex inhibited the growth of 38% of NSCLC cell lines examined, whereas the growth of all SCLC cells was insensitive to Dex. This anti-proliferative effect was directly proportional to the cellular concentration of GRs (Hofmann *et al.*, 1995; Lu *et al.*, 2005). All cell lines sensitive to Dex had high receptor concentrations, with the NSCLC A549 cells having the greatest GR concentration, hence experiencing the greatest anti-proliferative effect. SCLC cell lines have comparatively lower amounts of GR. High GR content is thus a prerequisite for growth inhibition induced by Dex (Hofmann *et al.*, 1995; Sommer *et al.*, 2007).

In the juvenile rat hippocampus, Dex has been shown to down-regulate anti-apoptotic Bcl-2 and Bcl-xL, and up-regulate the pro-apoptotic Bax protein. Down-regulation of Bcl-2 expression is thought to contribute to Gc-induced apoptosis in U-2 OS (osteosarcoma) cells (Lu *et al.*, 2007). The mechanism whereby the GR regulates these genes remains unclear (Sommer *et al.*, 2010).

Gcs induce apoptosis of lymphoid cells (Herr *et al.*, 2003; Herr *et al.*, 2007). However haematological cells may also be resistant to Gc-induced apoptosis. Possible molecular mechanisms for Gc resistance include a low number of GRs, mutations of the GR, abnormal expression of GR binding proteins (e.g. Hsp90 and Hsp70), dysregulation of transcription factors (e.g. AP-1 and NF-κB), of GR target genes, or of members of the apoptosis pathway, to name a few (Herr *et al.*, 2007). Cytosol analyses of SCLC biopsies have implied a complete absence of GR (Hofmann *et al.*, 1995). Moreover, transfection of SCLC cells with GR restores Dex-mediated inhibition of proliferation (Sommer *et al.*, 2007).

Mifepristone (RU486) is a synthetic Gc commonly used as a tool to study mechanisms of steroid receptor function. RU486 binds with high affinity to both progesterone receptors and GRs, where it exhibits potent antagonistic activity. This anti-Gc is also anti-gestagenic, widely used for the termination of unwanted pregnancy (Hofmann *et al.*, 1995; Ghoumari *et al.*, 2003). RU486 is virtually inactive when administered alone, but blocks the growth inhibitory effect of Dex on NSCLC cell lines when administered in conjunction with Dex (Hofmann *et al.*, 1995). In addition, apoptosis induced by over-expression of the GR in Gc-resistant SCLC cells, was slightly increased by Dex treatment, but inhibited by RU486 in a dose-dependent manner.

RU486 therefore competitively opposes the GR-mediated actions of Dex by binding GR, hence blocking GR access to Dex (Sommer *et al.*, 2007).

1.3.4. Ligand-independent GR expression

Gcs are steroid hormones which act through intracellular ligand-stimulated steroid receptors such as the GR and/or the chicken progesterone receptor (cPR) (Bai *et al.*, 1997). However, many steroid receptors can become activated in the absence of their cognate ligands. The concept of ligand-independent activation of GR/cPR function originates from findings that steroid receptor function is not only regulated by steroid hormone ligand binding, but also by signal transduction pathways driven by compounds unrelated to steroids (Bai *et al.*, 1997; Pariante and Miller, 2001).

Steroid receptors are phosphoproteins, hence their transcriptional activity is regulated by the phosphorylation induced by ligand binding. Steroid receptor transcriptional activity is also regulated by modulators of signal transduction pathways. However little is known about the molecular mechanisms of ligand-independent activation of steroid receptors. Since steroid receptors are phosphoproteins, ligand-independent activation may be mediated by changes of receptor phosphorylation in response to different treatments (Bai *et al.*, 1997). A study by Bai *et al.* (1997) revealed that phosphorylation of the cPR is not absolutely required for ligand-independent activation. This indicated that the ligand-independent activation of cPR may instead be mediated through alterations in the phosphorylation of receptor-associated proteins such as co-activators and chaperone proteins (e.g. Hsps), which play important roles in receptor regulation. Phosphorylation of Hsps, many of which are phosphoproteins, could cause an alteration in either the expression level of the Hsp, or their affinity toward steroid receptors, resulting in receptor activation. Moreover, alterations in the phosphorylation cofactors that interact with steroid receptors and are involved in their activation process, may contribute to ligand-independent activation of steroid receptors (Bai *et al.*, 1997).

Other studies have shown that GR function can be influenced by a multitude of non-steroid compounds including pro-inflammatory cytokines such as interleukin 1, and participants in the cyclic adenosine monophosphate cascade which includes protein kinase A (Pariante and Miller, 2001). Diminished GR function via alterations in ligand-independent factors that regulate the GR, may be a mechanism of Gc resistance (Pariante and Miller, 2001).

1.3.5. Resistance to Gc action in SCLC cells

SCLCs are insensitive to negative feedback of the POMC pro-hormone by Gcs (Schlossmacher *et al.*, 2011). This is due to impaired function of the GR. Turney and Kovacs (2001) found that in one SCLC cell line this occurred as a result of a mutation in the GR gene that generated a truncated protein form of the GR, known as GR-P. In a different SCLC cell line, the GRγ isoform was produced as one allele of the GR had an amino acid transition mutation in the DNA-binding region of the GR (Ray *et al.*, 1994; Ray *et al.*, 1996). In the CORL 103 SCLC cell line, over-expression of the GR co-repressor, NCoR, resulted in decreased transactivation of the GR and is therefore considered to be accountable for Gc resistance (Waters *et al.*, 2004). Sommer *et al.* (2007) and Kay *et al.* (2011) identified an overall reduction in GR expression across a panel of SCLC cell lines.

Gc sensitivity in the DMS 79 SCLC cell line can be restored by transient transfection of wild-type GR. In addition, retroviral over-expression of exogenous GR in DMS 79 cells induced massive apoptosis. These data suggest that low level expression of the GR in SCLC cell lines is responsible for apoptosis resistance and may contribute to cancer progression (Schmidt *et al.*, 2004; Kay *et al.*, 2011; Schlossmacher *et al.*, 2011).

1.4. Apoptosis

Resistance to apoptosis is a characteristic feature of SCLC. This suggests that apoptosis of the cancer cells is essential for the prevention of SCLC tumour development and progression (Hopkins-Donaldson *et al.*, 2003). Two major signalling pathways of apoptosis have been described: the 'extrinsic' death receptor pathway, and the 'intrinsic' mitochondrial signalling pathway (Schmidt *et al.*, 2004; Motadi *et al.*, 2007).

1.4.1. The extrinsic pathway

The extrinsic pathway is initiated by ligand-mediated activation of membrane death receptors, or the tumour necrosis factor (TNF)/nerve growth factor superfamily of cell surface receptor proteins such as FasL/CD95L and TNF-related apoptosis-inducing ligand (TRAIL)/APO2L. Binding of the cognate ligand to the cell surface receptor induces the receptor to trimerize and leads to clustering of the receptor death domains. A death inducing signalling complex (DISC) is subsequently formed by the cytoplasmic domains of the death receptors. DISC then associates with the Fas-associated death domain (FADD) containing protein adaptor molecule, forming

the DISC-FADD complex. Through its death effector domains, the DISC-FADD complex, which is regulated by p53, binds to initiator caspases 8 and 10, thereby stimulating the autocatalytic cleavage of procaspase -8 and -10 and activation of downstream executioner caspases, resulting in apoptosis (Hopkins-Donaldson *et al.*, 2003; Motadi *et al.*, 2007).

Caspases are proteases that disassemble the cell. Bcl-2 and related proteins promote cell survival by inhibiting adaptors required for activation of caspases, whereas pro-apoptotic proteins promote apoptosis through mechanisms that include displacing the adaptors from the pro-survival proteins. Bcl-2 proteins participate in the intrinsic mitochondrial signalling pathway of apoptosis (Adams and Cory, 1998).

1.4.2. The intrinsic pathway

The intrinsic pathway is mediated by mitochondrial cytochrome *c* and members of the Bcl-2 family (Schmidt *et al.*, 2004; Motadi *et al.*, 2007). Apoptosis is regulated by a balance between pro-survival and pro-apoptotic proteins. Bcl-2 proteins regulate apoptosis by 'tipping the scale' from anti- to pro- apoptotic Bcl-2 family members. This scale is termed the 'Bcl-2 rheostat' (Schlossmacher *et al.*, 2011). The Bcl-2 protein family comprises both pro- and anti-apoptotic members, and has been divided into three subfamilies: the anti-apoptotic Bcl-2 subfamily which includes Bcl-2 and Bcl-xL; the pro-apoptotic Bax subfamily; and the pro-apoptotic BH3 subfamily which contains Bad (Motadi *et al.*, 2007). Activated pro-apoptotic proteins attach to the outer mitochondrial membrane, forming conducting channels that allow cytochrome *c* to translocate from the inter-membrane matrix into the cytoplasm. In the cytoplasm, cytochrome *c* binds ATP, Apaf-1 and procaspase 9 to form an apoptosome, which activates caspase 9 and subsequently caspase 3, leading to apoptosis (Herr *et al.*, 2007; Motadi *et al.*, 2007).

1.4.3. GR-mediated apoptosis

The intrinsic pathway responds to intracellular signals such as those generated by GR signalling (Herr *et al.*, 2007). Activation of the GR by Gc binding can stimulate apoptosis, and this Gc-induced apoptosis has proven to be critically dependent on sufficient levels of cellular GR (Schmidt *et al.*, 2004; Herr *et al.*, 2007). SCLC however, has reduced GR expression. Restoration of the GR in SCLC cells by retroviral over-expression *in vitro* was found to induce apoptosis via up-regulation of the pro-apoptotic genes Bad and Bax (Sommer *et al.*, 2007). In xenograft, over-expression of the GR resulted in apoptotic cell death by up-regulation of Bad and down-

regulation of the anti-apoptotic, pro-survival genes Bcl-2, Bcl-xL and Mcl-1 (Sommer *et al.*, 2010). Restoration of GR expression to SCLC cells therefore results in apoptosis *in vitro* and similarly *in vivo* (Sommer *et al.*, 2010).

Interaction of Gcs with the GR can induce apoptosis through activation of pro-apoptotic members of the Bcl-2 family such as Bim, Bid and Bad, and/or repression of pro-survival proteins including Bcl-2, Mcl-1 and Bcl-xL (Schlossmacher *et al.*, 2011). Bad interacts with and transmits apoptotic stimuli to anti-apoptotic Bcl-2 and Bcl-xL to prevent their pro-survival function (Fig. 1.4). This stimulates activation of Bax, which commits the cell to apoptosis (Adams and Cory, 1998). The expression of Bax is regulated by mitochondrial p53, and over-expression of Bax induces apoptosis in lung cancer cell lines (Motadi *et al.*, 2007).

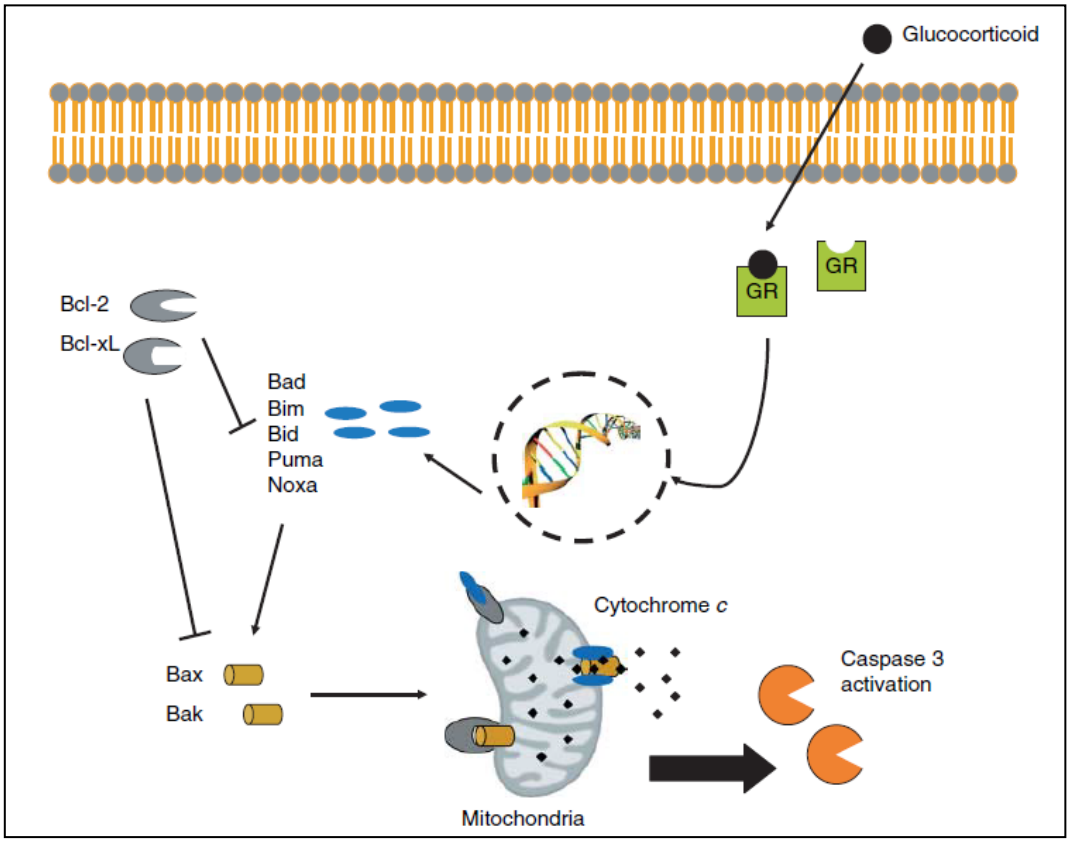

Figure 1.4. The mechanism of Gc-mediated apoptosis. While the exact pathway is not clear and may vary in different cell types, it is thought that Gcs act via the mitochondrial pathway to stimulate caspase activation. Image adapted from Schlossmacher *et al.* (2011).

Up to 90% of SCLC tumours and cell lines over-express Bcl-2. Bcl-2 down-regulates the intrinsic apoptotic pathway by inhibiting cytochrome *c* release from mitochondria, preventing apoptosis induced by UV irradiation, cytotoxic drugs, p53 and c-Myc. This indicates that Bcl-2 may play a critical role in the development of SCLC (Hopkins-Donaldson *et al.*, 2003; Motadi *et al.*, 2007).

1.5. Epigenetic modifications

Reduced GR expression confers a survival advantage to SCLC cells (Sommer *et al.*, 2007). The GR itself is a ubiquitously expressed gene and it is surprising that it is not expressed in SCLC cells. Many cancers inactivate unwanted genes by epigenetic mechanisms such as methylation and deacetylation (Kay *et al.*, 2011). Epigenetic modifications refer to heritable changes in gene expression that do not involve changes in the DNA sequence i.e. not genetic alterations. Many of these modifications include changes to the chromatin (Geutjes *et al.*, 2012). Resistance to apoptosis in SCLC cell lines is associated with increased methylation of the GR promoter, by mechanisms similar to those observed with conventional TSGs (Kay *et al.*, 2011).

1.5.1. Histone deacetylation

Histone deacetylases (HDACs) mediate the removal of acetyl groups from histone lysine residues (Ting *et al.*, 2006). Deacteylation of histones causes an increase in the positive charge of the histone protein, which increases the protein's voracity for DNA or for other histones. The resulting compaction of the chromatin may block access of transcription factors to the DNA or hinder the movement of RNA polymerase (Tycko, 2000). Actively transcribed genes are typically surrounded by acetylated histones, but by deacetylated histones when aberrantly silenced in cancer in collaboration with DNA hypermethylation (Ting *et al.*, 2006). HDACs sequentially deacetylate histones to maintain chromatin in a repressed state (Worm and Guldberg, 2002; Nephew and Huang, 2003).

1.5.2. DNA methylation

DNA methylation is an epigenetic event whose pattern is frequently altered in a wide variety of human cancers (Vaissière *et al.*, 2009). Tumour cells display global hypomethylation, with region-specific hypermethylation (Robertson, 2001). Conversely, normal cells display global hypermethylation interspersed with, on average, 1000 bp long regions of CG-rich hypomethylated DNA (Deaton and Bird, 2011).

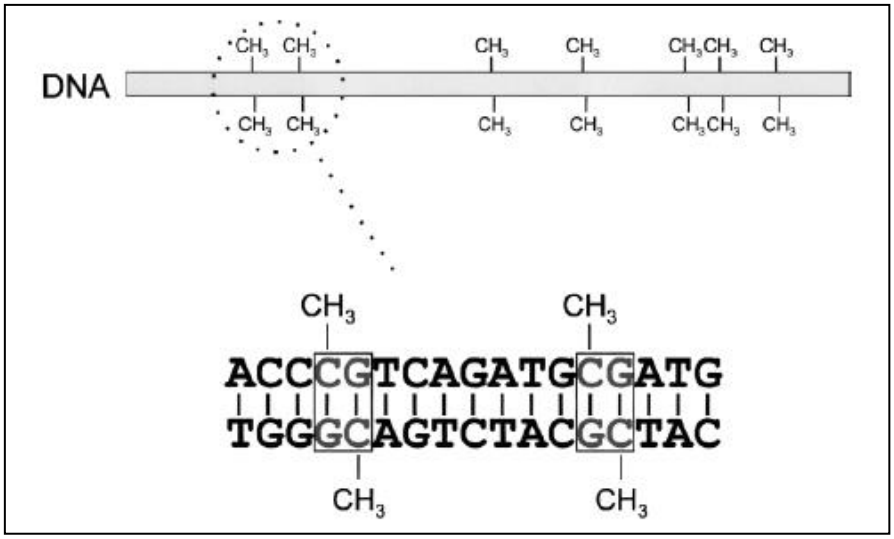

Figure 1.5. DNA methylation in CpG islands. Methylation entails the covalent addition of a methyl group at the fifth position of the cytosine ring and occurs almost exclusively in CpG islands, which are concentrated in gene promoters. Image taken from Worm and Guldberg (2002).

DNA methylation participates in many processes including DNA repair, genome stability, and chromatin structure (Robertson, 2001). It involves the covalent addition of a methyl group at the fifth position of the cytosine ring and predominantly occurs in CpG islands, concentrated in gene promoter regions where the transcription of DNA to RNA begins (Baylin *et al.*, 2004) (Fig. 1.5). CpG islands occur at transcription start sites in the promoter regions of more than half of the genes of the human genome, including nearly all reference genes. It is believed that CG richness is a feature that adapts CpG islands to promoter function, as CG richness increases the probability that ubiquitous transcription factors will bind (Deaton and Bird, 2011). These CpG islands are usually unmethylated (Fig. 1.6). However, promoter-associated CpG islands are more likely to become methylated in cancer cells than in normal cells, preventing transcription and resulting in "silencing" of the gene i.e. hypermethylation causes loss of gene function (Hopkins-Donaldson *et al.*, 2003; Baylin *et al.*, 2004). CpG island methylation is rare in normal cells, and contributes to X-chromosome inactivation in females and genomic imprinting (Robertson, 2001). Methylation is frequently accompanied by histone modifications such as deacetylation and, together, these conformational changes physically obstruct the transcriptional machinery of the cell from accessing the promoter region (Baylin *et al.*, 2004).

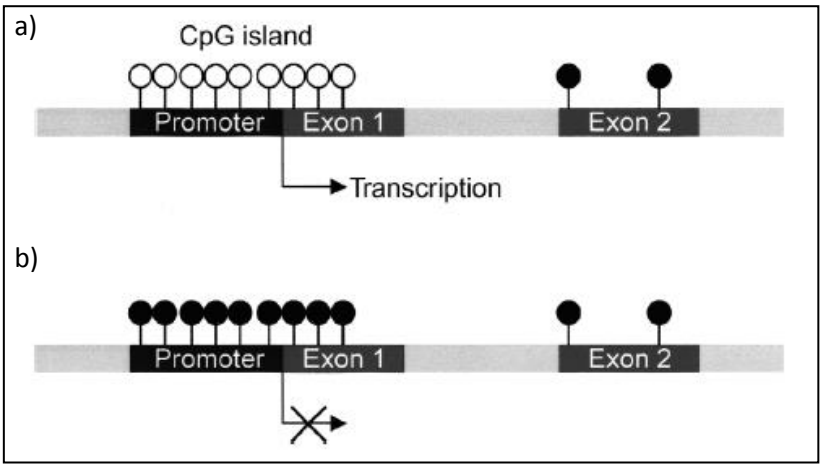

Figure 1.6. a) Promoter-associated CpG islands in normal cells are unmethylated (open lollipops), allowing transcription. However in b) cancer cells, promoter CpG islands are densely methylated (closed lollipops), which causes transcriptional silencing. Image adapted from Worm and Guldberg (2002).

In addition to DNA methylation, CpG island promoters can also be silenced by polycomb group proteins (PcGs). The two PcGs present in mammals are polycomb-repressive complex 1 (PRC1) and PRC2. PRC2 is possibly recruited to CpG islands by an unknown CpG island-binging factor, where it trimethylates histone H3K27 to form H3K27me3. H3K27me3 is recognized by PRC1, which inhibits transcriptional elongation by a mechanism involving H2A ubiquitylation and/or chromatin compaction, thereby silencing genes (Deaton and Bird, 2011).

1.5.3. Methyl-CpG binding domain proteins

HDACs couple with methyl-CpG binding domain proteins (MBDs), a family of proteins that 'interpret' the DNA methylation code of the cell, and mediate between DNA methylation and histone acetylation/deacetylation to maintain a transcriptionally silent chromatin state (see Fig. 1.7). The MBD family consists of methyl-CpG binding protein 2 (MeCP2), and MBD1, MBD2, MBD3 and MBD4 (Jones and Baylin, 2002; Esteller, 2007). MBDs bind methylated cytosines in promoters, and have been identified in many DNA hypermethylated promoters of aberrantly silenced cancer genes (Jones and Baylin, 2002; Ting *et al.*, 2006; Esteller, 2007). MeCP2, MBD1 and MDB2 also associate with transcriptional co-repressor proteins, such as Sin3A, which can bind HDACs directly. MBDs can thereby repress gene transcription through the recruitment of a HDAC-containing complex to methylated DNA. This provides a mechanistic link between DNA methylation and transcriptional repression by the modification of protein i.e. histone deacetylation (Tycko, 2000; Jones and Baylin, 2002; Esteller, 2007).

HDACs also form complexes with, and can be recruited by, DNA methyltransferases (DNMTs), specifically DNMT 1 (Worm and Guldberg, 2002; Nephew and Huang, 2003; Ting *et al.*, 2006).

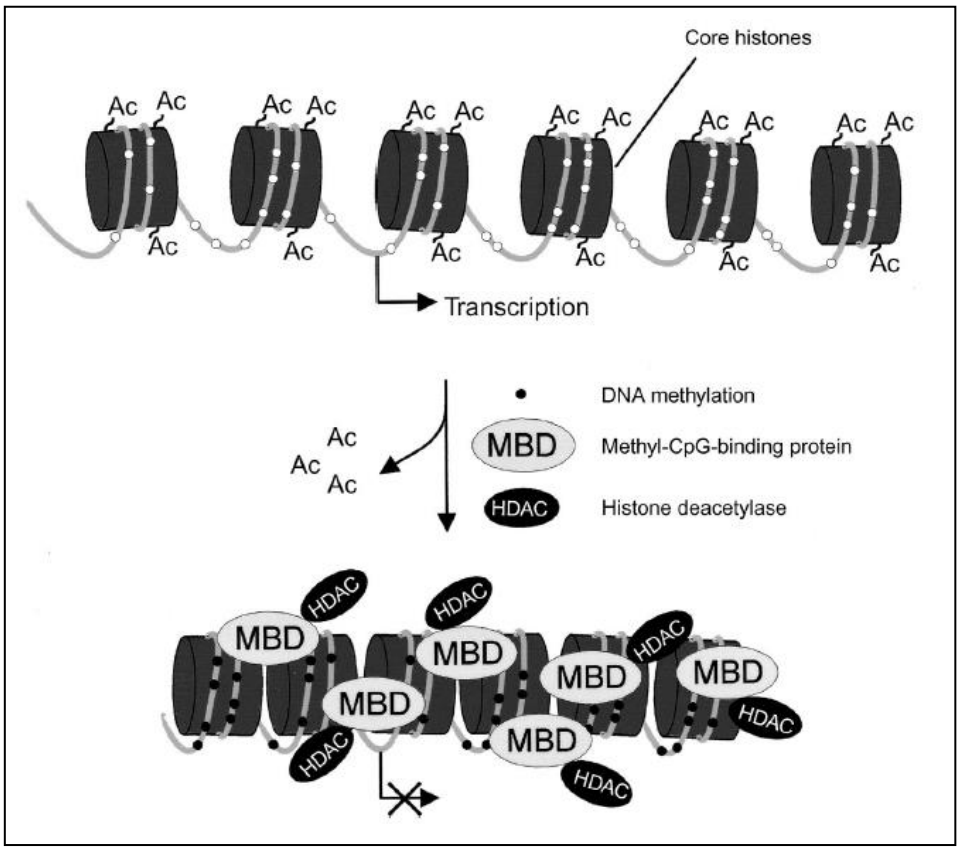

Figure 1.7. A model for methylation-dependent gene silencing. Histone acetylation causes an open chromatin configuration that is associated with a transcriptionally active state. MBDs recognise m^5C and subsequently recruit HDACs to the site of methylation, converting the chromatin into a closed structure that can no longer be accessed by the transcriptional machinery. Image taken from Worm and Guldberg (2002).

1.5.4. The mammalian DNA methyltransferases

Methylation is maintained by at least three individually encoded DNMTs: DNMT 1, DNMT 3a and DNMT 3b. A fourth DNMT, DNMT 2, has been identified but its catalytic activity has yet to be determined (Robertson, 2001). It is thought to be involved in the recognition of DNA damage, DNA recombination and repair (Turek-Plewa and Jagodziński, 2005). The reaction mechanism of the DNMTs involves the extrusion of the target cytosine from the double helix into the active site cleft of the enzyme where it is reacted upon by a conserved active site cysteine (Robertson, 2001).

DNMTs can also silence genes by a non-enzymatic transcriptional repressor function: these proteins all have transcriptional repressor domains, and furthermore each can recruit HDACs and/or other co-repressors to methylated DNA in a manner analogous to MBDs (Karpf and Jones, 2002).

The addition of methyl groups is mediated by the maintenance DNMT, DNMT 1 (Baylin *et al.*, 2004; Turek-Plewa and Jagodziński, 2005; Lin *et al.*, 2010). However, more than half of the DNMT 1 protein is not involved in catalysis, but instead is essential for protein-protein interactions and substrate recognition. A crucial aspect of substrate recognition is an affinity for DNA that is methylated on one strand, but not the other i.e. hemi-methylated DNA. A second function of the regulatory domain is targeting of DNMT 1 to foci of DNA replication in the nucleus. The preference for hemi-methylated DNA, combined with the physical proximity of the enzyme to newly synthesized DNA, enables the enzyme to faithfully copy methylation patterns to daughter strands (Tycko, 2000).

Methylation patterns can be both created and erased. DNMT 3a and 3b are responsible for *de novo* methylation, particularly during embryogenesis. The *de novo* DNMTs methylate the cytosines of CpG dinucleotides to m^5C post replication in unmethylated DNA (Turek-Plewa and Jagodziński, 2005). It has been suggested that DNMT 3a and 3b also repair the errors made by DNMT 1 following DNA synthesis. Unlike DNMT 1, DNMT 3a and DNMT 3b are firmly anchored to nucleosomes, perhaps allowing these enzymes to remain closely associated with the DNA methylation that they produce to facilitate epigenetic inheritance (Baylin and Jones, 2011).

Increased mRNA and/or protein expression of all of the DNMTs has been detected in numerous cancers (Jones and Baylin, 2002; Nephew and Huang, 2003). DNMT 1 is usually over-expressed in lung and liver cancer patients that are smokers. Recently, it has been shown that NNK, a major carcinogen (Rom *et al.*, 2000) and key ingredient of tobacco smoke, induces nuclear accumulation of DNMT 1 (Fig. 1.8). DNMT 1 binds to the promoters of multiple TSGs thereby allowing hypermethylation of promoters (Lin *et al.*, 2010). Epimutations, like epigenetic silencing of TSGs by hypermethylation, have been implicated in lung cancer aetiology (Lyko and Brown, 2005; Vaissière *et al.*, 2009). DNMT 1 over-expression has been shown to correlate with poor prognosis for lung cancer. Therefore, NNK-induced DNMT 1

accumulation and subsequent TSG promoter hypermethylation provides a significant link between cigarette smoking and lung cancer (Lin *et al.*, 2010).

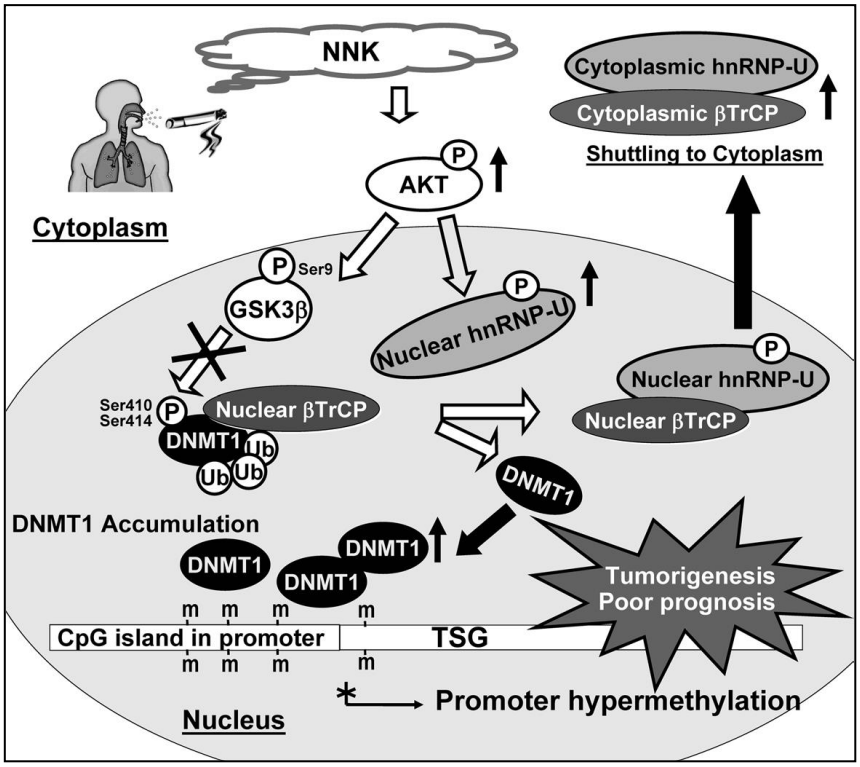

Figure 1.8. Proposed model to illustrate the accumulation of nuclear DNMT 1 by NNK-induced signaling leading to promoter hypermethylation, which ultimately leads to tumorigenesis and poor prognosis. Image taken from Lin *et al.* (2010).

1.5.5. 5-Aza-2'-deoxycytidine as a DNA methyltransferase inhibitor

5-Aza-2'-deoxycytidine (5-aza) is a potent inhibitor of the three biologically active DNMTs i.e. it is a DNMT inhibitor (DNMTi) (Christman, 2002; Karpf and Jones, 2002; Lyko and Brown, 2005; Baylin and Jones, 2011). It is incorporated into the DNA of dividing cells at the 5' of the cytosine ring (the position of methylation). DNMT 1 irreversibly bound to m^5C, is inactivated as soon as 5-aza integrates into CpG sites opposite the methylated CpG on the template strand. DNMT 1 recognises 5-aza, then forms a covalent adduct with the DNMTi. A stable reaction intermediate results via the sulfhydryl side chain of the catalytic cysteine residue (Fig. 1.9). The DNMT 1 enzyme is thus trapped and concomitantly degraded, causing rapid depletion of DNMT protein. DNA replication is then forced to proceed in the absence of methylation, which in turn leads to global demethylation and consequent reactivation of promoter

hypermethylated genes (Christman, 2002; Karpf and Jones, 2002; Lyko and Brown, 2005; Stresemann and Lyko, 2008; Geutjes *et al.*, 2012).

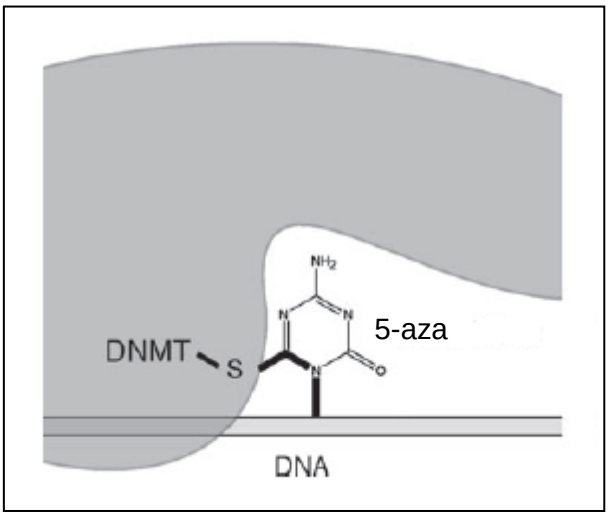

Figure 1.9. DNMT inhibition by enzyme trapping. 5-Aza is incorporated into DNA during replication and is then recognised by DNMTs. A stable reaction intermediate is formed via the sulfhydryl side chain of the catalytic cysteine residue. The DNMT enzyme is thus trapped, and concomitantly degraded. By this mechanism, cells are depleted of the DNMT protein. Image adapted from Lyko and Brown (2005).

5-Aza has been used to reverse methylation in a variety of cell lines. Virmani *et al.* (2003) found that target of methylation-induced silencing (TMS) 1, a CpG island-associated gene, is aberrantly methylated in SCLC, NSCLC, and breast cancer cell lines, and that 5-aza treatment removed methylation and restored TMS1 expression. In renal cancer cell lines the E-cadherin gene is silenced by promoter CpG hypermethylation. Treatment of the renal cancer cell lines with 5-aza resulted in re-expression of E-cadherin (Nojima *et al.*, 2001). Moreover, many cancer cells exhibit reduced caspase-8 expression due to promoter hypermethylation. 5-Aza treatment led to reactivation of caspase-8 and restored sensitivity for chemotherapy (Worm and Guldberg, 2002).

DNMTs are thus attractive therapeutic targets due to the reversible nature of DNA methylation. 5-Aza, however, initially proved too toxic for clinical use. Pioneering clinical work lead to the discovery that therapeutic efficacy could be achieved at low drug doses (Baylin and Jones, 2011). 5-Aza has been extensively tested in phase I-III clinical trials (Lyko and Brown, 2005). Known clinically as decitabine, it is currently used to treat myelodysplastic syndrome (MDS), a pre-leukaemic bone marrow disorder (Lyko and Brown, 2005; Baylin and Jones,

2011). A large clinical trial in MDS patients showed decitabine increased the conversion time of MDS to true leukaemia, as well as improved overall patient survival (Baylin and Jones, 2011). It has also demonstrated clinical efficacy in the treatment of acute myelogenous leukaemia and chronic myelogenous leukaemia (Christman, 2002; Lyko and Brown, 2005; Geutjes *et al.*, 2012). Decitabine is presently being investigated for the treatment of solid tumours (Brueckner *et al.*, 2007).

1.6. Aim and objectives

Sommer *et al.* (2007) showed that SCLCs have reduced GR, and that SCLC cells die by apoptosis if the GR is over-expressed. The GR promoter region in peripheral blood mononuclear cells is extensively methylated, specifically in the CpG islands (Turner *et al.*, 2008). Recent evidence in our laboratory suggests that the GR promoter in SCLC cells is methylated (Kay *et al.*, 2011). Since it is possible to remove epigenetic methyl marks by treatment with a DNMTi, we aimed to establish whether allowing re-expression of endogenous GR would commit the cells to apoptosis.

Bisulphite sequencing suggests that there are CpG islands in the GR promoter approximately 3.1 kb upstream of the start codon that show reversible methylation after treatment with 5-aza (Kay *et al.*, 2011). These methylation marks are not present in non-SCLC cell lines (Kay *et al.*, 2011).

The aim of this project is to establish whether re-expression of endogenous GR by treatment with the DNMTi, 5-aza, induces apoptosis of SCLC cells. To better understand the role of GR-induced apoptosis, the effects of 5-aza, Dex and RU486 will be examined on the SCLC cell line, DMS 79; the Gc-sensitive non-SCLC cell line, A549; and the Gc-resistant HEK 293 cell line. The HEK 293 cells will serve as the control because, like DMS 79 cells, they express very little GR, but do not undergo apoptosis when the GR is re-expressed (Sommer *et al.*, 2007). Because demethylating agents are not specfic, treatment with 5-aza will demethylate all methylated genes. It is therefore difficult to establish whether apoptosis resulting from treatment with 5-aza is solely due to re-expression of the GR, or due to re-expression of other genes that were previously silenced. The GR antagonist, RU486 (Schaaf and Cidlowski, 2003), will thus be used to determine whether apoptosis is specifically a result of endogenous GR re-expression. Dex is a synthetic GR agonist i.e. it stimulates GR action via a ligand-dependent mechanism (Schaaf

and Cidlowski, 2003). To establish whether Dex accelerates apoptosis, the effect of Dex on lung cancer cell lines was also examined.

The objectives of this project were as follows:

1) To determine whether treatment with 5-aza results in re-expression of endogenous GR.

2) To establish whether 5-aza is toxic to cells, affecting cell viability.

3) To determine whether endogenous GR re-expression is sufficient to activate the pro-apoptotic and suppress the anti-apoptotic pathway, leading to apoptosis.

4) To establish whether apoptosis associated with 5-aza treatment is due to demethylation and subsequent expression of the GR, or to demethylation and expression of other previously silenced genes.

5) To determine whether Dex treatment can enhance apoptosis.

Restoration of GR expression in SCLC cells by transfection or viral transduction is sufficient to restore Gc sensitivity (Ray *et al.*, 1994). Sommer *et al.* (2007) have shown that retroviral over-expression of the GR induces apoptosis of SCLC cells both *in vitro*, and also in a xenograft model (Sommer *et al.*, 2010). It is therefore clear that repression of GR expression in SCLC confers a significant survival advantage to the cancer cells. This raises the possibility that the GR is an as yet uncharacterised TSG for SCLC cells, and that loss of GR expression is implicated in SCLC pathogenesis.

2. MATERIALS AND METHODS

2.1. Cell culture

2.1.1. Cell lines

DMS 79, human embryonic kidney 293 (HEK) and A549 cells were utilised for this study (see Fig. 2.1). The DMS 79 cell line was derived from an ACTH-producing SCLC (Turney and Kovacs, 2001). This SCLC cell line is GR deficient. HEK cells are also GR deficient, and like the DMS 79 cells, are resistant to Gcs. The A549 human lung epithelial carcinoma cells express abundant GR, hence are sensitive to Gc action. The DMS 79, HEK and A549 cell lines were all obtained from the American Type Culture Collection.

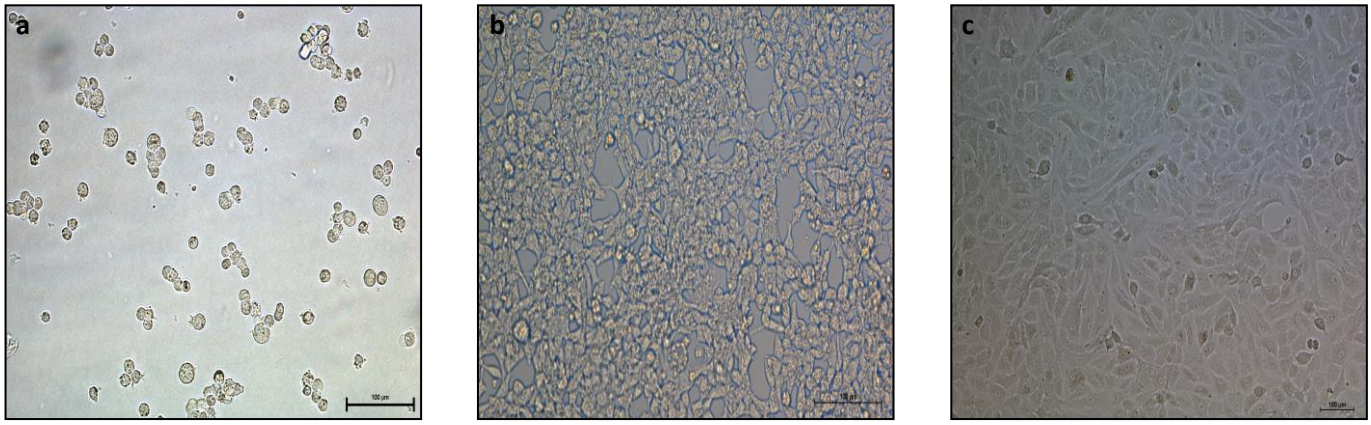

Figure 2.1. Differential interference contrast (DIC) photographs of (a) DMS 79 cells (X200) grown in suspension; (b) HEK cells (X100) and (c) A549 cells (X100) cultured as monolayers. The images were taken using a Nikon Eclipse T*i*-S microscope.

2.1.2. Cell culture technique

Cell culture was conducted in a Class II Type 2A laminar flow (Logic Labconco®) using dedicated cell culture equipment. The DMS 79 cells, which grow as spheroids in suspension, were cultured in 75 cm^3 (T75) or 25 cm^3 (T25) flasks (Corning) in 30 mL or 5 mL respectively of RPMI 1640 (PAA) medium containing 10 mM HEPES, supplemented with 1% GlutaMAX™ Supplement (Gibco), 10% heat-inactivated foetal bovine serum (FBS) Gold (PAA) and 2% 100x Penicillin-Streptomycin (PAA) to a final concentration of 100 units/mL. The HEK and A549 cells, which are adherent cells that grow as a monolayer, were cultured in 10 cm^3 or 6 cm^3 culture dishes (Corning) in Dulbecco's Modified Eagle Medium (DMEM) (PAA) containing 584 mg/L L-glutamine supplemented with 10% heat-inactivated FBS Gold and 2% 100x Penicillin-

Streptomycin. Cells were cultured aseptically at 37°C in an air-jacketed incubator (Shel Lab) and a humidified atmosphere of 5% CO_2. Cell growth was monitored using an inverted microscope (Nikon TMS) at a total magnification of X200. DMS 79 cells determined to be confluent were passaged by centrifuging up to 15 mL of medium (containing the cells) for 3 min at 2000 rpm. The supernatant/medium was removed, the cells re-suspended in 1 mL of fresh medium and split accordingly. The HEK and A549 cells determined to be confluent were split by the addition of 1 mL of 1x Trypsin-EDTA solution (PAA) (Appendix B.i) to the culture dish, followed by incubation for 5 min at 37°C. Trypsin-EDTA activity was inactivated by the addition of 1 mL DMEM.

2.1.3. Treatment with a DNA methyltransferase inhibitor (DNMTi)

The DNMTi, 5-aza-2'-deoxycytidine (5-aza) (Sigma®) (Appendix B.ii), was dissolved at 50 mg/mL in 50% filter sterilised acetic acid. A 1:100 dilution (in the appropriate culture medium i.e. RPMI 1640 or DMEM) was prepared. The cells were treated with either 0.5 µM, 1 µM, or 5 µM 5-aza (Fig. 2.2) for 72 h.

For the vehicle control (Appendix B.iii), a 1:100 dilution of 50% filter sterilized was made in the appropriate cell culture medium. The cells were treated with a 5 µM concentration of vehicle, as 5 µM was the highest concentration of 5-aza used (Fig. 2.2).

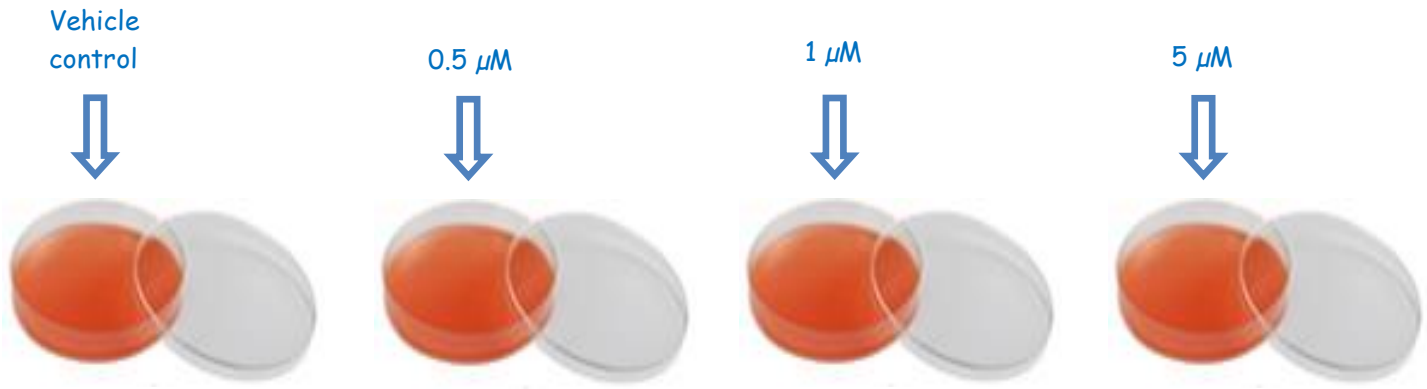

Figure 2.2. Representation of the vehicle control and 5-aza treatments of HEK or A549 cells, grown in 10 cm^3 culture dishes.

For quantitative real-time polymerase chain reaction (qPCR) analysis, DMS 79 cells in four T75 flasks or four 10 cm^3 dishes of HEKs and A549s were treated with either 0.5 µM, 1 µM, 5 µM 5-aza, or vehicle (Fig. 2.2) for 72 h for total RNA extraction. For the cell viability assay, a total of

five T25s (DMS 79) and five 6 cm^3 dishes (HEK and A549) comprising the vehicle control, 0.5 µM, 1 µM, and 5 µM 5-aza, plus one 'no treatment', were treated for 72h. Similarly, five culture vessels for each cell line were treated for flow cytometry. For the immunoblots, protein was extracted from two 10 cm^3 dishes per treatment for the HEK and A549 cells, whereas only one T75 flask per treatment was required for the DMS 79 cells.

2.2. RNA extraction

RNA was extracted from the three cell lines using the RNeasy® Mini Kit (QIAGEN). For the HEK and A549 cells, the media was removed, and the cells washed with 1 mL 1x phosphate-buffered saline (PBS) (Appendix B.iv). 1 mL 1x Trypsin-EDTA was added to the culture dishes to break the junctions between the adherent cells. Following a 5 min incubation at 37°C, during which the cells lifted from the bottom of the dish, 1 mL DMEM was added to inactivate the trypsin. The cells were then transferred to micro-centrifuge tubes (Starlab), which were centrifuged for 3 min at 2000 rpm. All the supernatant (cell culture medium) was carefully removed by aspiration.

For the DMS 79 cells, excess medium was removed from each flask. Up to 15 mL of medium (containing the cells) was placed into a 15 mL centrifuge tube (Corning) and centrifuged for 3 minutes at 2000 rpm. All the supernatant was then carefully removed from the cell pellet by aspiration.

RNA was extracted using the RNeasy® Mini Kit according to the 'Purification of Total RNA from Animal Cells Using Spin Technology' protocol. After all of the supernatant (cell culture medium) was carefully removed from the pelleted cells by aspiration, the pellet was disrupted by addition of 600 µL Buffer RLT (to lyse the cells) containing β-mercaptoethanol (to denature RNases released during lysis). The cell pellet was pipetted up-and-down, and vortexed (Vortex-Genie 2, Scientific Industries) to thoroughly mix. To create a homogenous lysate and shear DNA molecules, the lysate was transferred into a QIAshredder spin column, and centrifuged for 2 min at full speed. 600 µL 70% Ethanol (Appendix B.v) were then added to the homogenised lysate and mixed by pipetting. 700 µL of the sample was transferred to an RNeasy spin column and centrifuged for 15 s at 8000 x g. The flow-through was then discarded. 700 µL Buffer RW1 were added to the RNeasy spin column to wash the spin column membrane, and centrifuged for 15 s at 8000 x g, then the flow-through discarded. 500 µL

Buffer RPE were added to the RNeasy spin column to wash the spin column membrane, centrifuged for 15 s at 8000 x g, and the flow-through discarded. 500 µL Additional Buffer RPE was added to the RNeasy spin column and centrifuged for 2 min at 8000 x g and the flow-through discarded. The longer centrifugation dried the spin column membrane, ensuring that no ethanol, which may interfere with downstream reactions, was carried over during RNA elution. The RNeasy spin column was placed in a new 2 mL collection tube and centrifuged at full speed for 1 min. This step was performed to eliminate any possible carryover of Buffer RPE and/or residual flow-through which may have remained on the RNeasy spin column after the previous step. The RNeasy spin column was placed in a new 1.5 mL collection tube. 30 µL RNase-free water was added to the spin column membrane and centrifuged for 1 min at 8000 x g to elute the RNA. The samples were placed on ice and the RNA was quantitated using a Spectrophotometer ND1000 (NanoDrop Technologies) (Appendix A.3.1). The RNA samples were then aliquoted and stored at -80°C until cDNA synthesis.

2.2.1. Validation of RNA integrity

In accordance with the MIQE guidelines (Bustin *et al.*, 2009), the integrity of each RNA sample was validated before use in qPCR analyses. Two µg RNA samples were prepared in micro-centrifuge tubes. Two volumes of RNA Sample Loading Buffer (Sigma®) were added to each sample. The samples were vortexed, spun down, then denatured at 65°C for 10 min. The samples were subsequently cooled on ice and centrifuged to pull condensation down off the cap. The samples were run on 1.5% agarose 2.2 M formaldehyde gels (Appendix B.vi) with the 10 kb GeneRuler™ DNA Ladder Mix (0.5 µg/µL) (Fermentas) as the DNA molecular weight marker (MWM), in 1x MOPS running buffer (Appendix B.vi). The gels were imaged using a ChemiDoc™ XRS+ Imaging System with Image Lab™ software (Bio-Rad). The presence of two distinct, intact bands of 18 S rRNA and 28 S rRNA subunits were used to verify good quality RNA.

2.3. cDNA synthesis

cDNA was initially synthesized from RNA using the High Capacity RNA-to-cDNA Master Mix (Applied Biosystems), but this was later replaced by the Tetro cDNA Synthesis Kit (Bioline) as the former was discontinued by the manufacturer. RNA was defrosted on ice prior to cDNA synthesis. All incubation steps of each cDNA synthesis protocol were performed in the Bio-Rad MyCycler™ thermal cycler.

2.3.1. cDNA synthesis using the High Capacity RNA-to-cDNA Master Mix

cDNA was synthesized from RNA samples using the High Capacity RNA-to-cDNA Master Mix. 4 µL Reverse transcriptase (RT) Master Mix, 1 µg RNA (up to 16 µL) and nuclease-free H_2O sufficient to 20 µL, were pipetted into a PCR tube (Bio-Rad). The volume of nuclease-free H_2O and concentration of RNA was calculated to achieve the final required reaction mix volume (20 µL). Each PCR tube was centrifuged to spin down the contents and eliminate any air bubbles. The tubes were then loaded into the thermal cycler. Reverse transcription cycling conditions were as follows: 5 min at 25°C, 1 h at 42°C, and 5 min at 85°C. The cDNA was plunged into ice and spun-down immediately. The cDNA was then diluted 1:1 with 20 µL RNase-free water, and aliquoted. Aliquots were stored at -20°C until use.

2.3.2. cDNA synthesis using the Tetro cDNA Synthesis Kit

cDNA was later synthesized from RNA using the Tetro cDNA Synthesis Kit. All solutions from the kit were vortexed and spun-down before use.

2.3.2.1. Poly(A) tail priming

The poly(A) tail priming premix was prepared on ice: 2 µg RNA (up to 5 µL), 1 µL oligo $(dT)_{18}$ primer, 1 µL dNTP mix and up to 7 µL diethyl pyrocarbonate (DEPC)-treated water (supplied in the kit) was added to a PCR tube. DEPC-treated water prevents RNases from degrading the RNA. The volume of DEPC-treated water and concentration of RNA was calculated to create the required priming premix volume of 10 µL. The samples were spun-down and incubated at 70°C for 5 min in the thermal cycler, then chilled on ice for at least 1 min. Oligo $(dT)_{18}$ primers anneal to the 3' poly(A) tails of mRNA molecules and designate the starting sites for RT activity (Nam *et al.*, 2002).

2.3.2.2. First strand cDNA synthesis

For multiple samples, a mastermix was prepared in a micro-centrifuge tube. Preparation per sample included 4 µL 5x RT buffer, 1 µL Ribosafe RNase inhibitor to reduce template degradation and increase the yield of PCR product, 1 µL Tetro RT, and 4 µL DEPC-treated water. The reaction premix was spun-down to mix. 10 µL of the reaction premix was added to each sample of priming premix and gently spun-down to mix.

For each treatment of every cell line, a no-RT control was included in the experiment to evaluate sample contamination with genomic DNA. The priming premix was prepared as above. In the reaction premix, however, the 1 µL Tetro RT was substituted with 1 µL DEPC-treated water. 10 µL of reaction premix was transferred to the PCR tubes and centrifuged to spin down, as above.

Following the addition of the reaction premix, the samples were loaded into the thermal cycler and incubated at 45°C for 1 h. The reaction was terminated by incubation of the PCR tubes at 85°C for 5 min, then chilled on ice. The cDNA was placed on ice and spun-down immediately, then diluted 1:1 with 20 µL RNase-free water. Each cDNA sample was spun-down, aliquoted, and stored at -20°C until use in qPCR.

2.4. Polymerase chain reaction (PCR)

2.4.1. Primers

Three primer sets specific to GRα, glyceraldehyde-3-phosphate dehydrogenase (GAPDH) and β-actin were used for qPCR analyses. The specificity of the primers was evaluated by BLASTing them against the *Homo sapien* genome in the NCBI database (www.ncbi.nlm.nih.gov) using the Primer BLAST resource (http://www.ncbi.nlm.nih.gov/tools/primer-blast/) (see Appendix A.5.1). Primer sets were evaluated at an annealing temperature of 60°C. The relevant primer information is provided in Table 2 (p. 29). All primers were manufactured by Inqaba Biotec, and reconstituted in TE buffer (Appendix B.vii) to 100 µM stock solutions. The primer stock solutions were diluted 1:10 in nuclease-free water, and used at a concentration of 10 µM. The primers were stored at -20°C until use. Conventional PCR was used to optimise the primers sets prior to qPCR analysis.

2.4.2. Conventional PCR

Conventional PCR was performed to test the specificity and evaluate the efficiency of each primer set. A single 20 µL PCR reaction consisted of 1 µL cDNA, 1 µL forward primer, 1 µL reverse primer, 2 µL 10x NH_4 buffer (Fermentas), 2 µL 2mM dNTPs mix (Promega), 0.2 µL *Taq* polymerase (Fermentas), 1.8 µL 25mM $MgCl_2$ (Fermentas), and 11 µL nuclease-free water. A 'blank' reaction was included for each PCR run, in which 1 µL cDNA was substituted with 1 µL nuclease-free water. The 'blank' served as a negative control. PCR was carried out in a Bio-Rad MyCycler™ thermal cycler using the following cycling conditions: an initial denaturation step at

95°C for 4 min; 35 cycles of 95°C for 30 seconds, 60°C for 1 minute and 72°C for 1 minute; and an extra elongation step of 72°C for 7 minutes.

2.4.2.1. Agarose gel electrophoresis

PCR products were run on a 1.5% agarose (TopVision™, Fermentas) gel (Appendix B.viii) in 1x Tris-base EDTA (TBE) running buffer (Appendix B.ix). 0.5 µg/mL Ethidium bromide was included in the gel. 3 µL 6x DNA Loading Dye (Thermo Scientific) was added to each 20 µL PCR sample. The samples were vortexed and spun-down prior to loading. The MWM, GeneRuler™ DNA Ladder Mix (0.5 µg/µL), was run in the first well of the gel and 12 µL of each sample was loaded into individual wells. All agarose gels were run at 85 V for 55 min. Gels were visualised using a ChemiDoc™ XRS+ Imaging System (Bio-Rad) and the software package Image Lab™ (Bio-Rad).

2.5. Quantitative real-time PCR (qPCR)

qPCR analysis was performed to quantify the relative expression levels of the gene of interest, the GRα gene. qPCR was run with primers for GRα, and for the two reference genes GAPDH and β-actin.

2.5.1. qPCR experimental design

qPCR experiments were conducted and interpreted in accordance with the Minimum Information for Publication of Quantitative Real-Time PCR Experiments (MIQE) guidelines. Following the MIQE guidelines promotes better experimental procedure and allows more reliable, consistent and transparent interpretation of qPCR results (Bustin *et al.*, 2009). All relevant information as required by the MIQE guidelines is presented in Appendix A.

No-RT controls and no-template control (NTC) reactions were included in qPCR runs. This was done to verify that the gene expression results obtained were true reflections of the mRNA expression levels and that they were not influenced by genomic DNA contamination, amplicons, or RNA contamination.

The specificity of each primer set was evaluated by melt curve analysis of the qPCR product. The melting temperature (T_m) of each product corresponded to a single product, which was confirmed by agarose gel electrophoresis (as above in section 2.4.2.1.) (Appendix A.7).

Table 2. Primer information and sequences used for qPCR

Primer	Sequence (5' - 3')	Amplicon size (bp)	Reference sequence	Intron-exon spanning	Annealing temperature (°C)	Source
GRα	Fwd: CCATTGTCAAGAGGGAAGGA	173	NM_000176 (UCSC)	No	54	Sommer *et al.* (2007)
	Rev: CAGCTAACATCTCGGGGAAT					
GAPDH	Fwd: GAAGGTGAAGGTCGGAGT	226	NM_002046 (UCSC)	No	60	Sommer *et al.* (2007)
	Rev: GAAGATGGTGATGGGATTTC					
β-Actin	Fwd: GGCCACGGCTGCTTC	208	NM_001101.3 (NCBI)	No	60	Alt *et al.* (2010)
	Rev: GTTGGCGTACAGGTCTTTGC					

Due to problems with the supplier, qPCR was performed using 5x HOT FIREPol® EvaGreen® qPCR Mix Plus (no ROX) (Solis BioDyne) (Appendix A.6.1) and/or SYBR® Green JumpStart™ *Taq* ReadyMix™ (Sigma®) (Appendix A.6.2) as per the manufacturer's instructions. qPCR was carried out in a MiniOpticon™ Real-Time PCR Detection System (Bio-Rad).

Fluorescence was read from a baseline of 0.2 RFU, determined using the single threshold setting in the CFX Manager program. This baseline was used for all qPCR experimental runs when both EvaGreen and SYBR Green were used.

2.5.2. qPCR using 5x HOT FIREPol® EvaGreen® qPCR Mix Plus (no ROX)

A single 20 µL EvaGreen reaction consisted of 2 µL 5x HOT FIREPol® EvaGreen® qPCR Mix Plus (no ROX), 16 µL nuclease-free water, 0.5 µL forward primer, 0.5 µL reverse primer and 1 µL cDNA. qPCR was carried out in a MiniOpticon™ Real-Time PCR Detection System, and cycling conditions were as follows: a denaturation step at 95°C for 15 min; 40 cycles at 95°C for 15 s, at 60°C for 30 s, and at 72°C for 1 min. A plate read was then inserted. This was followed by a final extension of 72°C for 10 min. For the melt curve analysis, the temperature was dropped to 50°C, then subsequently increased to 95°C in 1°C increments, for a total of 5 s. This step was followed by another plate read.

2.5.3. qPCR using SYBR® Green JumpStart™ *Taq* ReadyMix™

A single 25 µL SYBR green reaction consisted of 12.5 µL SYBR® Green JumpStart™ *Taq* ReadyMix™, 10.5 µL nuclease-free water, 0.5 µL forward primer, 0.5 µL reverse primer and 1 µL cDNA. qPCR cycling conditions were as follows: an initial denaturation at 95°C for 2 min; 40 cycles at 95°C for 15 s, at 60°C for 30 s, and at 72°C for 1 min. A plate read was then inserted. This was followed by a final extension of 72°C for 10 min. For the melt curve analysis, the temperature was dropped to 50°C, and then subsequently increased to 95°C in 1°C increments, for a total of 5 s. This step was followed by another plate read.

2.5.4. Analysis of qPCR reactions

Results were analysed using the CFX Manager™ Software package version 2.1 (Bio-Rad). The data was transformed using the $2^{-\Delta\Delta CT}$ method (Livak and Schmittgen, 2001). Relative fold change of gene expression levels in treatments were represented as bar graphs with standard error of the mean (SEM). As two reference genes were used, the relative fold change in GRα

expression was also calculated with reference to the geometric mean of the two reference genes (Vandesompele *et al.*, 2002).

2.5.4.1. The $2^{-\Delta\Delta CT}$ method

Each single EvaGreen/SYBR green qPCR reaction was repeated in triplicate for each of the three genes for every treatment in all qPCR experimental runs. Three experimental runs were performed for each result obtained for the first biological repeat of the DMS 79 and A549 cells (n=3). Two experimental runs were performed for the first biological repeat of the HEK cells (n=2). Two experimental runs were conducted for the second biological repeat of all three cell lines (n=2). The mean quantification cycle (C_q) value for GRα (the target gene) of each treatment in an experimental run was calculated and then normalised against the average C_q values of the reference genes GAPDH and β-actin, both individually and as a geometric mean (Vandesompele *et al.*, 2002). The relative fold change values of the treatments relative to the control were thus obtained.

2.5.4.2. Validation of the $2^{-\Delta\Delta CT}$ method

For the $2^{-\Delta\Delta CT}$ method of qPCR analysis to be applicable, the reaction efficiency of the gene of interest (GRα) should ideally be equal to the reaction efficiencies of the reference genes (GAPDH and β-actin). A standard curve with an $r^2 > 0.98$ must be obtained for each target gene (Livak and Schmittgen, 2001). cDNA template dilutions were used to evaluate the reaction efficiencies of the target genes (Livak and Schmittgen, 2001) (see Appendix A.7.2).

cDNA was synthesized from 2 µg of RNA using the Tetro cDNA Synthesis Kit as in section 2.3.2. above. The fresh cDNA was not initially diluted. A series of 10-fold dilutions were then performed to obtain low template concentrations. This comprised a total of four dilutions. These dilutions, together with the undiluted cDNA, were analysed by qPCR using the primer sets of GRα, GAPDH and β-actin.

The average C_q of each gene, for each of the four dilutions, was calculated. The average C_q values were then plotted against the dilution concentration with each gene on its own set of axes values (see Appendix A.7.2).

2.5.4.3. Statistical analyses of qPCR data

Statistical analyses of the relative fold change values for GRα expression were carried out using IBM SPSS Statistics Version 21. Comparisons were by one-way analysis of variance (ANOVA). Two assumptions of the one-way ANOVA must be satisfied in order for the ANOVA results to be valid. The assumptions of the ANOVA apply to the residuals rather than the observations. One-way ANOVA assumptions are as follows:

The residuals from the analysis are normally distributed. This was determined by the one-sample Kolmogorov-Smirnov test.

The variance of the residuals must be equal in all treatments (residuals must be homoscedastic). Homoscedasticity was tested with the Levene's test, which is running the ANOVA again but with the residuals in the place of the dependant variable *viz.* relative fold change in GRα expression.

The samples from each treatment were independent of the other samples. The Bonferroni t-test was the multiple comparison analysis performed to determine whether there were significant differences between the GRα expression of the control and the GRα expression of the treatments. Significance was set at $p < 0.05$ for all statistical tests.

2.6. Immunoblot

2.6.1. Protein extraction

DMS 79 cells grown in T75 flasks were treated with either vehicle control, 0.5 µM, 1 µM or 5 µM 5-aza. One T75 was cultured per treatment. Media containing the cells were transferred into 15 mL centrifuge tubes. Two 10 cm^3 dishes were used per treatment for the adherent HEK and A549 cells. The cell culture medium was removed from the dishes by aspiration and discarded. The lightly adherent HEK cells were washed off the dishes with 2 mL 1x PBS and the cells collected in a 15 mL centrifuge tube. A cell scraper (Biologix Research Company) was used to dislodge the intensely adherent A549 cells from the 10 cm^3 dishes. Any remaining cells were washed off with 2 mL 1x PBS and collected in 15 mL centrifuge tubes. The cells from the two dishes of each treatment were transferred into the same centrifuge tube.

The 15 mL tubes were centrifuged in a 5810 R (Eppendorf) centrifuge at room temperature for 5 min at 1200 rpm. The supernatant was poured out of the tube. The remaining supernatant was carefully removed from above the cell pellet with a 1 mL pipette. The pellet was re-

suspended in 1 mL of 1x PBS, centrifuged at 1200 rpm for 2 min at 4°C, and the supernatant discarded. Each cell pellet was then treated with a protease-phosphate inhibitor cocktail.

2.6.1.1. Preparation of the protease and phosphatase inhibitor cocktail

250 µL Radio-immunoprecipitation assay (RIPA) buffer (Sigma®) was prepared in a micro-centrifuge tube. The protease and phosphatase inhibitor cocktail (Sigma®) was thawed on ice then spun-down. 25 µL was added to the RIPA buffer. The cocktail contains 2 mg/mL each of leupeptin, pepstatin A, aprotinin. 0.5 µL Chymostatin (also 2 mg/mL; Sigma®) and 2.5 µL phenylmethylsulfonyl fluoride (PMSF) were also added to the RIPA buffer inhibitor cocktail mixture.

Each cell pellet was re-suspended in 50 µL of the buffer-cocktail mixture. The cells were mixed by vortexing at medium speed. The cells were incubated for 5 min at room temperature and then plunged into ice for 30 min. The tubes were centrifuged at 4°C for 15 min at 4000 rpm. The cell lysate was then removed and stored in micro-centrifuge tubes, ready for sample preparation. The quantity of lysate removed from each tube was recorded. The lysate was mixed by pipetting, and 10 µL of protein lysate was removed before the sample preparation, to be used for protein quantification.

2.6.1.2. Sample preparation

Reducing sample treatment buffer/loading buffer (Appendix C.i) was vortexed and then added to the protein samples in a 1:1 ratio. The samples were quickly vortexed, spun-down, and placed in the heating block for 4 min at 95°C. Thereafter the samples were again quickly vortexed and centrifuged, and stored in the -80°C freezer until protein quantification.

2.6.2. Protein quantification

Protein was quantified using the Pierce® Bicinchoninic Acid (BCA) Protein Assay Kit (Thermo Scientific), according to the 'Microplate Procedure'. Protein concentrations were determined with reference to standards of the protein bovine serum albumin (BSA). A series of dilutions of known concentrations were prepared from BSA and assayed alongside the unknowns. The concentration of each unknown was subsequently determined, based on the standard curve.

2.6.2.1. Preparation of diluted BSA standards

The protein standards were prepared by diluting the contents of one BSA ampule (Thermo Scientific). Each 1 mL ampule has a concentration of 2 mg/mL. 300 µL of BSA stock, with a BSA concentration of 2000 µg/mL, was serial diluted into seven micro-centrifuge tubes. The seventh micro-centrifuge tube had a final BSA concentration of 25 µg/mL. A blank standard, containing only ultra-pure water, was also prepared. Each standard was thoroughly mixed before dilution to ensure the generation of an accurate standard curve.

2.6.2.2. Preparation of the BCA working reagent (WR)

The 10 µL lysate set aside during protein extraction was prepared for protein quantification by dilution in ultra-pure water in a 1:10 ratio i.e. 90 µL ultra-pure water was added to 10 µL of each sample. The samples were mixed by tapping, centrifuged, and incubated on ice until needed. The total WR volume, consisting of Reagent A and Reagent B, was prepared according to the following equation:

WR required = [(number of standards x number of replicates) + (number of samples x number of replicates) + 1 extra for pipetting error] x 200 µL

The WR was prepared by mixing 50 parts of BCA Reagent A with 1 part of BCA Reagent B (50 Reagent A : 1 Reagent B) in a 15 mL centrifuge tube. The WR was mixed by inverting the tube.

2.6.2.3. Microplate preparation and reading

The standards and samples were spun-down and 25 µL of each standard or sample was pipetted into a microplate (Sero-Wel) well. Two replicates per standard and three replicates per sample were included. 200 µL of the WR was added to each well and the plate was thoroughly mixed by gentle agitation for 30 s. The microplate was covered with cling wrap and incubated at 37°C for 30 min. Following incubation, the plate was cooled to room temperature and read using the PowerWave XS plate reader and KC4™ v.3.2. software. The absorbance was measured at 562 nm. The average 562 nm absorbance measurement of the blank standard replicates was subtracted from the 562 nm measurement of all other individual standard and sample replicates. A standard curve was generated by plotting the average blank-corrected 562 nm measurement for each BSA standard vs. its concentration in µg/mL. The standard curve was used to determine the protein concentration of each sample.

2.6.2.4. Standard curve generation and calculation of protein concentration

The absorbance readings from the two wells of each duplicate BSA standard were averaged. The average 'blank' absorbance was then subtracted from these absorbance means. The concentration of the BSA standards are known. A standard curve could thus be constructed from plotting the absorbance vs. concentration. An equation was generated from the trendline.

The absorbance readings from the three wells of each triplicate sample were then averaged, and the 'blank' absorbance subtracted from each mean absorbance. The 1:10 concentration (as the protein was diluted with 90 µL ultra-pure water) of each sample was subsequently calculated using the equation of the trendline. This concentration was multiplied by 10 to obtain the concentration of the protein stock. The quantity of protein (in µL) required to obtain 40 µg protein was then determined, as 40 µg protein was loaded into each well of the acrylamide gel.

2.6.3. Western blot

2.6.3.1. Acrylamide gel assembly

Glass plates for 1.5 mm thick gels (see Fig. 2.3) were washed with 1% sodium dodecyl sulphate (SDS) (see Appendix C.ii), and wiped with 70% ethanol to ensure that they were completely clean. The two plates were sealed together with one strip of Parafilm (Pechiney Plastic Packaging) along each side. The plate was inserted into the casting frame (Bio-Rad), and the plate and casting frame were secured in the casting stand (Bio-Rad) (see Fig. 2.3), with the bottom of the plate tightly pressed against the casting stand gasket (Bio-Rad).

It was previously established in the laboratory that a 13.5% SDS polyacrylamide gel electrophoresis (PAGE) gel (Appendix C.iii) is optimal for resolution of the GRα isoform. The 13.5% resolving gel (see Appendix C.iii) was made up first in a 15 mL centrifuge tube. The components were gently mixed by slowly inverting the tube, so as not to foam the SDS. The resolving gel was then immediately added, very quickly, in the centre of the glass plate with a 1 mL pipette (Gilson). 1 mL Deionised water (di.H_2O) was then added very slowly along the width of the plate, to form a layer on top of the resolving gel. The gel was allowed a minimum of 25 min to set. After 25 min, the plate and casting frame were removed from the casting stand and

the di.H_2O was poured off. A piece of absorbent filter paper was used to absorb the remaining water. The plate and casting frame were returned to the casting stand and secured.

The 4% stacking gel (see Appendix C.iii) was then prepared in a 15 mL centrifuge tube and gently mixed, as with the resolving gel. The stacking gel was added very quickly to the centre of the plate with a 1 mL pipette, on top of the resolving gel, until it over-flowed. A 15-well comb (see Fig. 2.3) for 1.5 mm thick gels was inserted into the stacking gel. The sides of the comb/plate were sealed with Parafilm to minimize air bubble formation. The gel was allowed a minimum of 25 min to set. Following 25 min, the Parafilm was removed, the comb was removed from the gel and the plate and casting frame were taken out of the casting stand. The wells of the gel were washed out with 1x electrode buffer (Appendix C.iv) using a 1 mL pipette. The plates were removed from the casting frame, and the Parafilm taken off. The outside of the plates were wiped with tissue paper to remove any traces of gel. The gel was then inserted into the electrode assembly placed in a tank filled with 1x electrode buffer, with the thinner plate facing the gasket. The tank was placed in a Tupperware container so that ice could be added around the tank to prevent the apparatus from becoming too hot.

Figure 2.3. Equipment used in acrylamide gel assembly. The casting frame (green), casting stand (clear), combs and glass plates for 1.5 mm thick gels are presented. Image adapted from www.bio-rad.com.

2.6.3.2. Sample preparation

The protein samples were thawed and centrifuged for 2 min at 2000 x g. 40 µg Protein was loaded in duplicate or triplicate into each well. The PageRuler™ Prestained Protein Ladder (Fermentas, Thermo Scientific) was used as a MWM. The protein ladder was spun-down, then 2.5 µL loaded into the first and last wells.

2.6.3.3. PAGE gel electrophoresis

The protein samples were run through the stacking gel for 30 min at 90 V using the Mini-PROTEAN 3 Cell (PowerPac Basic™, Bio-Rad) system. The run was then paused and ice was placed around the tank. The protein samples were subsequently separated by the resolving gel, which was run at 120 V for 1 h. After 1 h, the gel was removed from the tank.

The glass plates with the gel were placed in a blot assembly tray (Bio-Rad) containing protein transfer buffer (Appendix C.v). A gel releaser (Bio-Rad) was used to separate the two plates and loosen the gel. The stacking gel was discarded. The gel holder cassette (Fig. 2.4) was laid out. A foam pad (Bio-Rad) was dipped into the protein transfer buffer and placed on the black half of the gel holder cassette. Four pieces of filter paper, cut to size, were individually dipped in protein transfer buffer and placed on top of the foam pad. The gel was placed on top of the fourth filter paper, and smoothed with a 1 mL pipette tip (Tip One, Starlab) to eliminate any air bubbles. A sheet of Amersham™ Hybond™-ECL nitrocellulose membrane (GE Healthcare), also cut to size, was soaked in the protein transfer buffer, and carefully placed on top of the gel. An additional four pieces of filter paper were soaked in the protein transfer buffer and placed on top of the nitrocellulose membrane. Each piece of filter paper was smoothed with a 1 mL pipette tip. Another foam pad was soaked and placed on top of the filter paper stack. The gel holder cassette was closed and slotted into the electrode assembly in the tank (see Fig. 2.4) (placed in a Tupperware container) filled with protein transfer buffer. A magnetic stirrer was placed in the tank, and the tank was put on the IKA® big-squid. An ice brick was inserted into the tank, and ice was placed in the Tupperware around the tank to prevent it from over-heating. The protein transfer was run for 1 h at 100 V.

Figure 2.4. Equipment used for PAGE gel electrophoresis. The tank, gel holder cassette and electrode assembly are presented. Image adapted from www.bio-rad.com.

2.6.3.4. Blotting

2.6.3.4.1. Primary antibody incubation

Following protein transfer, the nitrocellulose membrane was removed from the gel holder cassette and cut to yield two strips of nitrocellulose – one corresponding to each protein. The membrane was cut at 55 kDa as the GAPDH protein is found between 30-40 kDa, and GRα is located between 60-94 kDa. The strips were rinsed in tris-buffered saline-tween (TBST; Appendix C.vi), each in one compartment of a plastic pill container, to remove the protein transfer buffer.

The TBST was poured off the membranes and 6% skim milk blocking buffer solution (Appendix C.vii) was added. The container was placed on the MiniMix (Enduro™, Labnet) for 1 h at room temperature to block non-specific binding of primary antibody. After the blocking procedure, the skim milk was poured off and the nitrocellulose strips were rinsed with TBST to remove excess blocking solution. All the TBST was sucked off with a 1 mL pipette. The nitrocellulose membranes were then probed with the primary antibodies: purified mouse anti-GR, Clone 41 (611226, BD Biosciences), and monoclonal rabbit anti-GAPDH (14C10, Cell Signalling). The GR primary antibody was diluted ½:12000 in 6% skim milk, whereas the GAPDH primary antibody was diluted 1:3000 in TBST. The nitrocellulose membranes were incubated overnight at 4°C.

2.6.3.4.2. Secondary antibody incubation

The primary antibodies were removed the following day. The nitrocellulose membrane with GAPDH was rinsed twice with TBST, whereas the GR nitrocellulose membrane was rinsed three times. Fresh TBST was added to each membrane, which were then agitated on the shaker (IKA® KS 130 Basic) for 8 min at 240 rpm. GAPDH was washed an additional three times. The GR was washed an additional six times, and rinsed in between washes. The membranes were agitated on the shaker for 8 min at 240 rpm after every wash. The purpose of washing with TBST was to remove any unbound or non-specifically bound primary antibody.

After the final wash, all the TBST was removed. The nitrocellulose membranes were probed with the secondary antibodies, HRP goat anti-mouse for GR (554002, BD Biosciences) and anti-rabbit IgG, HRP-linked antibody for GAPDH (7074, Cell Signalling) at room temperature for 1 h at 160 rpm on the shaker. The GR secondary antibody was diluted 1:2000 in TBST, whereas GAPDH was diluted 1:4000 in TBST. The GR nitrocellulose membrane was rinsed twice with

TBST, whereas the GAPDH nitrocellulose membrane was rinsed once with TBST. As above, the nitrocellulose membranes were washed six and three times for GR and GAPDH respectively, for 8 min at a time. This step removed any unbound secondary antibody.

2.6.4. Imaging the Western blot

Proteins were visualised using the Immun-Star™ HRP Chemiluminescent Kit (Bio-Rad). A chemiluminescent solution was made up in a 1:1 ratio by combining 1.5 mL of Immun-Star™ HRP Peroxide Buffer with 1.5 mL Immun-Star™ HRP Luminol/Enhancer. The membranes were imaged in the ChemiDoc™ XRS+ System (Bio-Rad) with Image Lab™ Software version 2.0.1 (Bio-Rad).

The nitrocellulose membranes were imaged individually. The membrane was dabbed on tissue paper to remove excess TBST and placed on a plastic plate, which was then placed on the glass plate of the ChemiDoc. 300 µL of the chemiluminescent solution was pipetted onto the membrane on the plastic plate. The plastic plate was tilted to evenly distribute the solution. In the Image Lab™ program, the camera was zoomed to 7.2 magnification and the plastic plate positioned so the image appeared in the centre of the screen. The membrane was imaged according to the Western Blot protocol. The protein ladder was then imaged according to the Molecular Marker protocol. The two images captured were merged and flipped to produce one representative image. The bands on the image were then analysed by densitometry.

2.6.5. Densitometry

In the Image Lab™ program, a rectangle was constructed around the band of interest (GRα and/or GAPDH), to fit each band of every treatment. The rectangle was copied and positioned around each band of interest, and the number of pixels was calculated.

The calculated values were exported into Microsoft Excel 2010. The ratio of the GR and corresponding GAPDH value was determined, then the average of the three values calculated. The averages were plotted on a bar graph with the SEM.

2.6.5.1. Statistical analyses on densitometry

As in section 2.5.4.3.

2.7. Cell viability assay

5-Aza is an exceptionally cytotoxic compound (Christman, 2002). The CellTiter 96® AQ_{ueous} One Solution Cell Proliferation Assay (Promega) was performed to establish whether treatment of the cells with 5-aza affected cell viability. The DMS 79, HEK and A549 cells were treated with either vehicle, 0.5 µM, 1 µM or 5 µM 5-aza for a total of 72 h. A 'no treatment' control was also included for each cell line.

2.7.1. Plate preparation

After 48 h of treatment, the cells were harvested and collected by centrifugation in 15 mL centrifuge tubes (as in section 2.1). The supernatant was removed and a cell suspension of 1 x 10^5 cells prepared by addition of the appropriate volume of medium. As per the manufacturer's instructions, 50 µL of the suspension (5000 cells) was seeded into six wells of a 96-well plate (Corning), creating six replicates. 50 µL of the appropriate cell culture medium was added to each well to make a total volume of 100 µL. As the HEK and A549 cell lines grow as monolayers, they were allowed 24 h to stick to the bottom of the 96-well plate and acclimatise. After 24 h, a triplicate set of control wells (without cells) were prepared, containing 100 µL of each culture medium. This served as a 'blank' to account for background 490 nm absorbance. The 'blank' medium was allowed 1 h to equilibrate, after which 20µl/well of CellTiter 96® AQueous One Solution Reagent (Promega) was added to the wells. The 96-well plate was covered with tin foil and incubated for 2½ h at 37°C in a humidified, 5% CO_2 atmosphere.

2.7.2. Plate reading and viability determination

The 96-well plate was read on the PowerWave XS plate reader (Bio-Tek®) using KC4™ v.3.2. software. The absorbance was measured at 490 nm. The data was exported to Microsoft Excel 2010. The average 490 nm absorbance of the 'blank' control wells was subtracted from the 490 nm absorbance measurement of all other individual wells, to yield corrected absorbances. The average of each set of replicates was then calculated. The average of each untreated sample was normalised to 100% and the rest of the samples were converted to percentages normalised to the respective untreated sample. A bar graph was constructed by plotting the normalised values against percentage cell viability.

2.7.3. Statistical analyses of cell viability data

As in section 2.5.4.3.

2.8. Flow cytometry

Flow cytometry was performed to determine whether re-expression of the GR induced cell death, and whether cell death was by apoptosis. Flow cytometry was carried out in a BD FACSCalibur Flow Cytometer (BD Biosciences).

2.8.1. Apoptosis and cell death analysis

DMS 79 and HEK cells were treated with either vehicle control, 0.5 µM, 1 µM or 5 µM 5-aza for 72 h. An untreated control sample was included for each cell line, as well as an unstained control. A camptothecin (Sigma®) (Appendix D.i) control was also included. Camptothecin disrupts DNA processing by topoisomerase I. It binds reversibly to DNA-topoisomerase I complexes, but not to the enzyme or DNA alone. It appears that camptothecin reversibly traps an intermediate involved in DNA unwinding by topoisomerase I and perturbs the equilibrium, resulting in increased DNA cleavage (Hertzberg *et al.*, 1989). Hence, treatment with camptothecin induced apoptosis of the cell populations, and therefore served as the positive control. Cells were treated with 6 µM camptothecin for 4 h.

2.8.1.1. Sample preparation

Samples were prepared according to the FITC Annexin V Apoptosis Detection Kit I (BD Pharmingen™) protocol. HEK cells were harvested by gentle washing with PBS, whereas the DMS 79 cells were transferred to 15 mL centrifuge tubes and collected by centrifugation. All cell lines were collected by centrifugation at 1400 rpm for 5 min. The supernatant was carefully removed and the cell pellets re-suspended in 500 µL 1x Annexin V Binding Buffer (Appendix D.ii). The cells were then counted using a haemocytometer. The required cell number of 1 x 10^6 cells/mL was achieved by adjusting the volume of the 1x Annexin V Binding Buffer-cell suspension. Each sample was then pipetted into a 50 mL centrifuge tube (Corning) through a 40 µm cell strainer (BD Biosciences) to create single cell suspensions. 100 µL of the cell suspension (1 x 10^5 cells) was transferred to a 5 mL round-bottom tube (BD Falcon). 5 µL FITC Annexin V and 5 µL Propidium Iodide Staining Solution (PI) were added to each sample. However neither FITC Annexin V nor PI was added to the unstained treatment. The camptothecin sample was divided between two round-bottom tubes. One camptothecin

sample was treated with 5 µL FITC Annexin V only, whereas the other camptothecin sample was treated with 5 µL PI only. The cell samples were then gently vortexed and incubated for 15 min at room temperature (25°C) in the dark. 400 µL of 1x Annexin V Binding Buffer was added to each tube, and the cells analysed by flow cytometry within 1 h.

2.8.1.2. Apoptosis and cell death detection

Cell populations were recorded with the BD CellQuest™ Pro (BD Biosciences) program. The unstained control was analysed first as it was used to set the parameters of each experiment. The cell population was adjusted by electronic compensation of the applied voltage, so that no cells fell in the regions of the graph where only cells stained with FITC Annexin V or PI would appear. The camptothecin-treated populations were subsequently analysed, and served as positive controls. The untreated/treated cell samples could then be analysed. The untreated population was used to define the basal level of apoptotic and dead cells. Cells (10 000) were gated and analysed for red fluorescence (613/20 nm) to determine the percentage of PI-positive cells, and green fluorescence (519/25 nm) to determine the percentage of FITC Annexin V-positive cells.

2.8.2. Pharmacological blockade

2.8.2.1. GR activation

DMS 79 cells were exposed to the GR agonist, Dex (Sigma®) (Appendix D.iii), to determine whether glucocorticoid binding accelerates apoptosis. The cells were treated with 0.5 µM 5-aza for 72 h. A separate culture was treated with Dex only for 24 h, which served as a control. Following 48 h of treatment, 100 nM Dex was added to the 5-aza treated cells for 24 h, to a total of 72 h. An untreated control sample as well as an unstained and camptothecin control were included for each experiment.

The cell samples were prepared using the FITC Annexin V Apoptosis Detection Kit I protocol as in section 2.8.1.1, and the cell populations detected as above in section 2.8.1.2.

2.8.2.2. GR antagonism

To establish whether apoptosis was due to re-expression of the GR, or due to re-expression of previously silenced genes, cells were treated with the GR antagonist RU486 (Sigma®) (Appendix D.iv). The cells were treated with 0.5 µM 5-aza for 72 h, and a separate culture was

treated with RU486 only for 24 h. This culture served as a control. Following 48 h of treatment, 100 nM RU486 was added to the 5-aza treated cells for 24 h, to a total of 72 h. The usual untreated, unstained and camptothecin controls were included for each experiment.

Similarly, the samples were prepared and the cell populations detected as in sections 2.8.1.1. and 2.8.1.2, respectively.

2.8.3. Flow cytometry data analysis

The flow cytometry data was analysed using FlowJo 7.6.1. (Tree Star, Inc.). The data files were transferred into the FlowJo program and transformed into scatter plot cell graphs. Each graph was divided into four quadrants between the $10^2 – 10^3$ values of each axis. The percentage of cells in each quadrant was calculated. Quadrant 2 represented dead cells whereas quadrant 3 represented apoptosing cells. The quadrant 2 and 3 values were copied into Microsoft Excel 2010 and the means of each quadrant calculated. Graphs were constructed displaying the mean ± SEM.

2.8.4. Statistical analyses of flow cytometry data

As in section 2.5.4.3.

2.9. Microscopy

Due to problems accessing the flow cytometer, microscopy was also performed to determine whether re-expression of the GR induced cell death, and whether cell death was by apoptosis. Microscopy was performed on the Nikon ECLIPSE 80*i* fluorescent microscope in the Electron Microscope Unit at the UKZN, Westville campus.

2.9.1. Apoptosis and cell death analysis

DMS 79, HEK and A549 cells were treated as in section 2.8.1. In addition, a DAPI (4',6-diamidino-2-phenylindole) (Sigma®) control was included for each cell line as it served as a positive control to establish whether cells had taken up stain.

2.9.1.1. Sample and slide preparation

The samples were prepared according to the FITC Annexin V Apoptosis Detection Kit I protocol. The HEK and DMS 79 cells were collected as above in section 2.8.1.1. The A549 cells were

trypsinized to detach the cells from the bottom of the dish. Following centrifugation at 1400 rpm for 5 min, the supernatant was carefully removed and the cell pellets re-suspended in 200 µL 1x Annexin V Binding Buffer. 100 µL of the cell suspension was transferred to a micro-centrifuge tube. 5 µL FITC Annexin V and 5 µL PI were added to each sample. However neither FITC Annexin V nor PI was added to the unstained treatment, or the DAPI control sample. The camptothecin sample was divided between two micro-centrifuge tubes. One camptothecin sample was treated with 5 µL FITC Annexin V only, whereas the other camptothecin sample was treated with 5 µL PI only. The cell samples were then gently vortexed and incubated for 15 min at room temperature (25°C) in the dark. Following incubation, the cells were centrifuged for 5 min at 1400 rpm, and the supernatant removed. To wash the cells, each pellet was re-suspended in 300 µL 1x PBS, centrifuged at 1400 rpm for 5 min, and then the supernatant was removed. The cell pellets were re-suspended in 50 µL DAPI (Appendix D.v), a nucleic acid stain, and incubated for 10 min at room temperature in the dark. The samples were then centrifuged for 5 min at 1400 rpm and the supernatant was removed. The remaining cells were re-suspended in 10 µL 1x PBS and mounted on slides using mowiol mounting medium (Appendix D. vi). Slides were analysed within 1 h by microscopy using the Nikon ECLIPSE 80*i* fluorescent microscope at the UKZN Electron Microscope Unit (Westville campus).

2.9.1.2. Apoptosis and cell death detection

The unstained control was examined first to ensure that there was no fluorescence in either of the 3 channels used to view DAPI (V-2A), PI (G-2A) or FITC Annexin V (B-2A). The population stained with DAPI only was subsequently viewed, to determine whether fluorescence could only be detected in the channel used to view DAPI. Similarly, the samples stained only with PI and only with FITC Annexin V were examined to resolve whether the stains fluoresced in the correct channels. The treated cells were then examined for blue fluorescence (455/70 nm) to visualise the cells, red fluorescence (613/20 nm) to determine the percentage of PI-positive cells, and green fluorescence (519/25 nm) to determine the percentage of FITC Annexin V-positive cells. Images were obtained using the software program NIS-Elements D 3.2.

2.9.2. Pharmacological blockade

2.9.2.1. GR activation and GR antagonism

DMS 79, HEK and A549 cells were treated as in sections 2.8.2.1 and 2.8.2.2 respectively. In addition to the untreated, unstained and camptothecin controls, a DAPI control was included for each experiment.

The cell samples and slides were prepared as in section 2.9.1.1, and the cell populations detected as above in section 2.9.1.2.

2.9.3. Analysis of microscopy data

A total of 300 cells were counted from the images of various fields of view. From the 300 cells, the number of cells exhibiting chromatin condensation (DAPI stained), PI positive and FITC Annexin V positive cells were determined. The percentages of fluorescent cells were plotted on a bar graph with ± SEM.

2.9.4. Statistical analyses of microscopy data

As in section 2.5.4.3.

3. RESULTS

3.1. Validation of RNA integrity

DMS 79, HEK and A549 cells were used for qPCR gene expression analyses. RNA was extracted from the different cell types and cDNA synthesized. This cDNA was used in qPCR analyses. In accordance with the MIQE guidelines (Bustin *et al.*, 2009), the integrity of all RNA samples were validated before use in qPCR analyses. RNA samples (2 µg) were run on 1.5% agarose 2.2 M formaldehyde gels. A 10 kb DNA MWM (Fermentas) was run in each gel and gels were stained with ethidium bromide. The presence of two distinct, intact bands of 18 S rRNA and 28 S rRNA subunits were used to verify good quality RNA. The RNA gels showed that all RNA samples were of a suitable quality to be used for cDNA synthesis and qPCR analyses (Fig. 3.1, Fig. 3.2 and Fig. 3.3).

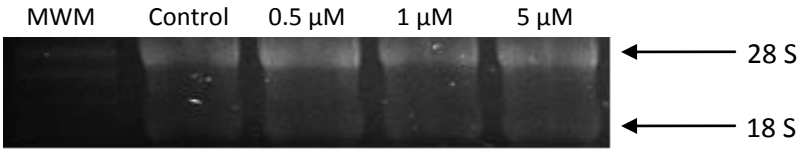

Figure 3.1. Integrity of RNA samples extracted from DMS 79 cells following treatment with vehicle control or 0.5 µM, 1 µM and 5 µM 5-aza for 72 h. RNA extracted for the first biological repeat for qPCR is shown.

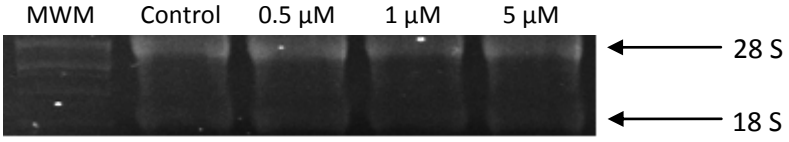

Figure 3.2. RNA integrity of samples extracted from HEK cells treated with vehicle control or 0.5 µM, 1 µM and 5 µM 5-aza for 72 h. RNA extracted for the second biological repeat for qPCR is shown.

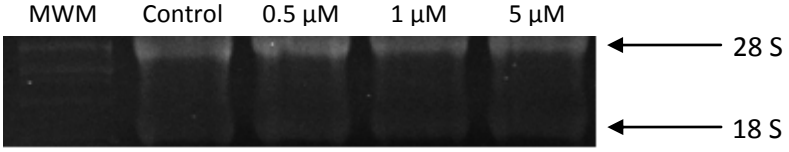

Figure 3.3. Integrity of RNA samples extracted from A549 cells following 72 h of treatment with either vehicle control, or 0.5 µM, 1 µM or 5 µM 5-aza. RNA extracted for biological repeat 2 for qPCR is shown.

Fulfilment of the MIQE requirements is presented in detail in Appendix A. qPCR reaction efficiencies were shown to be comparable (Appendix A.7.2) thus allowing comparison of the data. Data analyses are presented in greater detail in Appendix A.8.

3.2. GRα mRNA expression

Previous studies have shown that there is very little GR expression in DMS 79 and HEK cells, but abundant GR expression in A549 cells (Kay *et al.*, 2011). In this study, the cells were treated with a DNMTi, 5-aza, to determine whether lack of GR expression in the DMS 79 cell line is due to silencing by DNA methylation. qPCR was run with primers for GRα, and for the two reference genes GAPDH and β-actin. The HEK and A549 cells served as controls.

3.2.1. Treatment with 5-aza had no effect on GRα mRNA expression in A549 cells

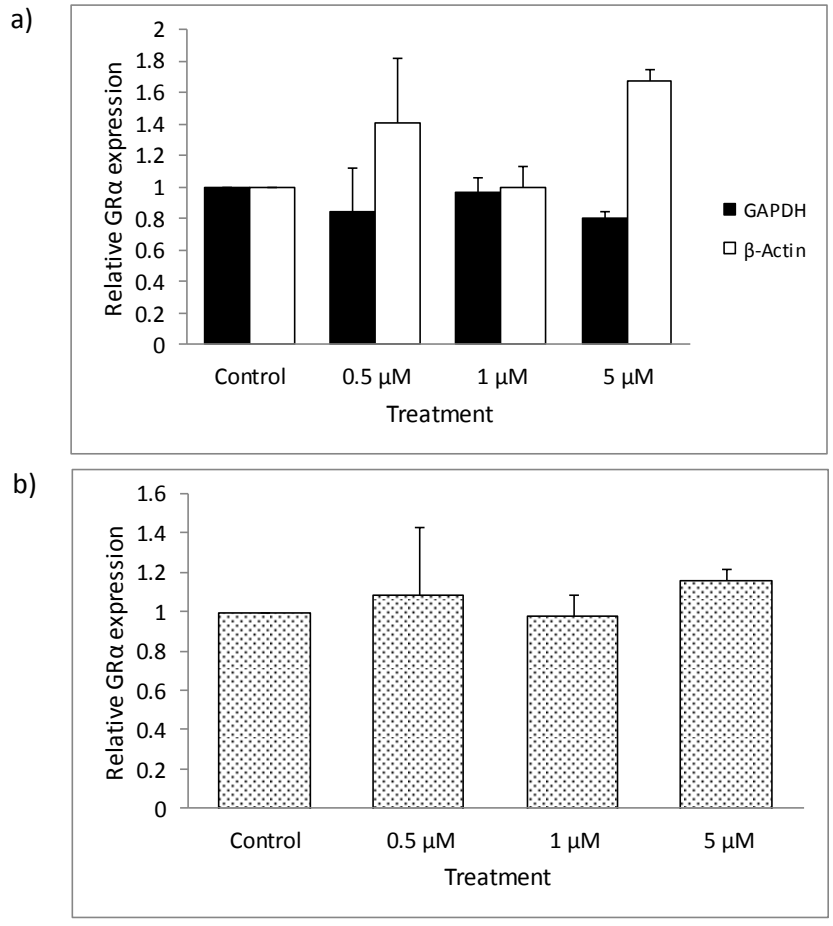

Figure 3.4. The relative fold change in GRα expression in the GR abundant A549 cells in response to 72 h treatment with 5-aza. GRα expression was normalised to (a) GAPDH and β-actin, and (b) the geometric mean of GAPDH and β-actin. qPCR was conducted using SYBR Green. The mean ± SEM is displayed (n = 3). These data represent the first biological repeat for A549 cells.

Owing to problems with the supplier, qPCR with the A549 cells had to be performed using both SYBR Green and EvaGreen. Firstly with SYBR Green, only minor changes in GRα were seen in the A549 cells following 72 h of treatment with 5-aza (Fig. 3.4a and Fig. 3.4b). In comparison to GAPDH, slight down-regulations in GRα expression were observed in response to the various concentrations of 5-aza (Fig. 3.4a). However in comparison to β-actin, the expression of GRα was seen to increase following treatment with 0.5 µM and 5 µM 5-aza, although not significantly more than the control (Fig. 3.4a). Negligible changes in GRα expression were seen when GRα was normalised to the geometric mean (Vandesompele *et al.*, 2002) of GAPDH and β-actin (Fig. 3.4b). None of the statistical tests reached significance.

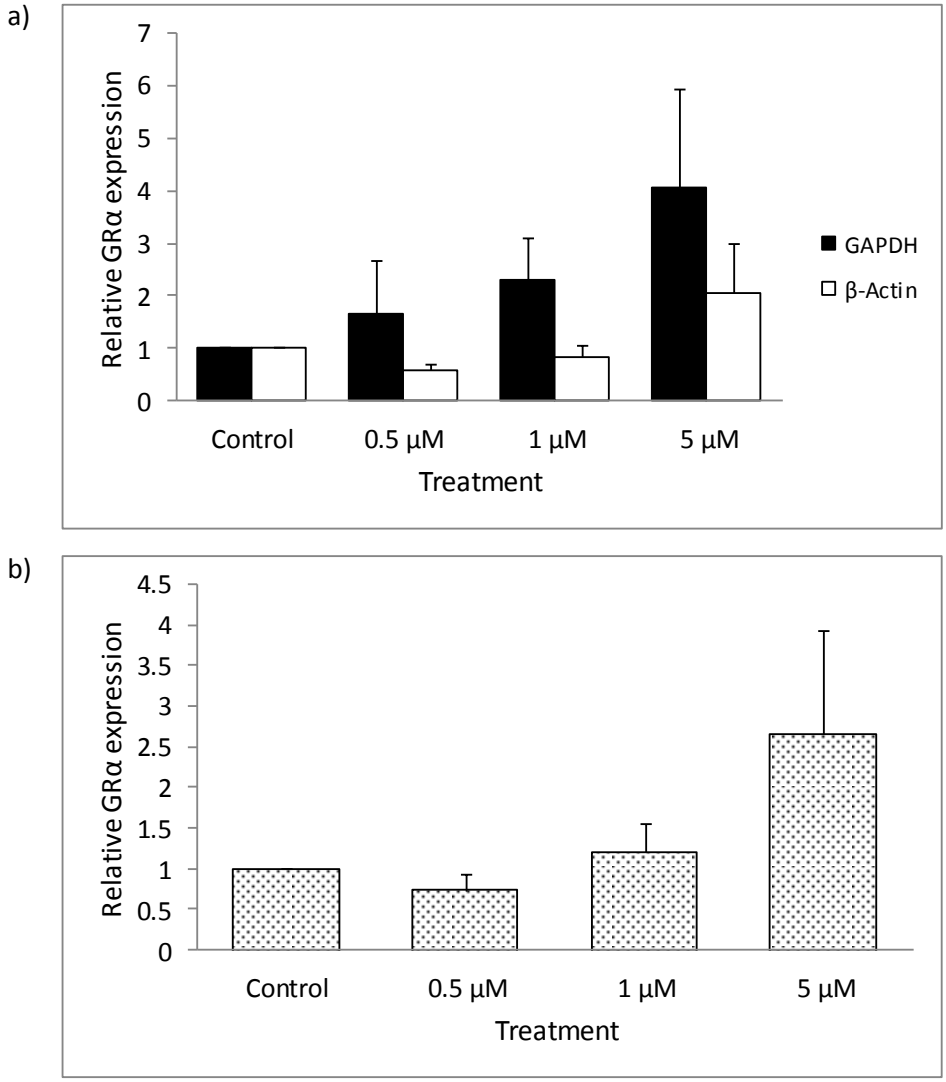

Figure 3.5. The relative GRα expression in A549 cells standardised to (a) GAPDH and β-actin, and (b) the geometric mean of GAPDH and β-actin following 72 h of 5-aza treatment. qPCR was conducted using EvaGreen. The mean ± SEM is displayed (n = 3). These data represent the mean fold change in GRα expression across biological repeats 2 and 3.

Using EvaGreen, no significant changes in GRα expression were seen in A549 cells following 72 h of treatment with 5-aza (Fig. 3.5a and 3.5b). With reference to GAPDH, the expression of GRα appeared to increase in relation to increasing 5-aza concentrations (Fig. 3.5a). Conversely small down-regulations in GRα expression were observed with 0.5 µM and 1 µM 5-aza, with reference to β-actin (Fig. 3.5a). GRα showed a minor increase in response to 5 µM 5-aza, but not significantly more than the control. A similar effect was seen when GRα was compared to the geometric mean (Vandesompele *et al.*, 2002) of GAPDH and β-actin, with GRα expression increasing in relation to increasing concentrations of 5-aza (Fig. 3.5b). None of the statistical tests reached significance. As no significant changes in GRα expression were seen when qPCR was conducted using either SYBR Green or EvaGreen, it can be concluded that the A549 cell line was suitable as a control.

3.2.2. Treatment with 5-aza had no effect on GRα mRNA expression in HEK cells

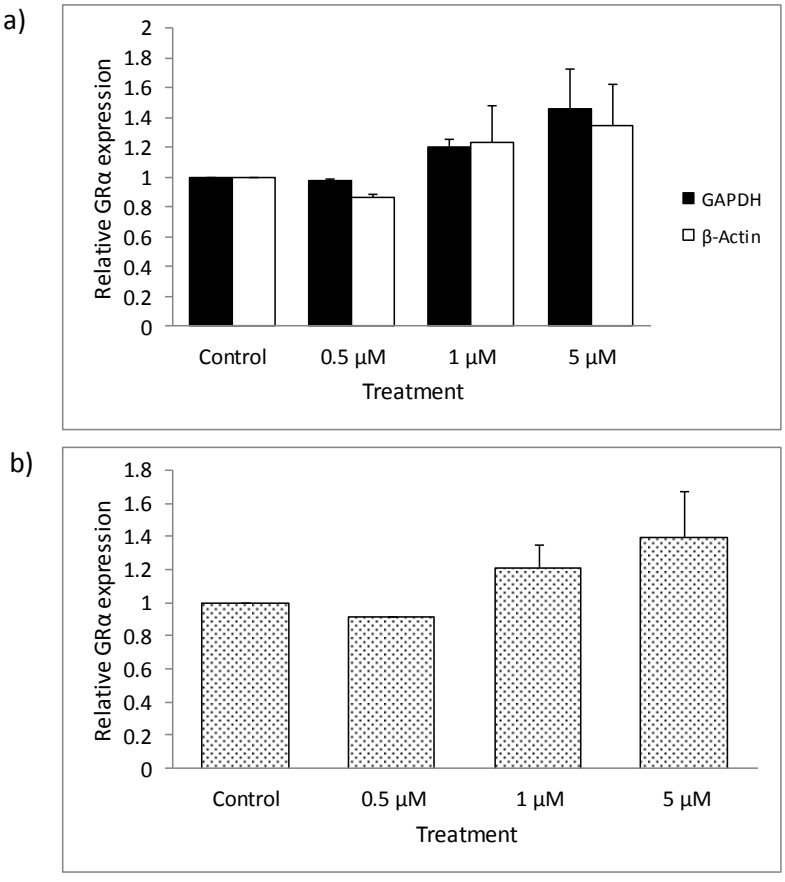

Figure 3.6. The relative fold change in GRα expression in GR deficient HEK cells following 72 h 5-aza treatments. GRα was standardised to (a) GAPDH and β-actin and, (b) the geometric mean of GAPDH and β-actin. qPCR was conducted using SYBR Green. The mean ± SEM is displayed (n = 3). These data represent the mean GRα expression across two biological repeats using HEK cells.

All qPCR gene expression analyses on HEK cells were performed using SYBR Green. Only minor changes in GRα expression were observed in the HEK cells following 72 h of treatment with 5-aza (Fig. 3.6a and Fig. 3.6b). In comparison to both GAPDH and β-actin, 0.5 µM 5-aza caused slight decreases in GRα expression relative to the control (Fig. 3.6a). 1 µM 5-aza effected minor increases in GRα expression with reference to GAPDH and β-actin (Fig. 3.6a). An up-regulation in GRα expression was also seen with 5 µM 5-aza, standardised to GAPDH and β-actin (Fig. 3.6a). GRα expression relative to the geometric mean (Vandesompele *et al.*, 2002) of the two reference genes (Fig. 3.6b) displayed the same effect as was observed when GRα expression was compared to GAPDH and β-actin individually. No changes in GRα expression following 5-aza treatment were statistically significant. Therefore methylation of the GR promoter is not the reason for reduced GR expression in HEK cells. This is consistent with the findings of Kay *et al.* (2011). Moreover as the GR is not methylated, HEK cells are a suitable control cell line.

3.2.3. Treatment with 5-aza had variable effects on GRα mRNA expression in DMS 79 cells

3.2.3.1. Using EvaGreen, 5-aza had no effect on GRα mRNA expression in DMS 79 cells

a)

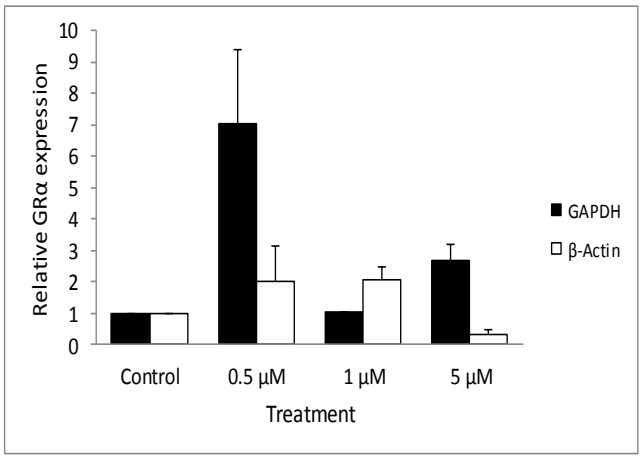

b)

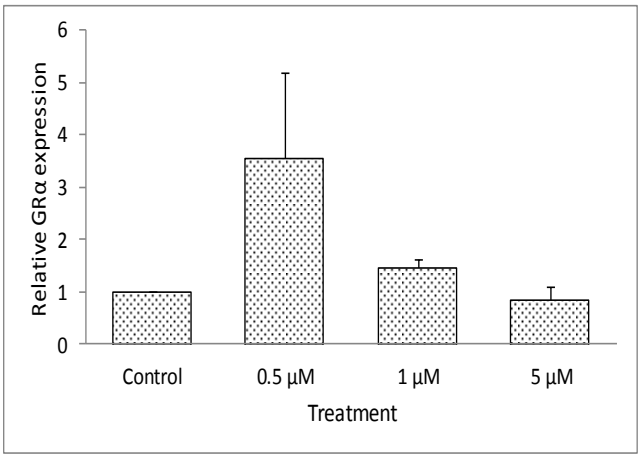

Figure 3.7. The relative fold change in GRα expression in GR deficient DMS 79 cells in response to 5-aza treatments for 72 h. GRα was normalised to (a) GAPDH and β-actin and, (b) the geometric mean of GAPDH and β-actin. qPCR was conducted using EvaGreen. The mean ± SEM is displayed (n = 3). These data represent the first biological repeat.

If the loss of GR expression in DMS 79 cells resulted from DNA methylation, perhaps consequent or as a prelude to carcinogenesis, GR expression would be predicted to increase

following reversal of methylation (Kay *et al.*, 2011). qPCR was performed on the DMS 79 cells using both EvaGreen and SYBR Green. With EvaGreen, variable changes in GRα expression were seen after 72 h of treatment with 5-aza. GRα expression normalised to GAPDH (Fig. 3.7a) differed between the control, 0.5 µM, 1 µM and 5 µM 5-aza treatments (p = 0.045). A relatively large up-regulation in GRα expression normalised to GAPDH was seen in response to 0.5 µM (Fig. 3.7a), although this was not significant relative to the control. 1 µM and 5 µM 5-aza produced insignificant down-regulation and up-regulation of GRα expression, respectively (Fig. 3.7a).

With reference to β-actin, minor increases in GRα expression were observed in response to 0.5 µM and 1 µM 5-aza (Fig. 3.7a), although these increases were not significantly greater than the control. In contrast, GRα expression was down-regulated by 5 µM 5-aza, but this was not significant relative to the control (Fig. 3.7a). Expression of GRα standardised to the geometric mean of GAPDH and β-actin showed that GRα expression was up-regulated by 0.5 µM and 1 µM 5-aza, although 0.5 µM 5-aza affected a greater increase than the 1 µM treatment (Fig. 3.7b). None of these increases in GRα expression were significant relative to the control. 5 µM 5-Aza down-regulated GRα expression (Fig. 3.7b), although not significantly. Therefore using EvaGreen, 5-aza had no effect on GRα mRNA expression in DMS 79 cells.

3.2.3.2. Using SYBR Green, 5-aza reduced GRα mRNA expression in DMS 79 cells

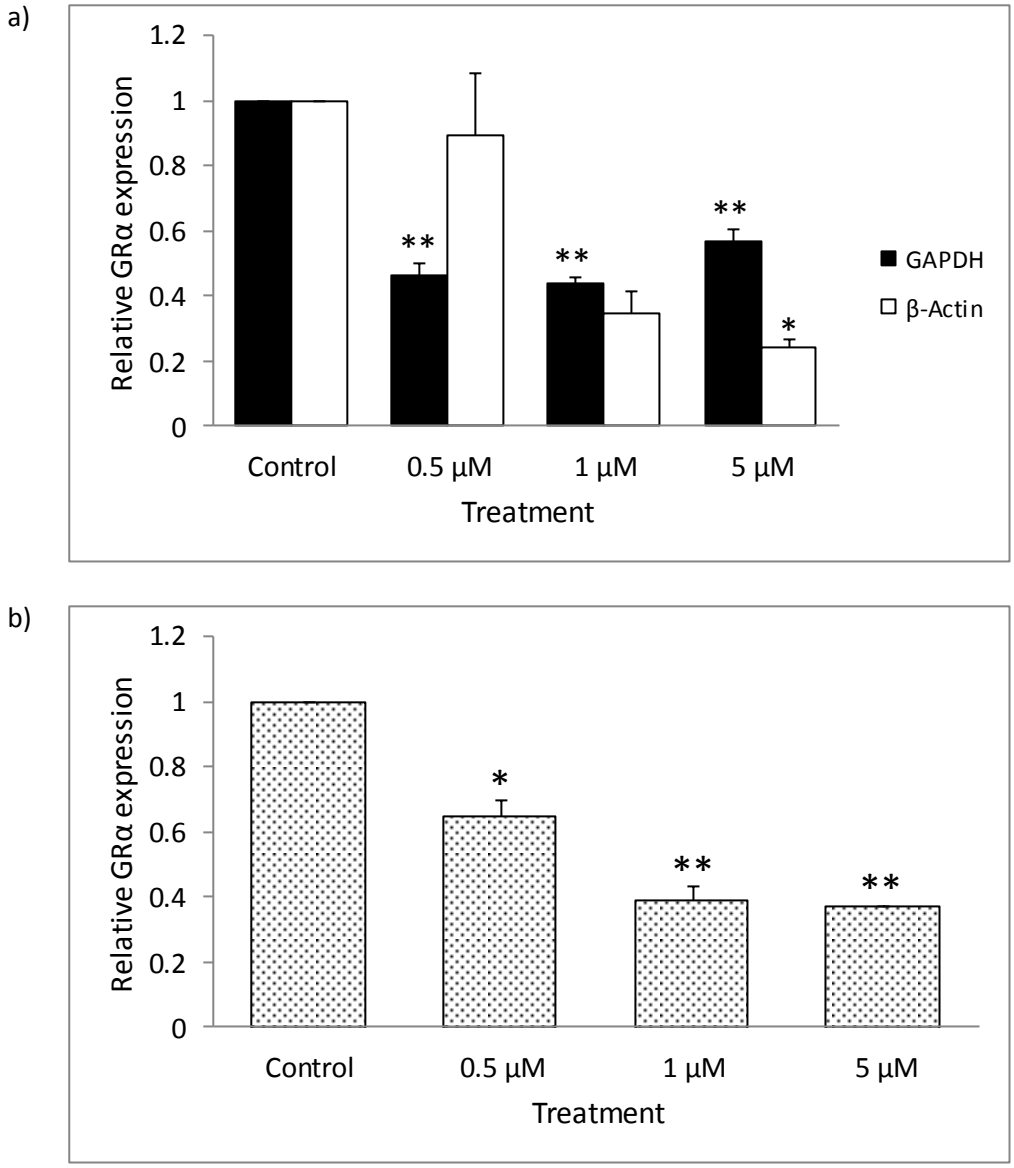

Figure 3.8. The relative GRα expression in DMS 79 cells standardised to (a) GAPDH ($p < 0.0005$) and β-actin ($p = 0.013$), and (b) the geometric mean of GAPDH and β-actin ($p < 0.0005$) following 72 h of 5-aza treatment. qPCR was conducted using SYBR Green. The mean ± SEM is displayed (n = 3). * indicates $p < 0.05$ and ** indicates $p < 0.005$ compared to vehicle-treated control. These data represent the second biological repeat.

Using SYBR Green, qPCR performed with the DMS 79 cells showed that GRα expression decreased in response to 72 h of treatment with 5-aza (Fig. 3.8a and Fig. 3.8b). GRα expression normalised to GAPDH was different in the control, 0.5 µM, 1 µM and 5 µM 5-aza treatments ($p < 0.0005$) (Fig. 3.8a). 0.5 µM 5-Aza cause a significant down-regulation in GRα expression

relative to the control (p = 0.001) (Fig. 3.8a). Expression of GRα was also significantly decreased relative to the control by 1 µM (p = 0.001) and 5 µM (p = 0.002) 5-aza (Fig. 3.8a).

Expression of GRα varied between the control, 0.5 µM, 1 µM and 5 µM 5-aza treatments (p = 0.013) when GRα expression was standardised to β-actin (Fig. 3.8a). A slight reduction in GRα expression was seen in response to 0.5 µM 5-aza (Fig. 3.8a), although this was not significantly less than the control. An insignificant decrease in GRα expression was also seen to be produced by 1 µM 5-aza (Fig. 3.8a). 5 µM 5-Aza significantly down-regulated GRα expression, relative to the control (p = 0.036) (Fig. 3.8a).

GRα expression normalised to the geometric mean of GAPDH and β-actin (Fig. 3.8b) was different in the control, 0.5 µM, 1 µM and 5 µM 5-aza treatments (p < 0.0005). Fig. 3.8b showed that, normalised to the geometric mean of the two reference genes, GRα expression was significantly reduced by 0.5 µM (p = 0.010), 1 µM (p = 0.001) and 5 µM (p = 0.001) 5-aza, relative to the control. Therefore using SYBR Green, 5-aza reduced GRα mRNA expression in DMS 79 cells.

3.2.3.3. Treatment with fresh 5-aza lead to massive re-expression of GRα mRNA in DMS 79 cells

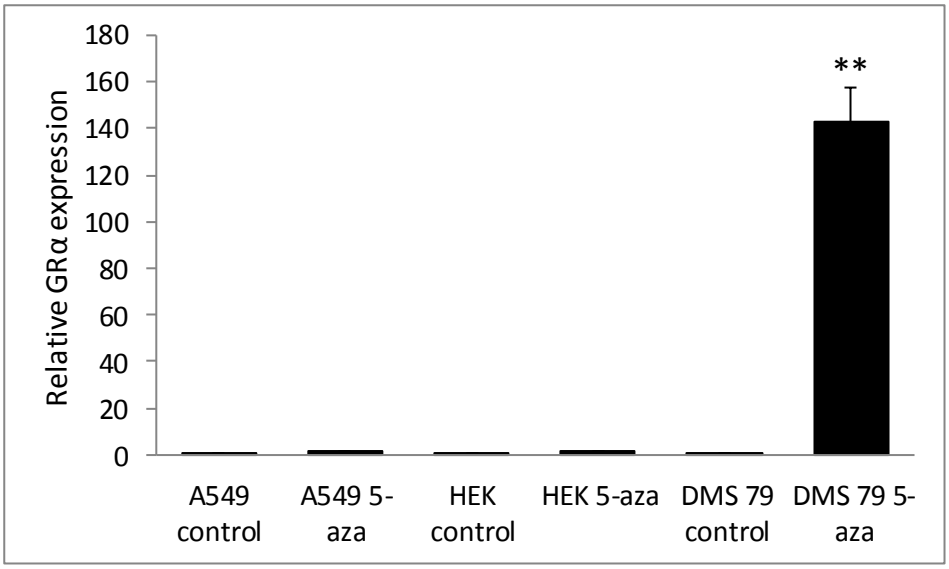

Figure 3.9. The relative fold change in GRα expression in A549, HEK and DMS 79 cells normalised to GAPDH. The cell lines were treated with 0.5 µM 5-aza for 72 h. qPCR was conducted using SYBR Green. The mean ± SEM is displayed (n = 3). ** indicates p < 0.005 compared to vehicle-treated control.

Previous to the experiment described in 3.2.1, 3.2.2 and 3.2.3, qPCR was performed on A549, HEK and DMS 79 cells using newly purchased and freshly prepared 5-aza. Following RNA extraction, cDNA was synthesized using the High Capacity RNA-to-cDNA Master Mix. qPCR was then performed using SYBR Green. GAPDH was the only reference gene used.

No change in GRα expression was observed in the A549 cells after treatment with 0.5 µM 5-aza (Fig. 3.9). In addition, treatment with 5-aza did not produce a change in GRα expression in the HEK cells either (Fig. 3.9). However in the DMS 79 cells, 5-aza produced massive GRα re-expression in comparison to the control ($p < 0.0005$) (Fig. 3.9). Thus, here, treatment with fresh 5-aza lead to massive re-expression of GRα mRNA in DMS 79 cells.

3.3. GRα protein expression

Western blots were performed to establish whether GRα mRNA transcribed as a result of possible demethylation of the GR promoter, was translated into protein. The DMS 79, HEK and A549 cells were treated with either vehicle control, 0.5 µM, 1 µM or 5 µM 5-aza for 72 h. Protein was extracted and run on a 13.5% SDS PAGE gel, then transferred onto a nitrocellulose membrane. The membrane was probed with primary monoclonal antibody specific for human GRα protein or GAPDH, and subsequently probed with a secondary HRP antibody. The effect of 5-aza on GRα protein expression was determined.

3.3.1. Treatment with 5-aza negatively affected GRα protein expression in A549 cells

3.3.1.1. Presence of the GRα protein in A549 cells

The Western blot of GRα protein and GAPDH protein in A549 cells is shown in Fig. 3.10. Two distinct GRα bands were seen at ~94 kDa and above 72 kDa (Fig. 3.10). These represent the two GRα isoforms found in A549 cells.

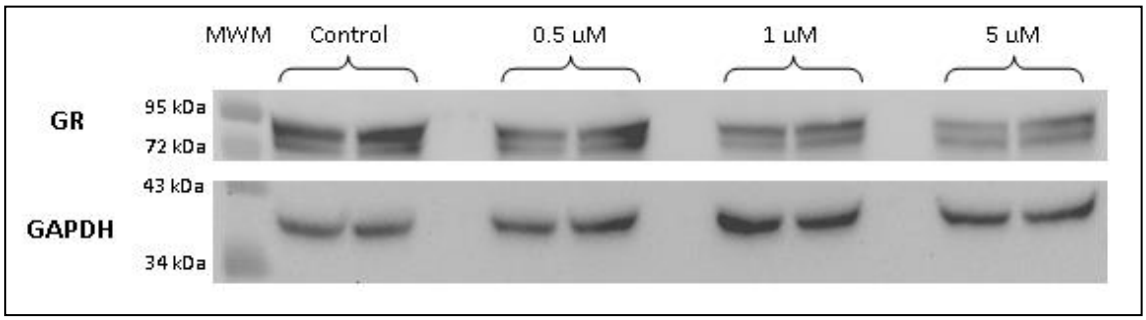

Figure 3.10. Western blot image of protein from A549 cells treated with either vehicle control, 0.5 µM, 1 µM or 5 µM 5-aza for 72 h.

3.3.1.2. Effect of 5-aza on GRα protein expression in A549 cells

Densitometry was carried out on the western blot image to quantitate band intensity. Band intensity is illustrative of GRα protein expression. The total GRα protein expression in the A549 cell line varied between the vehicle control, 0.5 µM, 1 µM and 5 µM 5-aza treatments (p = 0.023) (Fig. 3.11). Reductions in GRα protein expression were seen in response to all concentrations of 5-aza treatment, relative to the control (Fig. 3.11). However only 1 µM 5-aza significantly down-regulated GRα protein expression (p = 0.042) (Fig. 3.11). Hence, treatment with 5-aza negatively affected GRα protein expression in A549 cells.

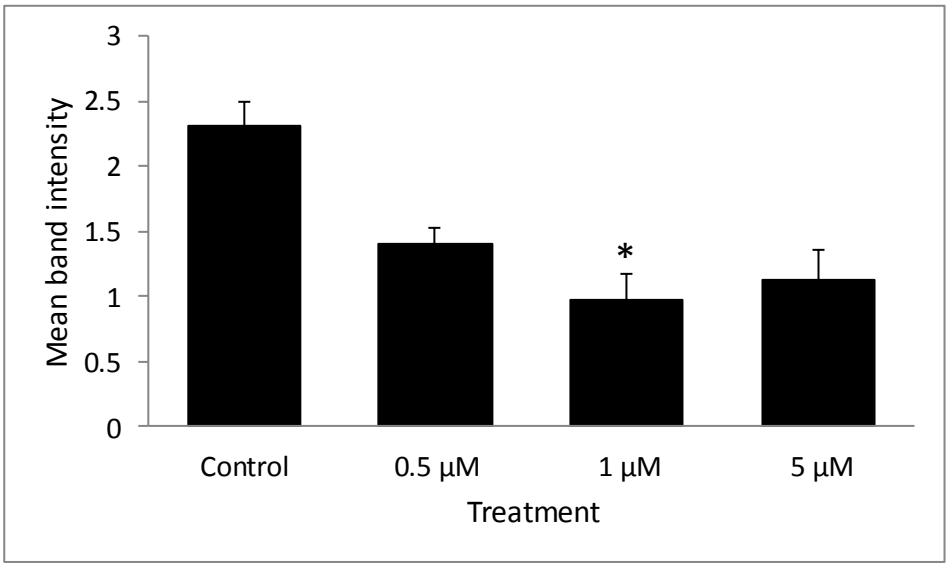

Figure 3.11. Densitometric analysis of the total GRα protein relative to GAPDH in A549 cells. The mean ± SEM is displayed (n = 2; p = 0.023). * indicates p <0.05 compared to vehicle-treated control.

3.3.2. Treatment with 5-aza negatively affected GRα protein expression in HEK cells

3.3.2.1. Presence of the GRα protein in HEK cells

The Western blot of GRα and GAPDH proteins in HEK cells is shown in Fig. 3.12. Three bands/isoforms were present at ~94 kDa, ~91 kDa and ~78 kDa in the HEK cells where the GRα protein is located (Fig. 3.12).

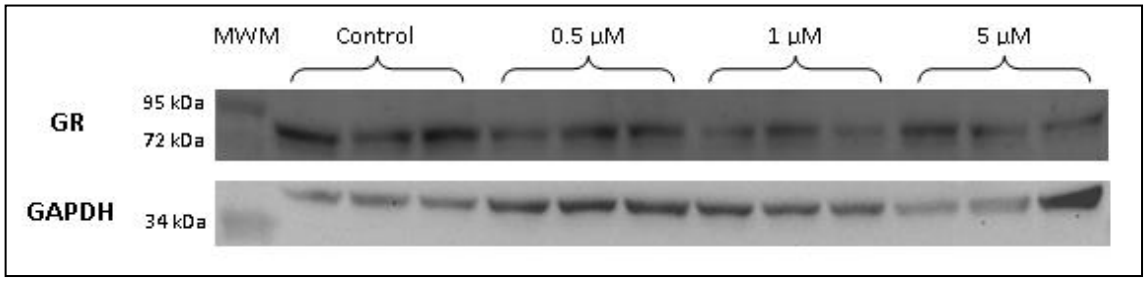

Figure 3.12. Western blot image of protein from HEK cells treated with either vehicle control, 0.5 µM, 1 µM or 5 µM 5-aza for 72 h.

3.3.2.2. Effect of 5-aza on GRα protein expression in HEK cells

Densitometry was performed on the Western blot images to quantitate band intensity. There was a significant difference in total GRα protein expression in the HEK cells between the vehicle control, 0.5 µM, 1 µM and 5 µM 5-aza treatments (p = 0.003) (Fig. 3.13). Down-regulations in GRα protein expression were observed in response to 0.5 µM, 1 µM and 5 µM 5-aza (Fig. 3.13). However only the 0.5 µM treatment (p = 0.006) and 1 µM treatment (p = 0.005) produced a significant reduction in GRα expression relative to the control (Fig. 3.13). Therefore treatment with 5-aza negatively affected GRα protein expression in HEK cells.

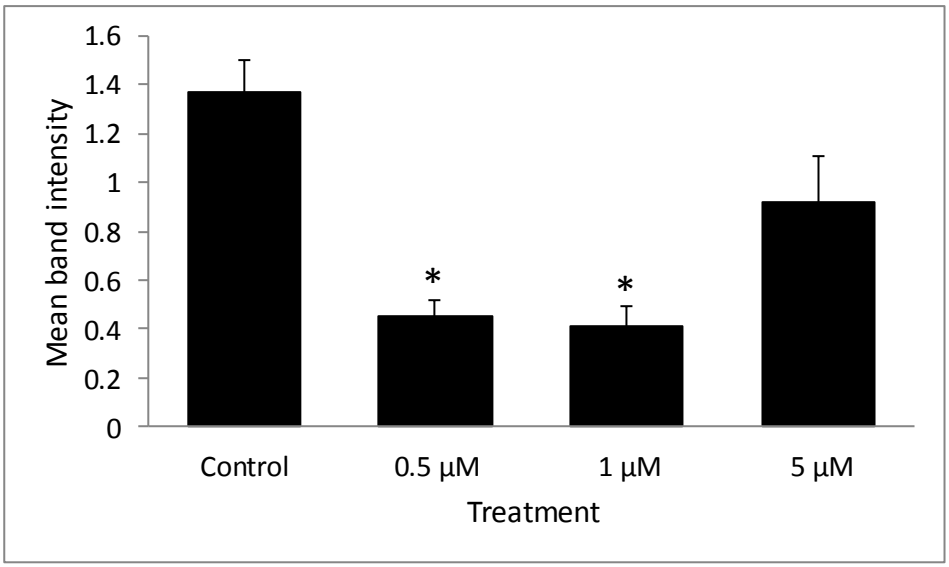

Figure 3.13. Densitometric analysis of the total GRα protein relative to GAPDH in HEK cells. The mean ± SEM is displayed (n = 3; p = 0.003). * indicates p <0.05 compared to vehicle-treated control.

3.3.3. Treatment with 5-aza had no effect on GRα protein expression in DMS 79 cells

3.3.3.1. Presence of the GRα protein in DMS 79 cells

The Western blots of GRα and GAPDH proteins in DMS 79 cells are shown in Fig. 3.14a and Fig. 3.14b. Four GRα bands were seen between 95 kDa and 55 kDa at ~94 kDa, ~91 kDa and two at ~78 kDa. These represent the four GRα isoforms found in DMS 79 cells (Fig. 3.14a and Fig. 3.14b).

a)

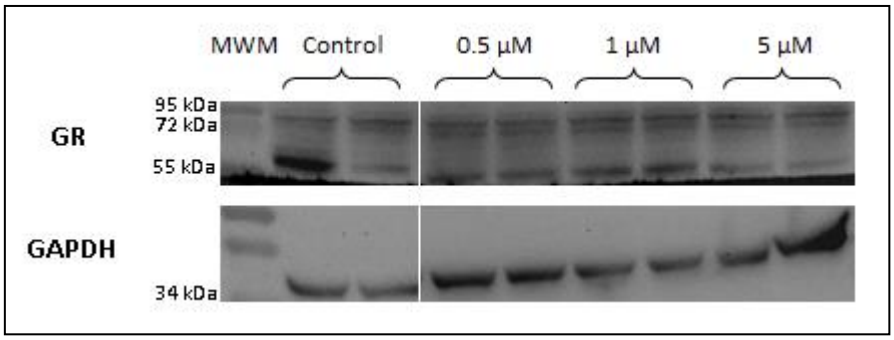

b)

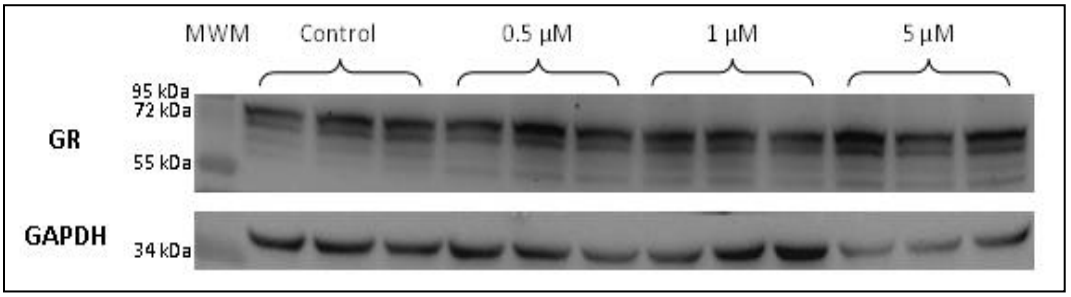

Figure 3.14. Western blot image of protein from DMS 79 cells treated with either vehicle control, 0.5 µM, 1 µM or 5 µM 5-aza for 72 h. (a) Represents the first biological repeat, whereas (b) represents the second biological repeat.

3.3.3.2. Effect of 5-aza on GRα protein expression in DMS 79 cells

Densitometry was carried out on the Western blot images to quantitate band intensity. In Fig. 3.15a, small increases in GRα protein expression were seen following treatment with 1 µM and 5 µM 5-aza. These increases however were not significant. There were also no significant differences in total GRα protein expression in the DMS 79 cells between the vehicle control, 0.5 µM, 1 µM and 5 µM 5-aza treatments (Fig. 3.15a).

There were no significant differences in total GRα protein expression in the DMS 79 cells between the vehicle control, 0.5 µM, 1 µM and 5 µM 5-aza (Fig. 3.15b). A minor decrease in

GRα protein expression was seen in response to treatment with 1 µM 5-aza, although it was not significant. In contrast, 0.5 µM and 5 µM 5-aza produced small increases in GRα protein expression. These changes were also not significant relative to the control. Treatment with 5-aza therefore had no effect on GRα protein expression in DMS 79 cells.

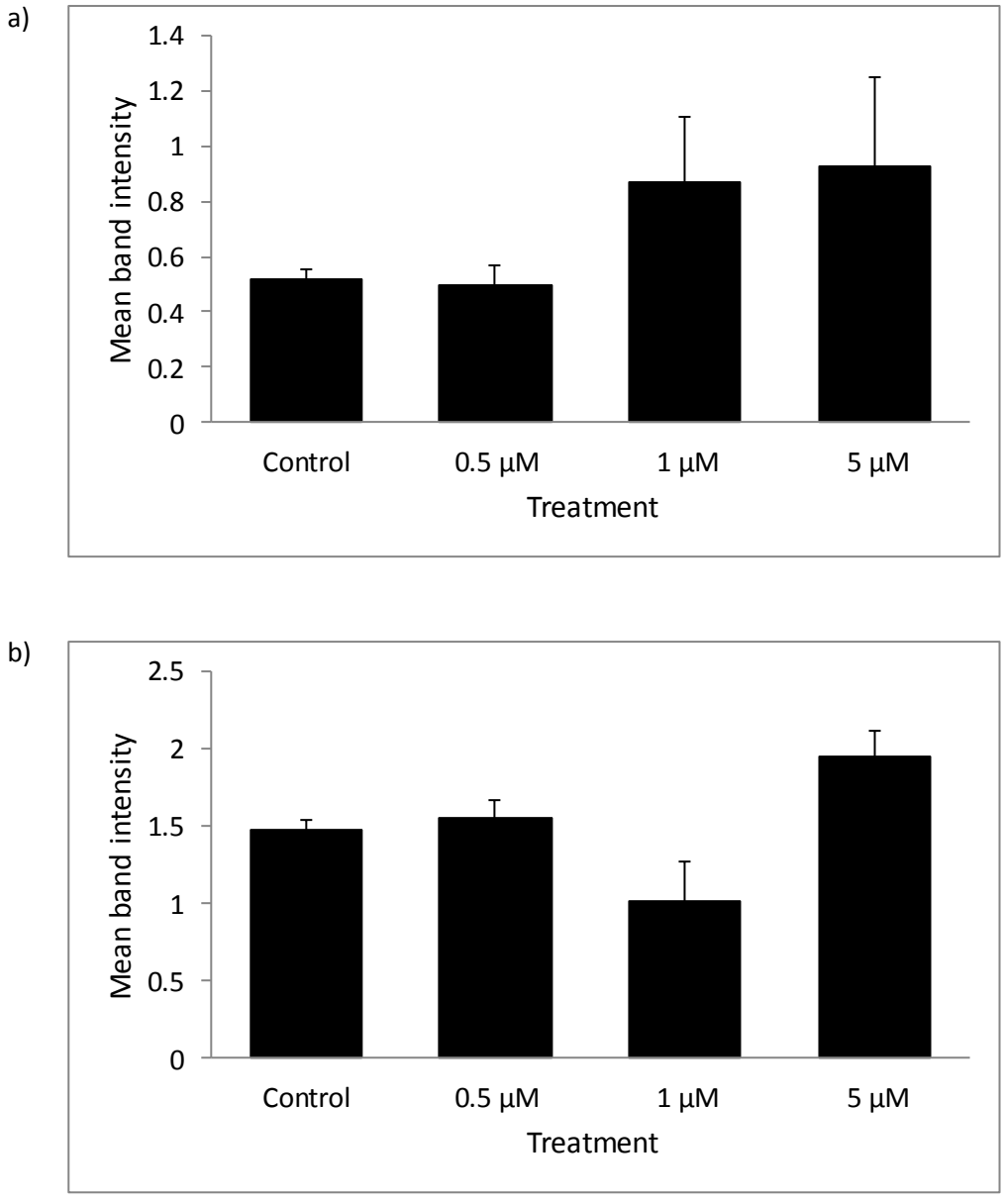

Figure 3.15. Densitometric analysis of the total GRα protein relative to GAPDH in DMS 79 cells. The mean ± SEM is displayed. (a) Represents the first biological repeat (n = 2), whereas (b) represents the second biological repeat (n = 3).

3.4. Cell viability

5-Aza displays considerable cytotoxic effects (Christman, 2002). This presents a problem in interpreting laboratory data as it is frequently unclear whether the effects on gene expression related to inhibitor treatment are due to cytotoxicity or DNA demethylation (Lyko and Brown, 2005). The CellTiter 96® AQ_{ueous} One Solution Cell Proliferation Assay was performed to establish whether the toxic effects of 5-aza affected cell viability.

This cell viability assay is a colorimetric method for determining the number of viable cells. The CellTiter 96® AQ_{ueous} One Solution Reagent contains a tetrazolium compound, inner salt (MTS) and an electron coupling reagent which combines with MTS to form a stable solution. Cells bioreduce the MTS tetrazolium compound (also known as Owen's reagent) into a coloured formazan product. The quantity of formazan product as measured by the absorbance at 490nm is directly proportional to the number of living/viable cells in culture.

The DMS 79, HEK and A549 cells were seeded into a 96-well plate at a density of 5 x 10^3 cells/100 µL. Six replicates per treatment were performed for each cell line. Cells were treated with either vehicle, 0.5 µM, 1 µM or 5 µM 5-aza for a total of 72 h. An untreated control was also included for each cell line.

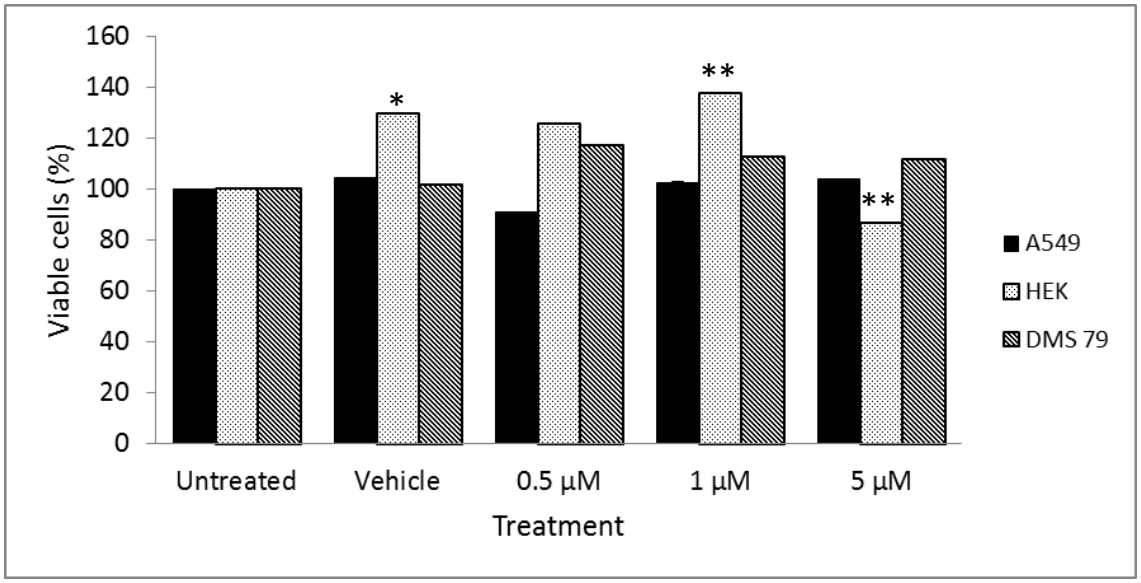

Figure 3.16. Absorbance of formazan product of A549, HEK and DMS 79 cells, normalised to percentages of the respective untreated samples. The cells were left untreated or exposed to 0.5 µM, 1 µM and 5 µM 5-aza, or vehicle, for a total of 72 h. The mean ± SEM is displayed (n = 6). * indicates $p < 0.05$; ** indicates $p < 0.005$.

3.4.1. Treatment with 5-aza had no effect on the viability of A549 cells

Slight changes in A549 cell viability were observed following treatment with vehicle control, 0.5 µM, 1 µM and 5 µM 5-aza (Fig. 3.16). The vehicle control, 1 µM and 5 µM 5-aza affected negligible increases in the number of living A549 cells relative to the untreated sample (Fig. 3.16). Slightly more viable cells were seen in the 1 µM and 5 µM 5-aza treatments compared to the vehicle control (Fig. 3.16). A minor decrease in the number of viable cells was seen with 0.5 µM 5-aza, relative to both the untreated sample and vehicle-treated cells (Fig. 3.16). None of the changes in A549 cell viability were significant. Treatment with 5-aza therefore did not affect the viability of the A549 cells.

3.4.2. Treatment with 5-aza had minimal effect on the viability of HEK cells

The viability of the HEK cells is different in the untreated control, vehicle control, 0.5 µM, 1 µM and 5 µM 5-aza treatments ($p < 0.0005$) (Fig. 3.16). There are a slightly greater number of viable cells in the vehicle control, 0.5 µM and 1 µM treatments, relative to the untreated sample (Fig. 3.16). The increased cell viability is significant in the vehicle control ($p = 0.029$) and 1 µM 5-aza ($p = 0.003$) treatments in comparison to the untreated sample (Fig. 3.16). Less viable cells were observed in the 5 µM 5-aza treatment relative to the untreated sample, but this was not significant (Fig. 3.16). However, there were significantly less viable cells in the 5 µM 5-aza treatment relative to the vehicle control ($p = 0.001$) (Fig. 3.16). Treatment with 5-aza had only a minimal effect on the viability of HEK cells.

3.4.3. Treatment with 5-aza had no effect on the viability of DMS 79 cells

Marginally more viable cells were seen with the 0.5 µM, 1 µM and 5 µM 5-aza samples in comparison to both the untreated sample and vehicle-treated cells (Fig. 3.16). A miniscule increase in the number of viable cells was observed with the vehicle control treatment, relative to the untreated cells (Fig. 3.16). None of the statistical tests on DMS 79 cell viability reached significance. Treatment with 5-aza therefore had no effect on the viability of DMS 79 cells.

3.5. Apoptosis and cell death

Loss of plasma membrane asymmetry is one of the earliest features of apoptosis. When cells commit to apoptosis their membranes involute, exposing the membrane phospholipid phosphatidylserine (PS) to the external cellular environment (Kerr *et al.*, 1994). Annexin V is a

calcium-dependent phospholipid-binding protein that has a high affinity for PS. Annexin V may be conjugated to fluorochromes such as FITC. FITC Annexin V binds to PS molecules, serving as a marker for early apoptosis. It is thereby used to quantitatively determine the percentage of cells within a population that are actively undergoing apoptosis (Lu *et al.*, 2007).

Propidium iodide (PI) is a standard flow cytometric dye used to distinguish viable from nonviable cells. Viable cells with intact membranes exclude PI, whereas the membranes of dead and damaged cells are permeable to PI. PI stains DNA, which is only accessible if the cell has ruptured i.e. is dead. Cells that stain positive for FITC Annexin V and negative for PI are in the process of apoptosing. Cells that stain positive for both FITC Annexin V and PI are either in the end stage of apoptosis, are undergoing necrosis, or are already dead. Cells that do not stain with FITC Annexin V and PI are alive and not undergoing measurable apoptosis.

Furthermore, condensation of the chromatin is one of the earliest recognised morphologic changes characteristic of apoptosis. It is accompanied by compaction of the cytoplasm, followed by convolution of the nuclear envelope and cell membrane. The early processes of apoptosis are distinctive, and chromatin condensation is commonly used to identify cells in early stage apoptosis (Kerr *et al.*, 1994).

To determine whether re-expression of endogenous GR induced apoptosis, the cells were stained with FITC Annexin V. Cells were stained with PI to establish whether endogenous re-expression of the GR resulted in cell death.

The DMS 79 and HEK cells were either untreated, or treated with either vehicle, 0.5 µM, 1 µM and 5 µM 5-aza for 72 h. The cells were subsequently prepared for flow cytometry by creating single cell suspensions and then stained with FITC Annexin V and PI. For microscopy, cells were stained with DAPI in addition to FITC Annexin V and PI, to identify whether the cells were in early stage apoptosis.

3.5.1. Overall, treatment with 5-aza induced negligible apoptosis and cell death of HEK cells

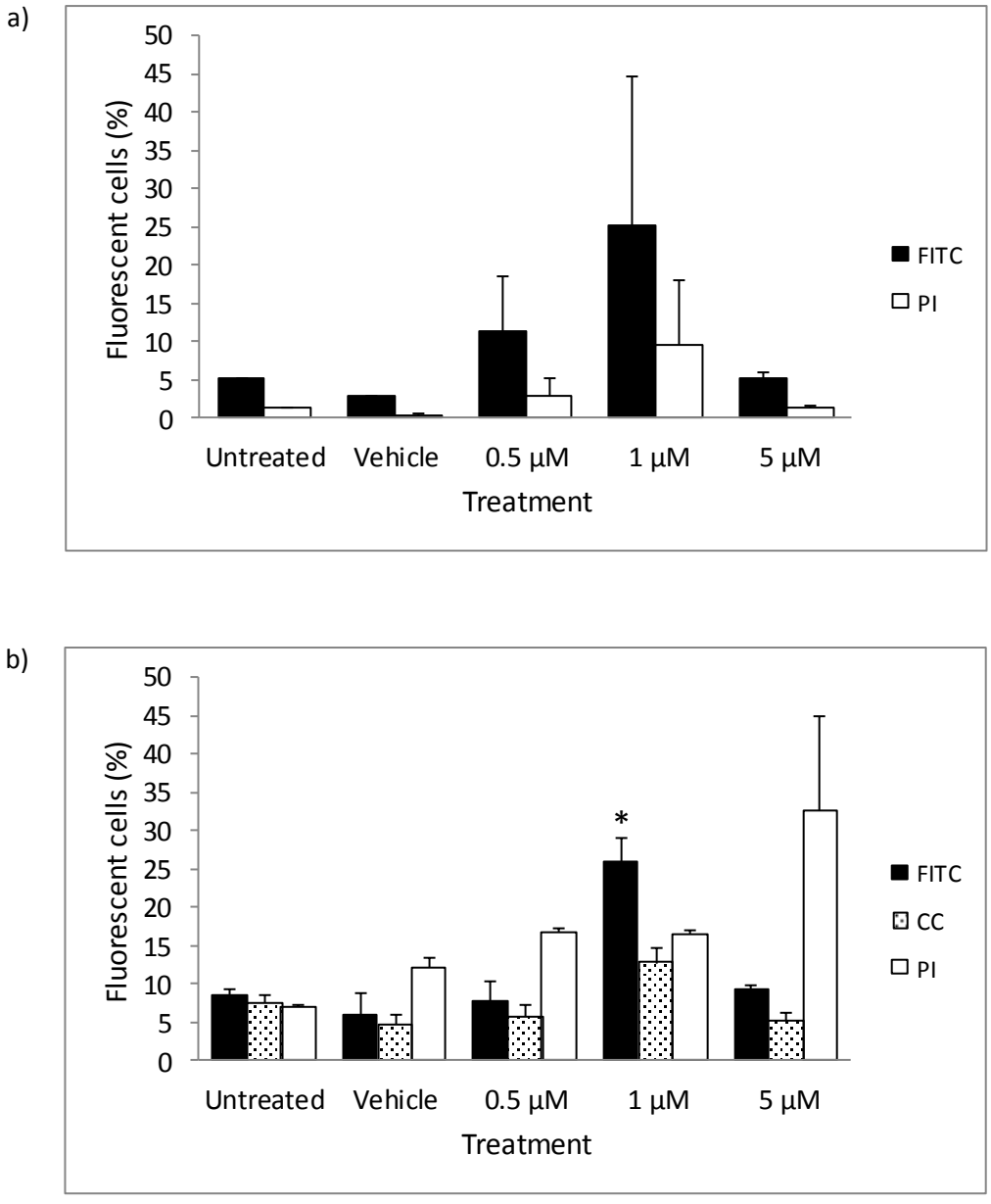

Figure 3.17. Treatment with 5-aza resulted in negligible apoptosis and cell death of HEK cells. The HEK cell line was treated with various concentrations of 5-aza for 72 h, or treated with vehicle, or left untreated. Cells were then analysed by (a) flow cytometry for viability by PI, and apoptosis by FITC Annexin V and (b) microscopy for FITC Annexin V, PI, and DAPI to visualise condensed chromatin. The percentage of FITC Annexin V positive, PI positive, and cells with chromatin condensation were established in the cells subsequent to treatment. The mean of two biological repeats ± SEM is displayed (n = 2). * indicates $p < 0.05$. CC – condensed chromatin.

The HEK cells were stained with FITC Annexin V, a marker of early apoptosis. With flow cytometry, a greater number of HEK cells treated with 0.5 µM (11.25%) and 1 µM (25.15%) 5-aza were in the process of apoptosis, relative to both the untreated control and vehicle control (Fig. 3.17a). Cells exposed to 5 µM 5-aza (5.22%) were experiencing a similar amount of apoptosis as the untreated control (5.06%), but slightly greater apoptosis than the vehicle control (2.77%) (Fig. 3.17a). Treatment with 0.5 µM (11.25%) and 1 µM (25.15%) 5-aza induced more apoptosis than the 5 µM (5.22%) 5-aza treatment (Fig. 3.17a). Strangely, a greater proportion of cells in the untreated control (5.06%) stained positive for FITC Annexin V than cells in the vehicle control (2.77%) (Fig. 3.17a). None of the statistical tests reached significance, suggesting that 5-aza did not affect apoptosis of the HEK cells.

The samples were also stained with PI, a marker of cell death. As with the FITC Annexin V-stained samples, HEK cells exposed to 1 µM 5-aza showed the greatest proportion of cell death (9.57%) relative to both the untreated control (1.24%) and vehicle control (0.40%), whereas 5 µM 5-aza induced the least cell death in comparison to the controls (Fig. 3.17a). Treatment with 0.5 µM (2.82%) and 1 µM (9.57%) 5-aza induced greater cell death than the 5 µM (1.26%) 5-aza treatment (Fig. 3.17a). Strangely, there were more dead cells in the untreated control (1.24%) than the vehicle control (0.40%) (Fig. 3.17a). None of the statistical tests reached significance, indicating that 5-aza did not affect HEK cell death.

For all 5-aza treatments, a greater proportion of cells were undergoing apoptosis than cell death (Fig. 3.17a), but this was not significant. The flow cytometry quadrant dot plots are shown in Appendix E.

To determine whether the results obtained by flow cytometry were reliable and comparable, cells were treated with either vehicle, 0.5 µM, 1 µM or 5 µM 5-aza for 72 h as above. The samples were then analysed by microscopy instead of flow cytometry, and incorporated nuclear morphology. The proportion of FITC Annexin V positive and PI positive, as well as the number of cells with condensed chromatin were ascertained. DAPI stains the nucleus of a cell. If the chromatin is condensed, it may indicate that the cell is in the early stages of apoptosis.

Using microscopy, it was determined that the greatest proportion of apoptosis was induced by 1 μM (26.0%) 5-aza (Fig. 3.17b). The population of cells undergoing apoptosis was significantly more than both the untreated control (8.5%) (p = 0.022) and vehicle control (6.0%) (p = 0.012) (Fig. 3.17b). 0.5 μM (7.83%) 5-Aza induced more apoptosis than the vehicle control (6.0%), but not the untreated control (8.5%) (Fig. 3.17b). Treatment with 5 μM (9.34%) 5-aza showed a miniscule increase in the proportion of apoptosing cells relative to both of the controls (Fig. 3.17b).

As with apoptosis, the greatest number of cells displaying chromatin condensation were seen in the 1 μM 5-aza sample (12.84%) (Fig. 3.17b). However there were not significantly more cells in early stage apoptosis in the 1 μM (12.84%) 5-aza sample, relative to both the untreated control (7.67%) and vehicle control (4.67%) (Fig. 3.17b). Cells treated with 0.5 μM (5.67%) and 5 μM (5.17%) 5-aza had slightly bigger populations of cells with condensed chromatin than the vehicle control (4.67%), but not the untreated control (7.67%). None of the statistical tests reached significance, implying that treatment with 5-aza did not affect apoptosis of the HEK cells.

0.5 μM (16.67%), 1 μM (16.34%) and 5 μM (32.5%) 5-aza caused cell death, in comparison to both the untreated control (7.0%) and vehicle control (12.0%) (Fig. 3.17b). 5 μM 5-Aza induced the greatest cell death (32.5%), but this was not significantly more than the controls (Fig. 3.17b). As was expected, a greater proportion of dead cells were present in the vehicle-treated control (12.0%) than the untreated control (7.0%) (Fig. 3.17b). None of the statistical tests reached significance. This conveyed that 5-aza did not affect HEK cell death.

Both flow cytometry and microscopy showed no significant cell death. In addition, only 1 μM 5-aza induced apoptosis of the HEK cells, as determined by FITC Annexin V fluorescence using microscopy. No other significant apoptosis was detected using flow cytometry, or microscopy by either FITC Annexin V staining or nuclear morphology. Therefore in general, 5-aza induced negligible apoptosis and cell death in the HEK cells.

For representative microscopy images, see Appendix F.

3.5.2. In general, treatment with 5-aza induced apoptosis and cell death of DMS 79 cells

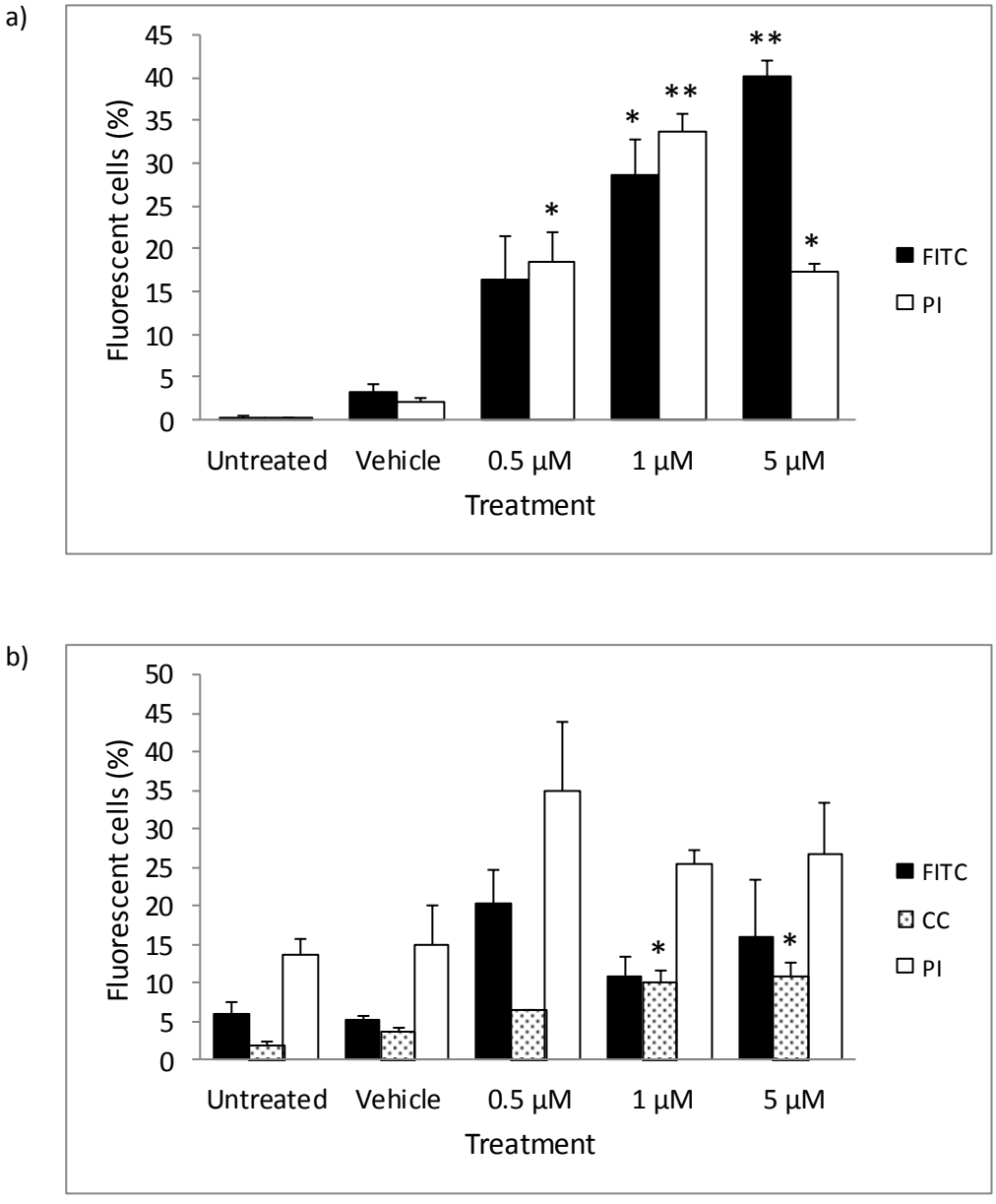

Figure 3.18. In general, treatment with 5-aza resulted apoptosis and cell death of DMS 79 cells. The DMS 79 cell line was treated with various concentrations of 5-aza for 72 h, or treated with vehicle, or left untreated. Cells were then analysed by (a) flow cytometry for viability by PI and apoptosis by FITC Annexin V, and (b) microscopy for FITC Annexin V, PI, and DAPI to visualise condensed chromatin. The percentage of FITC Annexin V positive, PI positive, and cells with chromatin condensation were established in the cells subsequent to treatment. The mean of two biological repeats ± SEM is displayed (n = 2). * indicates $p < 0.05$; ** indicates $p < 0.005$. CC – condensed chromatin.

FITC Annexin V was used to determine the mode of cell death. In contrast to the HEK cells, and as determined by flow cytometry, significant proportions of the DMS 79 cells stained positive for FITC Annexin V (p = 0.001) (Fig. 3.18a). The size of the cell populations in the process of apoptosis, increased with increasing 5-aza concentrations. 0.15% (untreated control), 3.24% (vehicle control), 16.31% (0.5 µM), 28.68% (1 µM) and 40.1% (5 µM) of the cell populations, respectively, committed to apoptosis (Fig. 3.18a). 0.5 µM 5-Aza did not induce a significant apoptosis (Fig. 3.18a). However, a significant percentage of the cells treated with 1 µM (p = 0.010) and 5 µM (p = 0.002) 5-aza were undergoing apoptosis, relative to the untreated control (Fig. 3.18a). Similarly, treatment with 1 µM (p = 0.017) and 5 µM (p = 0.003) 5-aza lead to significant apoptosis in comparison to the vehicle control (Fig. 3.18a).

Once again in contrast to the HEK cells, significant populations of the DMS 79 cells stained positive for PI (p < 0.0005) when the samples were analysed by flow cytometry (Fig. 3.18a). 0.1%, 2.05%, 18.37%, 33.7% and 17.3% of the untreated control, vehicle control, 0.5 µM, 1 µM and 5 µM 5-aza-treated populations respectively, were dead (Fig. 3.18a). With reference to the untreated control, treatment with 0.5 µM (p = 0.005), 1 µM (p < 0.0005) and 5 µM (p = 0.007) 5-aza caused significant DMS 79 cell death (Fig. 3.18a). In addition, 0.5 µM (p = 0.008), 1 µM (p < 0.0005) and 5 µM (p = 0.012) 5-aza also resulted in significant cell death in comparison to the vehicle-treated cells (Fig. 3.18a). The greatest amount of cell death was caused by 1 µM 5-aza (33.7%) (Fig. 3.18a). Therefore, treatment with 5-aza induced DMS 79 cell death.

Interestingly, the 0.5 µM and 1 µM 5-aza–treated DMS 79 cells had greater PI positive than FITC Annexin V positive populations (Fig. 3.18a). This was possibly a result of the stresses involved in preparation for flow cytometry, *viz.* the formation of single cell suspensions. Conversely, a greater proportion of the DMS 79 cells treated with 5 µM 5-aza stained positive for FITC Annexin V than PI (Fig. 3.18a).

With microscopy, a trend could be seen in each of the samples/treatments (Fig. 3.18b). In each sample, the greatest proportion of cells stained with PI, followed by FITC Annexin V, and the smallest proportion of cells displayed chromatin condensation (Fig. 3.18b). Treatment with 0.5 µM 5-aza (20.17%) resulted in the greatest population of cells that were FITC Annexin V positive, but this was not significant relative to the untreated control (5.88%) or vehicle control (5.17%) (Fig. 3.18b). The apoptosis caused by 1 µM (10.83%) and 5 µM (16.0%) 5-aza was

slightly less than that resulting from 0.5 µM (20.17%) 5-aza, and similarly not significant relative to the controls (Fig. 3.18b). Hence, treatment with 5-aza did not appear to induce apoptosis of DMS 79 cells when analysed for FITC Annexin V fluorescence, using microscopy.

The amount of cells with condensed chromatin varied across all treatments (p = 0.007) (Fig. 3.18b). Cells treated with 0.5 µM 5-aza (6.5%) had more cells with condensed chromatin than both the untreated control (1.83%) and vehicle control (3.67%). However this increase was not significantly greater than either control (Fig. 3.18b). In contrast to what was seen with FITC Annexin V fluorescence, the 1 µM (10.17%) 5-aza sample contained a significantly larger proportion of cells with condensed chromatin than the untreated control (1.83%) (p = 0.027) (Fig. 3.18b). In addition, the 5 µM (11.0%) sample contained significantly more cells with condensed chromatin than both the untreated control (1.83%) (p = 0.018) and vehicle control (3.67%) (p = 0.047) (Fig. 3.18b). According to microscopy on chromatin condensation, 1 µM and 5 µM 5-aza induced apoptosis of the DMS 79 cells.

The greatest quantity of cell death was also observed in the 0.5 µM 5-aza sample (34.84%) (Fig. 3.18b). In addition, more cell death was seen in the 1 µM (25.33%) and 5 µM (26.67%) 5-aza samples, relative to the untreated control (13.61%) and vehicle control (15.0%). However this increased cell death was not as much as that observed with 0.5 µM 5-aza, and also not significant (Fig. 3.18b). None of the statistical tests reached significance, suggesting that treatment with 5-aza did not cause DMS 79 cell death.

In general, flow cytometry showed that 5-aza treatment induced cell death and apoptosis of the DMS 79 cells. However microscopy showed that only 1 µM and 5 µM 5-aza induced apoptosis, but only when examined for chromatin condensation. This may be due to the limited number of cells that were analysed by microscopy. Taken together, these results indicate that treatment with 5-aza induced cell death and apoptosis of the DMS 79 cells.

For representative microscopy images, see Appendix F.

3.6. Pharmacological blockade

The pharmacological blockade on the HEK cells could only be investigated by microscopy due to problems accessing the flow cytometer. In addition, no images could be captured due to breakdown of the fluorescent microscope and camera. The HEK cells were counted live using the Nikon ECLIPSE E400 fluorescent microscope (as opposed to the Nikon ECLIPSE 80*i*). For representative microscopy images, see Appendix F.

3.6.1. Treatment with a GR agonist

To establish whether treatment with Dex, a synthetic Gc, can accelerate apoptosis (of the DMS 79 cells), cells were treated with Dex only as a control, or 5-aza and Dex together. For ease of comparison, 0.5 µM 5-aza data from previous experiments is included in these graphs.

3.6.1.1. In HEK cells, neither Dex, nor Dex and 5-aza significantly affected apoptosis; but 5-aza treatment enhanced cell death induced by Dex

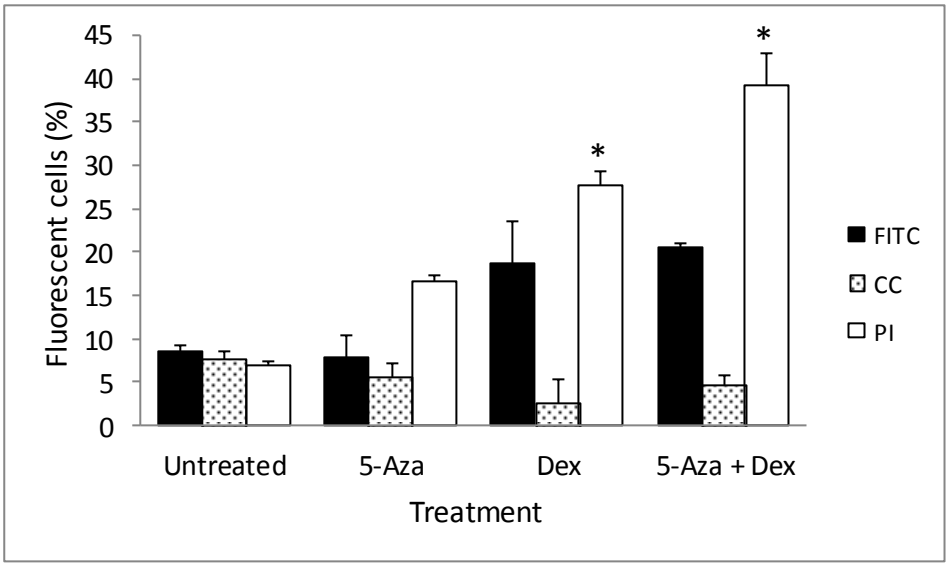

Figure 3.19. Treatment with neither Dex, nor Dex and 5-aza significantly affected apoptosis of HEK cells; but 5-aza amplified cell death induced by Dex. The HEK cell line was treated with 0.5 µM 5-aza for 72 h alone, or Dex was added for 24 h; or treated with Dex only for 24 h; or left untreated. Cells were then analysed using microscopy for viability by PI, apoptosis by FITC Annexin V, and DAPI to visualise condensed chromatin. The percentage of FITC Annexin V positive, PI positive, and cells with chromatin condensation were established subsequent to treatment. The mean of two biological repeats ± SEM is displayed (n = 2). CC – condensed chromatin.

The cells were treated with Dex to establish whether Dex could accelerate apoptosis. Strangely, there were slightly fewer FITC Annexin V positive HEK cells in the 5-aza sample (7.83%) than the untreated control (8.5%) (Fig. 3.19). More apoptotic cells were seen in the Dex (18.67%), and Dex and 5-aza (20.5%) samples, than the untreated control (8.5%) (Fig. 3.19). In contrast, smaller numbers of cells with condensed chromatin were observed in the Dex (2.67%), and Dex and 5-aza (4.67%) samples as well as the 5-aza only sample (5.67%), in comparison to the untreated control (7.67%) (Fig. 3.19). None of the statistical tests reached significance, suggesting that Dex treatment did not accelerate apoptosis of the HEK cells.

Large increases in the numbers of dead HEK cells were observed in response to treatment with both Dex only (27.67%), and Dex and 5-aza (39.17%), relative to the untreated control (7.0%) and the 5-aza treatment (16.67%) (Fig. 3.19). The cell death produced by Dex (p = 0.046), and Dex in combination with 5-aza (p = 0.005), was significant in comparison to the untreated control (Fig. 3.19). Furthermore, a significant increase in cell death was seen in the Dex and 5-aza treatment, relative to the 5-aza only treatment (p = 0.030) (only significance relative to the untreated control is displayed on the graph). As the GR is not methylated in HEK cells (Kay *et al.*, 2011), it is thought that Dex stimulated cell death in conjunction with genes that were re-expressed following 5-aza treatment.

3.6.1.2. In DMS 79 cells, 5-aza appeared to enhance cell death induced by Dex when analysed by flow cytometry; whereas microscopic analysis showed no significant effect on cell death

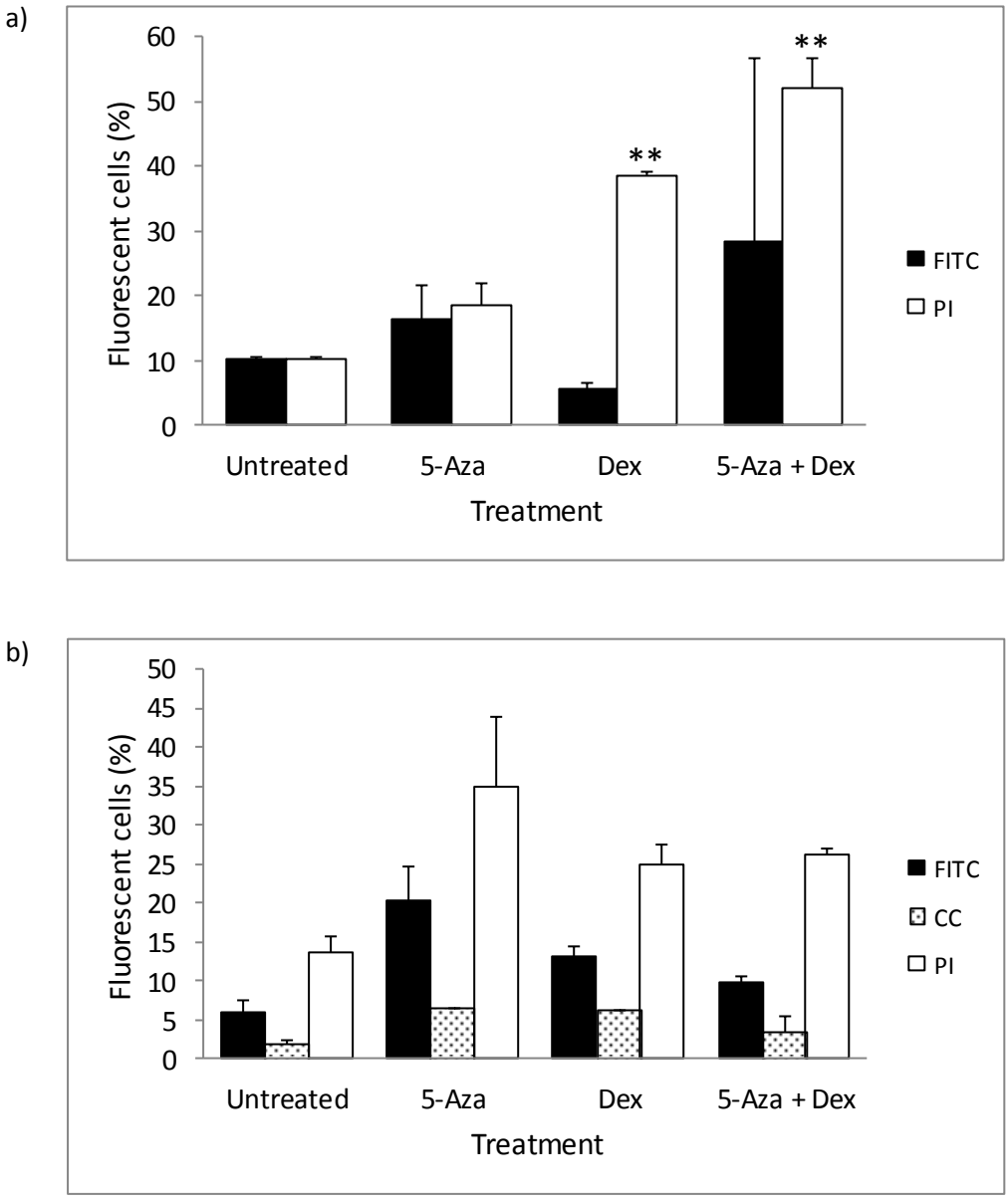

Figure 3.20. 5-Aza accelerated cell death induced by Dex in DMS 79 cells when analysed by flow cytometry, but not microscopy. The DMS 79 cell line was treated with 0.5 µM 5-aza for 72 h alone, or Dex was added for 24 h; or treated with Dex only for 24 h; or left untreated. Cells were then analysed by (a) flow cytometry for viability by PI, and apoptosis by FITC Annexin V and (b) microscopy for FITC Annexin V, PI, and DAPI to visualise condensed chromatin. The percentage of FITC Annexin V positive, PI positive, and cells with chromatin condensation were established subsequent to treatment. The mean of two biological repeats ± SEM is displayed (n = 2). CC – condensed chromatin.

To establish whether Gc action could accelerate apoptosis, the DMS 79 cells were treated with Dex. A reduced number of apoptotic cells were detected by flow cytometry in the Dex only sample (5.70%), relative to the untreated control (10.15%) (Fig. 3.20a). In contrast, a greater population of apoptotic cells was detected in the Dex and 5-aza sample (28.48%), in comparison to the untreated control (10.15%) (Fig. 3.20a). 5-Aza treatment (16.31%) resulted in slightly more apoptotic cells than the untreated sample (10.15%) (Fig. 3.20a). None of the statistical tests reached significance, suggesting that treatment with Dex does not affect apoptosis of the DMS 79 cells.

When the cells were examined by microscopy, a greater number of apoptotic cells were seen in the Dex (13.7%), and Dex and 5-aza sample (6.34%), than the untreated control (5.88%) (Fig. 3.20b). These increases however, were not significant relative to the untreated control. Cells treated with 5-aza experienced greater apoptosis (20.17%) than the other samples. In addition, more cells in the 5-aza (6.5%), Dex (6.34%), and Dex and 5-aza (3.5%) sample displayed condensed chromatin in comparison to the untreated control (1.83%) (Fig. 3.20b). None of the statistical tests reached significance. When examined by microscopy, Dex treatment appeared to slightly reduce apoptosis of the DMS 79 cells.

Using flow cytometry, significant cell death in comparison to the untreated control (10.1%) was seen in the Dex (38.35%) ($p = 0.003$), and Dex and 5-aza samples (52.1%) ($p < 0.0005$) (Fig. 3.20a). 5-Aza treatment alone did not result in significant cell death (16.31%) (Fig. 3.20a). Moreover, significantly greater populations of apoptotic cells were detected in the Dex ($p = 0.020$), and Dex and 5-aza ($p = 0.001$) samples, relative to the 5-aza treatment (only significance relative to the untreated control is displayed on the graph) (Fig. 3.20a). Furthermore, Dex and 5-aza together caused greater cell death than either Dex or 5-aza alone (Fig. 3.20a). Hence 5-aza appeared to enhance DMS 79 cell death induced by Dex, when analysed by flow cytometry.

As determined by microscopy, both Dex (24.84%), and Dex and 5-aza (26.17%) caused an increase in the number of dead cells in comparison to the untreated control (13.61%) (Fig.3.20b). However, this increase was not significantly greater than the untreated control and was surprisingly lower than treatment with 5-aza only, which caused 34.84% of the cells to die. Therefore, using microscopy, no significant effect of Dex on apoptosis was observed.

Taken together, these data indicate that 5-aza may enhance cell death induced by Dex, but Dex has negligible effect on apoptosis of the DMS 79 cells.

3.6.2. Treatment with a GR antagonist

To determine whether apoptosis associated with 5-aza treatment is due to demethylation and subsequent expression of the GR, or to demethylation and expression of other previously silenced genes, cells were treated with a GR antagonist, RU486, as a control, or 5-aza and RU486. To aid interpretation, 0.5 µM 5-aza data from previous experiments are included in these graphs.

3.6.2.1. In HEK cells, RU486 treatment in conjunction with 5-aza had negligible effects on apoptosis, but induced cell death

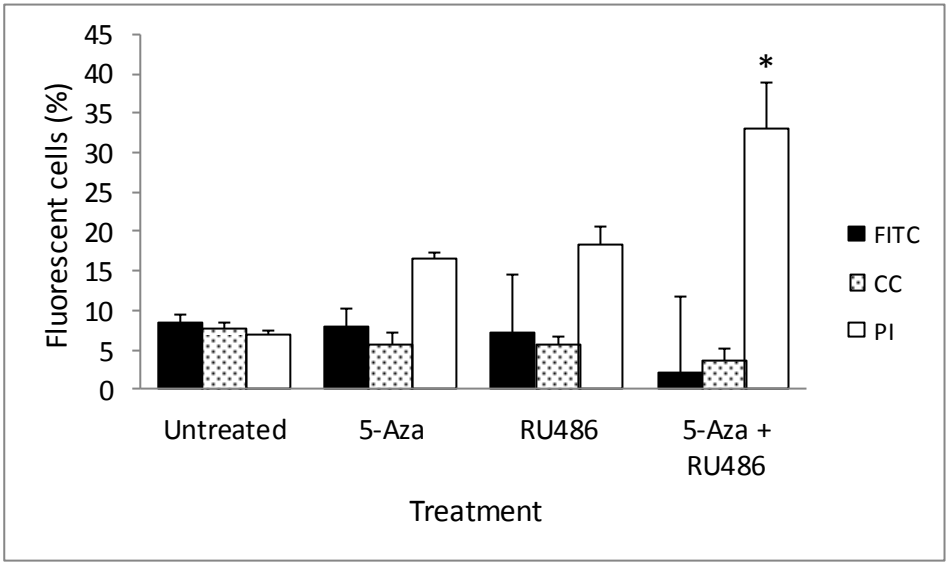

Figure 3.21. Treatment with RU486 in conjunction with 5-aza had negligible effects on apoptosis, but induced HEK cell death. The HEK cell line was treated with 0.5 µM 5-aza for 72 h alone, or RU486 was added for 24 h; or treated with RU486 only for 24 h; or left untreated. Cells were then analysed using microscopy for viability by PI, apoptosis by FITC Annexin V, and DAPI to visualise condensed chromatin. The percentage of FITC Annexin V positive, PI positive, and cells with chromatin condensation were established subsequent to treatment. The mean of two biological repeats ± SEM is displayed (n = 2). CC – condensed chromatin.

RU486 was used to determine whether apoptosis (of DMS 79 cells) is specifically due to re-expression of the GR, or to re-expression of other previously silenced genes. In HEK cells, fewer cells in the 5-aza sample were in the process of apoptosis, as detected by FITC Annexin V staining (7.83%) and chromatin condensation (5.67%), in comparison to the untreated sample (8.5% and 7.67% respectively) (Fig. 3.21). Smaller populations of cells were apoptotic (7.17%) and displayed condensed chromatin (5.67%) in the RU486 only sample, in comparison to the untreated control (Fig. 3.21). Similarly, smaller proportions of the RU486 and 5-aza samples were undergoing apoptosis (2.17%) and displayed chromatin condensation (3.67%), relative to the untreated control (Fig. 3.21). None of the statistical tests reached significance. Thus, treatment with RU486, and RU486 in conjunction with 5-aza, had negligible effects on apoptosis of HEK cells.

Treatment with 5-aza only, as well as treatment with RU486 alone, caused increases in the number of dead cells (16.67% and 18.34% respectively). But these increases were not significantly larger than the untreated control (7.0%) (Fig. 3.21). However significant cell death (p = 0.014) was seen in the sample treated with 5-aza and RU486 (33.0%), relative to the untreated control (7.0%) (Fig. 3.21). Treatment with RU486 in combination with 5-aza therefore induced significant death of the HEK cells.

3.6.2.2. In general, RU486 treatment appeared to inhibit apoptosis induced by 5-aza, while RU486 treatment as well as RU486 in combination with 5-aza induced cell death of DMS 79 cells

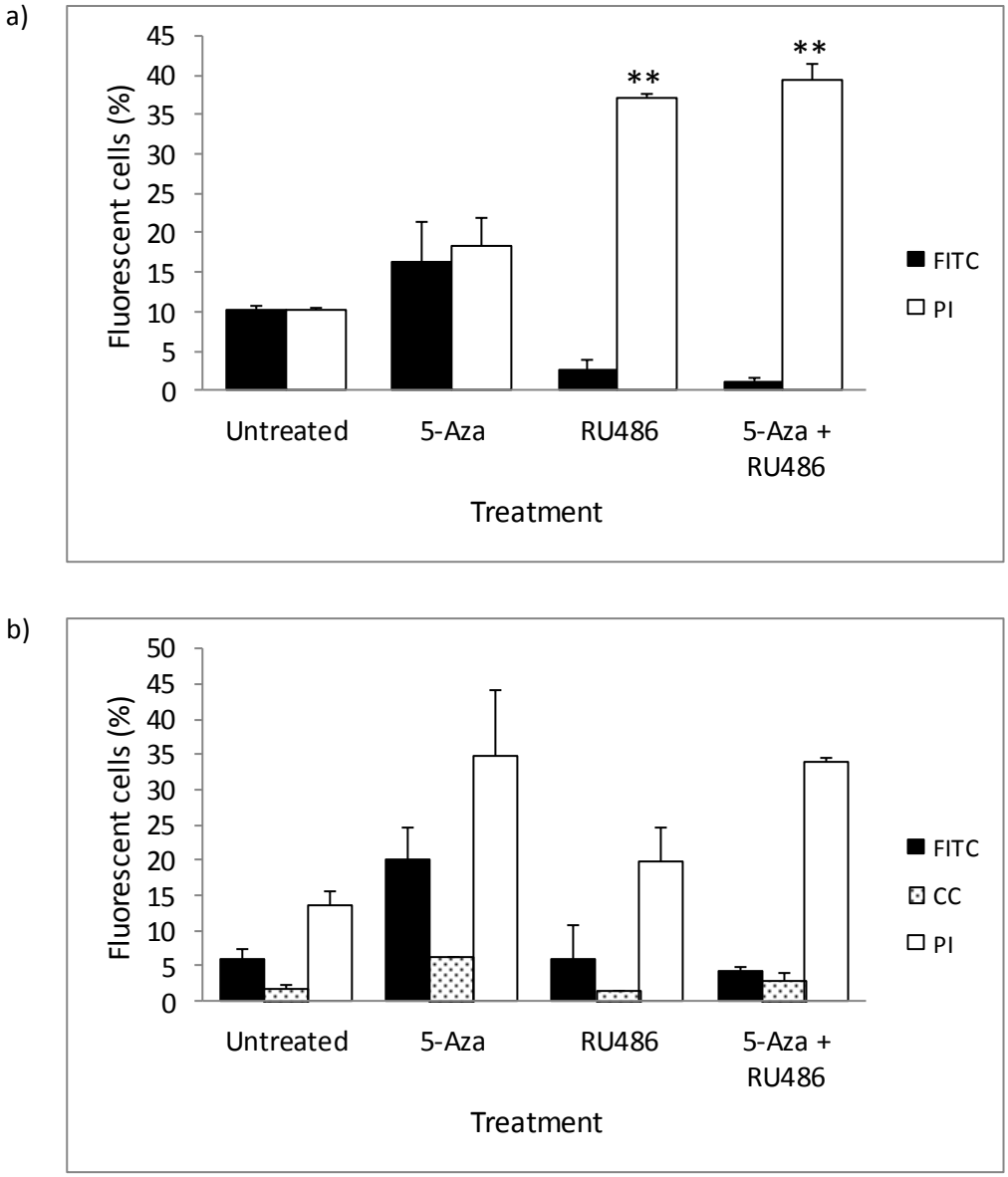

Figure 3.22. In general, RU486 treatment appeared to inhibit apoptosis induced by 5-aza, while RU486 treatment as well as RU486 in combination induced cell death of DMS 79 cells. The DMS 79 cell line was treated with 0.5 µM 5-aza for 72 h alone, or RU486 was added for 24 h; or treated with RU486 only for 24 h; or left untreated. Cells were then analysed by (a) flow cytometry for viability by PI, and apoptosis by FITC Annexin V and (b) microscopy for PI, FITC Annexin V, and DAPI to visualise condensed chromatin. The percentage of PI positive, FITC Annexin V positive, and cells with chromatin condensation were established subsequent to treatment. The mean of two biological repeats ± SEM is displayed (n = 2). CC – condensed chromatin.

DMS 79 cells were analysed by both flow cytometry and microscopy. The cells were treated with RU486 to determine whether apoptosis is due to re-expression of the GR, or to re-expression of other previously silenced genes as RU486 is a GR antagonist and will therefore block any GR activity. Flow cytometry revealed that although not significant, notable apoptosis occurred as a result of 5-aza treatment (16.31%) (Fig. 3.22a). With reference to the untreated control (10.15%), negligible apoptosis occurred in response to treatment with RU486 only (2.68%) (Fig. 3.22a). However, treatment with RU486 together with 5-aza (1.0%) produced a further reduction in apoptosis (Fig. 3.22a). Although not reaching statistical significance, RU486 treatment appears to inhibit apoptosis induced by 5-aza.

Using microscopy, the proportions of cells undergoing apoptosis were similar in the untreated control (5.88%) and the sample treated with RU486 alone (5.96%), whereas 5-aza induced a greater apoptosis (20.17%) than the untreated control (5.88%) (Fig. 3.22b). There were slightly less apoptotic cells in the RU486 and 5-aza sample (4.18%) than the untreated control (5.88%), but this difference was not significant (Fig. 3.22b). Furthermore, negligible differences in chromatin condensation were seen in the RU486 sample (1.67%), and RU486 in conjunction with 5-aza (3.0%), relative to the untreated control (1.83%) and 5-aza only sample (6.5%) (Fig. 3.22b). None of the statistical tests were significant, but it appears that RU486 treatment, and RU486 in conjunction with 5-aza decreased the number of apoptotic cells. The microscopy results mirror the trend seen with flow cytometry.

Using flow cytometry, 5-aza treatment (18.37%) resulted in an increase in dead cells relative to the untreated control (10.1%), but this was not significant. Treatment with RU486 only (37.24%) resulted in significant cell death (p = 0.004) relative to the untreated control (10.1%) (Fig. 3.22a). Treatment with RU486 and 5-aza together (39.54%) also caused significant cell death (p = 0.003) in comparison to the untreated control (10.1%) (Fig. 3.22a). In addition, significantly greater populations of dead cells were detected in the RU486 (p = 0.027), and RU486 and 5-aza (p = 0.015) samples, in comparison to the 5-aza treatment (only significance relative to the untreated control is displayed on the graph). Hence treatment with RU486, and 5-aza in conjunction with RU486, induced cell death.

Microscopic analysis showed increases in cell death when treated with 5-aza alone (34.84%), RU486 only (19.83%), and 5-aza together with RU486 (34.0%), in comparison to the untreated

control (13.61%) (Fig. 3.22b). None of the statistical tests reached significance. However using microscopy, 5-aza treatment, as well as 5-aza in combination with RU486, appears to induce DMS 79 cell death.

Overall, treatment with RU486, and treatment with RU486 in combination with 5-aza, induced cell death. Both flow cytometry and microscopy showed that RU486 treatment appeared to inhibit apoptosis induced by 5-aza in DMS 79 cells.

4. DISCUSSION

Lung cancer is the most frequently diagnosed major cancer type and the principal cause of cancer related deaths worldwide (Parkin, 2001). SCLC represents a highly aggressive form of the disease and comprises 20% of all lung cancers (Waters *et al.*, 2004; Panani and Roussos, 2006; Sommer *et al.*, 2007). SCLCs initially respond well to chemotherapy, yet the five year survival rate is less than 5% due to recurrent chemo-resistant tumours, producing a very poor prognosis (Hopkins-Donaldson *et al.*, 2003; Sommer *et al.*, 2007).

SCLC is a neuroendocrine tumour that secretes neuropeptides such as ACTH. This ectopic ACTH secretion is characteristically resistant to Gc action in SCLCs (Ray *et al.*, 1994; Schmidt *et al.*, 2004; Sommer *et al.*, 2007). The SCLC, Gc-resistant DMS 79 cell line shows reduced GR expression (Ray *et al.*, 1996). Therefore insensitivity of ACTH production by SCLC cells to Gc action is thought to be attributed to impaired GR expression in SCLC. Many tumours silence the expression of TSGs by epigenetic mechanisms (Baylin *et al.*, 2004; Lyko and Brown, 2005; Vaissière *et al.*, 2009; Lin *et al.*, 2010). New data in our laboratory suggest that the GR in SCLC cells is epigenetically silenced by methylation (Kay *et al.*, 2011). DNA methylation predominantly occurs in gene promoter regions (Baylin *et al.*, 2004). Demethylation of the GR promoter by 5-aza, and consequent GR re-expression, was investigated in this study.

Stresemann and Lyko (2008) conducted a study in which HCT116 (a human colon carcinoma cell line) cells were treated with 2 µM 5-azacytidine for a period ranging from 5 min to 48 h. Analysis of global m^5C levels of genomic DNA indicated progressive demethylation after 1 h of incubation, up to 48 h. The greatest demethylation was observed after 48 h. This confirmed that prolonged exposure to azanucleosides (such as 5-azacytidine and 5-aza-2'-deoxycytidine) resulted in more pronounced DNA demethylation. 5-Aza (5-aza-2'-deoxycytidine) is however a more potent inhibitor of methylation than 5-azacytidine (Stresemann and Lyko, 2008). Therefore only 0.5 µM, 1 µM and the highest concentration of 5 µM 5-aza were used for cell treatments to a maximum of 72 h. These concentrations have been used in a study incorporating the SCLC DMS 79 cell line, HEK, and NSCLC A549 cells (Kay *et al.*, 2011).

The first objective of this study was to determine whether treatment with the demethylating agent, 5-aza, obstructs DNMTs thereby preventing DNA methylation, hence allowing

endogenous GR re-expression. GRα mRNA expression and GRα protein expression were investigated.

4.1. The effect of a demethylating agent on GRα mRNA expression in A549, HEK and DMS 79 cells

Previous studies have shown that there is very little GR expression in DMS 79 and HEK cells. A549 cells, however, express abundant GR. The HEK and A549 cell lines therefore served as controls for little and abundant GR expression respectively. To determine whether lack of GR expression in the DMS 79 cell line was due to silencing by methylation, the cells were treated with the DNMTi, 5-aza. Treatment with a DNMTi results in a population of cells with unmethylated GR (and other gene) promoters, as 5-aza treatment removes all methyl marks. Relative GRα expression was evaluated because GRα is the major functional GR isoform, and its expression is a critical factor for Gc sensitivity in SCLCs (Schmidt *et al.*, 2004). GRα expression was normalized to GAPDH and β-actin individually, as well as the geometric mean of GAPDH and β-actin (Vandesompele *et al.*, 2002). The use of two reference genes is thought to be more accurate as experiments have shown that all genes in an 8000 gene array varied by ratios of at least 2-fold across a panel of 60 cell lines. Sets of commonly used reference genes, including GAPDH and β-actin, were found to vary in expression by 7- to 23-fold (Vandesompele *et al.*, 2002). These data demonstrate that universal control genes do not exist, and warrant the search for stably expressed genes in individual cell types. Our data reiterate this with differences seen when using the two different reference genes. Therefore, to produce more stringent data, in this study the two reference genes were used to facilitate more accurate gene expression profiling (Vandesompele *et al.*, 2002).

The discovery that 5-aza is incorporated into DNA, thereby inhibiting DNA methylation, resulted in extensive use of 5-aza to demonstrate the connection between loss of methylation in a specific gene region and re-expression of the associated gene (Christman, 2002; Lyko and Brown, 2005). This was attempted by Nojima *et al.* (2001) in kidney cancer cells. CpG methylation of the promoter region of the E-cadherin gene was believed to suppress its expression in renal cell carcinoma. E-cadherin was shown to be inactivated through CpG hypermethylation in its promoter region, and treatment of the renal cancer cells with 5-aza restored E-cadherin mRNA expression (Nojima *et al.*, 2001). In addition, Nephew and Huang (2003) reported that epigenetically silenced genes in ovarian cancer cells were reactivated by

5-aza. More recently, 5-aza was also used by Kay *et al.* (2011) to remove methylation from the heavily methylated GR 1C promoter in the DMS 79 SCLC cell line. The reversal of DNA methylation restored GR expression.

5-Aza has not only demonstrated efficacy on cells lines, but on tumour cells as well. Tessema *et al.* (2008) discovered that in primary lung adenocarcinoma tumours transcription of the three genes SYNE1, AKAP12, and IL20RA, was completely silenced by hypermethylation. Treatment with 5-aza resulted in their reactivation.

In our study, treatment with 5-aza had no effect on the A549 and HEK cells. No significant changes in GRα expression were seen in the A549 cells, relative to GAPDH, β-actin or the geometric mean of the two reference genes (Fig. 3.4 and Fig. 3.5). This was true for all biological repeats, and using either SYBR Green of EvaGreen (Fig. 3.4 and Fig. 3.5). Thus, as expected due to the abundant expression of GR, the GR in A549 cells is not methylated, consistent with the finding of Kay *et al.* (2011).

No significant changes in GRα expression were seen in the GR deficient HEK cells either (Fig. 3.6). This implies that the GR in HEK cells is not methylated and that other mechanisms are responsible for low GR expression. This, too, is in accordance with the study by Kay *et al.* (2011), in which treatment with 5-aza did not alter GR expression. These two cell lines are therefore appropriate controls.

DMS 79 cells are known to express reduced levels of the GR. If this is due to methylation, as has been recently shown (Kay *et al.*, 2011), GR expression should increase following reversal of methylation. However, in our study, a diverse range of effects were seen in the DMS 79 cells. Using EvaGreen and with reference to GAPDH, 0.5 µM 5-aza appeared to cause an increase in GRα expression, but this was not significant relative to the control (Fig. 3.7a). Treatment with 5 µM 5-aza effected a slight up-regulation in GRα expression with reference to GAPDH, whereas GRα expression was down-regulated with reference to β-actin (Fig. 3.7a). This was inconsistent with the findings of Kay *et al.* (2011), who demonstrated a dramatic increase in GR mRNA levels in DMS 79 cells following a 72 h exposure to 5 µM 5-aza.

qPCR performed using SYBR Green showed significant down-regulation of GRα expression in the DMS 79 cells, in response to all concentrations of 5-aza used (Fig. 3.8). Since 5-aza is a DNMTi and the GR promoter in DMS 79 cells is most likely methylated (Kay *et al.*, 2011), 5-aza was expected to demethylate the GR promoter and consequently up-regulate GRα expression. 5-Aza is known to be a very unstable compound. In acidic solutions such as acetic acid (in which the 5-aza was dissolved), the glycosidic bond of azanucleosides is cleaved, creating an instable compound. This would also interfere with the potential oral administration of decitabine, the clinical form of 5-aza (Stresemann and Lyko, 2008). Retrospective analysis revealed that storage of 5-aza aliquots had been compromised by thawing of the -80°C storage freezer for an unknown length of time. All the qPCR data described, with the exception of Fig. 3.9, were obtained using the probably degraded 5-aza.

Fig. 3.9 represents qPCR conducted in the laboratory before the 5-aza defrosted. There was no re-expression of GRα in the HEK and/or A549 cells after 5-aza exposure. In contrast, massive GRα re-expression was evident in the DMS 79 cells. Similarly observed by Kay *et al.* (2011), treatment with 5-aza resulted in re-expression of endogenous GRα mRNA. This occurred as the result of the DNMTi becoming irreversibly bound to CpG sites in the GR promoter. Methylation was prevented; hence the GR could be transcribed/expressed (Kay *et al.*, 2011). Inconsistencies between qPCR performed with the DMS 79 cells before and after the 5-aza defrosted, may be attributed to the instability and probable degradation of the chemical.

While GRα mRNA is re-expressed following treatment with 5-aza, it does not necessarily mean that GRα protein is expressed. Western blots were carried out to determine whether treatment with 5-aza results in re-expression of endogenous GRα protein.

4.2. The effect of a demethylating agent on GRα protein expression in A549, HEK and DMS 79 cells

The GR is encoded by a complex gene, consisting of seven constant coding/translated exons (exons 2-8), two exon 9s encoding the α and β protein isoforms, and nine 5'-non-coding/untranslated alternative first exons (exon 1) (Schaaf and Cidlowski, 2002; Alt *et al.*, 2010). Each exon 1 has its own promoter associated with an alternative transcription start site, from which genuine, full-length GR protein is generated, as the translation start site is located in the common exon 2 (Turner *et al.*, 2006; Alt *et al.*, 2010). Exon 2 – exon 9 forms the protein-

coding region. Multiple GR isoforms are generated from alternative RNA splicing, as well as alternative translation initiation and post-translational modifications such as phosphorylation, ubiquitination and sumoylation (Zhou and Cidlowski, 2005; Duma *et al.*, 2006). GRα is the major functional GR isoform (Schmidt *et al.*, 2004). Eight different GRα isoforms are translated from human GRα mRNA, *viz.* GRα-A, GRα-B, GRα-C1, GRα-C2, GRα-C3, GRα-D1, GRα-D2 and GRα-D3 (Duma *et al.*, 2006) (see Fig. 4.1).

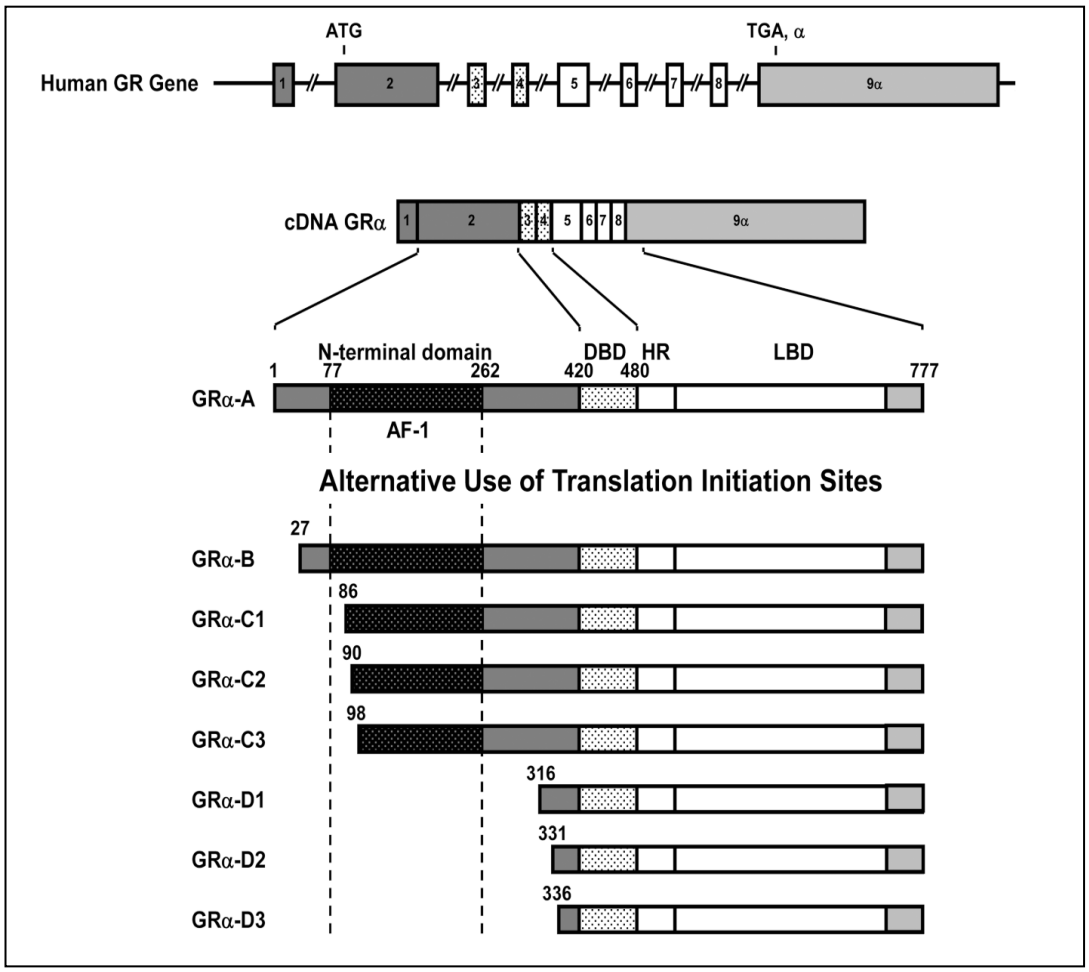

Figure 4.1. Genomic structure of the human GRα. Generation of multiple GRα protein isoforms are as a result of alternative translation initiation. Translation can be initiated in each of the AUG codons corresponding to positions 1, 27, 86, 90, 98, 316, 331 and 336 of the GRα N-terminal domain, resulting in a set of GRα isoforms with different lengths, sizes and functional domains. DBD – DNA binding domain; HR – hinge region; LBD – ligand binding domain. Image taken from Duma *et al.* (2006).

4.2.1. GRα isoform expression in A549, HEK and DMS 79 cells

The NSCLC, A549 cell line served as a control because the cells exhibit abundant GR protein expression. Two distinct bands were visualised at ~94 kDa and ~91 kDa (Fig. 3.10). These represent the putative GRα-A (94 kDa) and GRα-B (91 kDa) protein isoforms.

HEK cells were also used as a control because the cells have a relatively low expression of non-functional GR protein. Three protein bands were visualised at ~94 kDa, ~91 kDa and ~78 kDa, which represent the putative isoforms GRα-A, -B and -C, respectively (Fig. 3.12). Zhou and Cidlowski (2005) also observed expression of the GRα-B isoform in HEK cells, suggesting that alternative translation initiation of the different GRα isoforms is a normal occurrence in these cells.

In DMS 79 cells, four distinct protein bands were visualised between 55 kDa and 95 kDa, where the GRα protein is located (Fig. 3.14). The bands were at ~94 kDa, ~91 kDa and two at around ~78 kDa. These bands represent the four GRα isoforms present in DMS 79 cells. The GRα-A isoform is at 94 kDa, the GRα-B isoform at 91 kDa, and two different GRα-C isoforms are between 79 and 78 kDa (Zhou and Cidlowski, 2005; Duma *et al.,* 2006).

Importantly, 5-aza treatment did not affect isoform expression in any of these cell lines as there was no difference between the GRα isoforms expressed in control and treated cells for all the cell lines.

Lu *et al.* (2007) previously demonstrated that both common and distinct sets of genes were regulated by the GRα translational isoforms in the same cell. The human osteoblastic sarcoma cell line, U-2 OS, also lacks endogenous GR expression. Lu *et al.* (2007) expressed wild type human GRα and the individual GRα isoforms in these cells, and discovered that the GRα translational isoforms had distinct abilities to stimulate apoptosis. GRα-C isoforms were the most effective at inducing apoptosis in U-2 OS cells, followed by the -A and -B isoforms. GRα-D was the least effective at initiating cell death. The GRα isoforms activated many pro-apoptotic genes including caspase-7, TNF receptor superfamily members 1b and 10b, and caspase recruitment domain family members 12 and 14, among others. Pro-survival genes were also repressed by the GRα isoforms. These included Bcl-2, Bcl-xL and Mcl-1 (Lu *et al.*, 2007). These same anti-apoptotic genes were down-regulated when the GR was over-expressed in SCLC

xenograft (Sommer *et al.*, 2010). GRα isoforms therefore selectively regulate genes involved in apoptosis (Lu *et al.*, 2007). It is interesting here that the GRα-C isoform is expressed by the DMS 79 cells, and it would be worth investigating whether it is specifically this isoform that is involved in inducing apoptosis in this cell line.

4.2.2. The effect of demethylation on GRα protein expression in A549, HEK and DMS 79 cells

Densitometric analysis of the Western blot for the NSCLC A549 cells showed that control cells contained significantly more total GRα protein than cells treated with 1 μM 5-aza (Fig. 3.11). Cells treated with 0.5 μM and 5 μM 5-aza also displayed reduced total GRα protein expression in comparison to the control (Fig. 3.11). A549 cells contain abundant, Gc sensitive GR that is not methylated. It has been demonstrated that 5-aza can inhibit cell proliferation of cancer cell lines and reduce their viability (Stresemann and Lyko, 2008). Research by Yuan *et al.* (2004) demonstrated that growth of NSCLC cells was inhibited by treatment with 1 μM 5-aza. This is believed to be due to 5-aza–induced DNA demethylation and the consequent changes in mRNA expression of multiple genes (Yuan *et al.*, 2004). Such an event could have occurred in the A549 cells.

Densitometric analysis of the HEK Western blot showed that exposure to 0.5 μM and 1 μM 5-aza lead to a significant reduction in GRα protein expression, relative to the control (Fig. 3.13). This was unexpected as the GR promoter is known to be unmethylated in HEK cells, and the gene and protein, non-functional. In addition, the qPCR data (Fig. 3.6) implied that the GR in the HEK cell line is silenced by a mechanism other than methylation, and that other means are employed to ensure the gene is effectively non-functional (Kay *et al*., 2011). Such effects may be due to the toxicity of the 5-aza, leading to cell death.

Densitometric analyses of the DMS 79 Western blots showed that there was no significant difference in total GRα protein between the control and 5-aza–treated cells (Fig. 3.15). If the vehicle control were to be excluded, then 5-aza appears to increase the expression of total GRα protein in a dose dependent manner (Fig. 3.15a); but not significantly. Thus, treatment with 5-aza had no effect on re-expression of endogenous GRα protein in the DMS 79 cells. However, the replicates (even on the same blot) appeared to be dissimilar (Fig. 3.14), which is a confounding factor and higher GRα protein expression than expected was seen in the

control-treated cells (especially Fig. 3.15b). Moreover, this may have been due to an error made during cell treatment, protein extraction or protein loading.

These results are unexpected and retrospective analysis has revealed that these results may have been due to the use of possibly degraded 5-aza. At the time however, it was thought that the concentrations of 5-aza may have been toxic to the cells (Christman, 2002; Lyko and Brown, 2005), obscuring results. An MTS cell viability assay was thus performed to establish whether the toxic effects of 5-aza affected cell viability.

4.3. The effect of demethylation on A549, HEK and DMS 79 cell viability

Toxicity presents a problem in interpreting laboratory data as it is frequently unclear whether the effects on gene expression related to inhibitor treatment are due to cytotoxicity, or the DNA demethylation (Lyko and Brown, 2005). 5-Aza demonstrates substantial cytotoxic effects (Christman, 2002). Clinically this manifests as myelosuppression with neutropenic fever (Lyko and Brown, 2005). Paradoxically, 5-aza exerts its toxic effects through the formation of the DNMT 1–5-aza–DNA adducts. The presence of these adducts induce DNA damage response pathways necessary to clear the cell of protein-DNA adducts. The TSG p53 mediates DNA damage responses to chemotherapeutic drugs. p53 is activated, resulting in the death of 5-aza treated cells (Karpf and Jones, 2002).

The discrepancies in the data may have been due to 5-aza cytotoxicity. However, treatment with 5-aza did not seem to have an effect on cellular viability. Very slight changes in the numbers of viable A549 cells were seen in response to the various concentrations of 5-aza (Fig. 3.16). DMS 79 cell viability appeared to increase following treatment with 5-aza, relative to the controls (Fig. 3.16). Strangely, there were significantly more viable HEK cells in the control-treated sample and 1 μM 5-aza sample in comparison to the untreated sample. Furthermore, 5-aza reduced HEK cell viability at a concentration of 5 μM, relative to the vehicle control (Fig. 3.16).

The lack of an effect on cell viability may have been due to the unfortunate use of possibly degraded 5-aza for these experiments, confounding interpretation of these data.

4.4. The effect of a demethylating agent on HEK and DMS 79 cell death and apoptosis

To determine whether re-expression of the endogenous GR in SCLC cells is sufficient to activate the pro-apoptotic and suppress the anti-apoptotic pathway, cells were analysed by flow cytometry and/or microscopy. Both methods were used as access to the flow cytometer was suddenly restricted due to staff absences. These experiments were only performed on HEK and DMS 79 cells, and not A549 cells, due to additional malfunction of the microscope. For these experiments, freshly prepared 5-aza was used.

4.4.1. The effect of a demethylating agent on apoptosis of HEK and DMS 79 cells

FITC Annexin V binds to phosphatidylserine molecules, which become exposed when the cell membrane involutes – one of the earliest features of apoptosis (Lu *et al.*, 2007). FITC Annexin V fluorescence is therefore a marker of early apoptosis. Cells were stained with FITC Annexin V to establish whether cell death was by apoptosis. When analysed by flow cytometry, relatively small proportions of the HEK control and 5-aza treated cells were FITC Annexin V positive (Fig. 3.17a). Examination by microscopy revealed that only treatment with 1 µM 5-aza induced significant apoptosis in HEK cells (Fig. 3.17b).

Chromatin condensation is one of the earliest recognised morphologic changes characteristic of apoptosis, and is commonly used to identify cells in early stage apoptosis (Kerr *et al.*, 1994). No significant apoptosis of the HEK cells was identified by chromatin condensation (Fig. 3.17b). Taken together with the FITC Annexin V data from flow cytometry and microscopy, it can be concluded that 5-aza induced negligible apoptosis of HEK cells.

In contrast, much greater percentages of the DMS 79 cells stained positive for FITC Annexin V, and this proportion increased with increasing concentrations of 5-aza (Fig. 3.18a). 1 µM and 5 µM 5-aza induced significant apoptosis relative to the untreated and vehicle controls (Fig. 3.18a). The DMS 79 cells are therefore dying by apoptosis subsequent to demethylation. Hopkins-Donaldson *et al.* (2003) found that SCLC cells are resistant to apoptosis initiated by FasL and TRAIL activation, and that DNA methylation is responsible for the silencing of Fas, TRAIL-R1 and caspase-8 expression. Re-activation of these proteins leads to apoptosis. Thus, the apoptosis seen in the DMS 79 cells may be caused by re-expression of genes other than the GR. Kay *et al.* (2011) discovered that treatment with 5-aza inhibits expression of the Bcl-2 pro-

survival protein in DMS 79 cells and HEK cells. Thus, Bcl-2 suppression may contribute to the apoptosis and cell death observed in these cell lines.

When the DMS 79 cells were analysed by microscopy, significant apoptosis was not detected (Fig. 3.18b). This may be due to the difficulties in detecting FITC Annexin V fluorescence as the SCLC cells are characterised by a large round nucleus surrounded by very little cytoplasm, making it difficult to visualise cytoplasmic staining. It is possible that populations of FITC positive cells were not able to be distinguished. Although significant FITC positive cells were not seen, significant proportions of cells with condensed chromatin, which is easily seen in the small cells, were detected in the samples treated with 1 µM and 5 µM 5-aza (Fig. 3.18b). In conjunction with the flow cytometry data, it is thought that treatment with 1 µM and 5 µM 5-aza induced apoptosis of the DMS 79 cells.

Since cell death is the eventual outcome of cells undergoing apoptosis, cells in the late stages of apoptosis will have a damaged membrane and stain positive for propidium iodide (PI) as well as for FITC Annexin V. Thus PI- and FITC Annexin V-staining does not distinguish between cells that have already undergone an apoptotic cell death and those that have died as a result of the necrotic pathway, because in either case the dead cells will stain with both FITC Annexin V and PI.

4.4.2. The effect of a demethylating agent on HEK and DMS 79 cell death

PI stains the nucleus, which is only accessible if the cell has ruptured, as viable cells with intact membranes exclude PI. Therefore PI is used to detect dead cells. For the HEK cells, only very small proportions of the controls and 5-aza–treated samples detected by flow cytometry were dead (less than 10% of the respective populations) (Fig. 3.17a). With microscopy, greater proportions of dead cells were observed in the cell samples treated with 5-aza, but this was not significantly more than the control (Fig. 3.17b). This negligible cell death was probably the result of the trauma involved in preparation for flow cytometry and microscopy, *viz.* the formation of single cell suspensions.

In contrast to the HEK cells, flow cytometry detected significantly more dead DMS 79 cells in the 5-aza–treated samples, than the controls (Fig. 3.18a). Significance was in comparison to both the untreated control and vehicle control for all three concentrations of 5-aza used. 1 µM

5-aza produced the greatest amount of dead cells, followed by 0.5 µM 5-aza (Fig. 3.18a). The induction of cell death after 72 h of incubation with 5-aza may be the consequence of apoptosis or necrosis. If death was due to apoptosis, this could possibly be due to re-acquisition of GR expression, or regulation of other pro-apoptotic genes (Sommer *et al.*, 2007; Kay *et al.*, 2011). The large amount of dead cells could also be a result of the DNA damage response pathways induced by 5-aza, which could ultimately lead to cell death. It has been demonstrated that 5-aza caused the formation of double strand breaks in human tumour cell lines, and that DNMT 1 may be involved in mediating the cellular damage response to the drug (Stresemann and Lyko, 2008).

Microscopic analysis revealed that 5-aza treatment did not cause significant cell death of DMS 79 cells, but there did appear to be a greater number of dead cells in these samples (Fig. 3.18b). The differences may be due to the relatively small number of cells that were analysed by microscopy (300 cells), in comparison to flow cytometry (10 000 cells), resulting in a population that is not representative.

4.5. The effect of a GR agonist on HEK and DMS 79 cell death and apoptosis

Gcs induce apoptosis of lymphoid cells and osteoblasts. The synthetic Gc Dex has a range of effects on cell survival, cell signalling and gene expression (Herr *et al.*, 2003; Herr *et al.*, 2007). 5-Aza causes re-expression of the GR, which mediates the effects of Dex. To establish whether Dex could enhance apoptosis of SCLC DMS 79 cells, the cells were treated with Dex only and 5-aza only as controls, or with Dex in conjunction with 5-aza.

4.5.1. The effect of a GR agonist on apoptosis of HEK and DMS 79 cells

Expression of wild-type GRα has been previously shown to induce apoptosis in U-2 OS bone cells. The apoptotic effect was accelerated by Dex. Interestingly, treatment with Dex also resulted in more dead cells. Down-regulation of Bcl-2 expression is thought to contribute to Gc-induced apoptosis in U-2 OS cells (Lu *et al.*, 2007). The mechanism whereby the GR regulates these genes remains unclear (Sommer *et al.*, 2010). We wanted to establish whether the same apoptotic effect was evident in DMS 79 cells when endogenous GR was re-expressed.

In the control cells, no significant apoptosis of HEK cells resulted from treatment with Dex, as determined by FITC Annexin V-staining and chromatin condensation (Fig. 3.19). HEK cells exposed to Dex together with 5-aza, also did not undergo significant apoptosis (Fig. 3.19). Hofmann *et al.* (1995) found that cell lines responsive to Dex had high GR concentrations. HEK cells express very little GR, therefore the 'no effect' is in agreement with the finding by Hofmann *et al.* (1995).

Treatment with Dex alone produced no significant apoptotic effect (as determined by FITC Annexin V fluorescence and chromatin condensation) on the DMS 79 cells (Fig. 3.20). This was predicted as high levels of GR expression are necessary for Dex activity (Hofmann *et al.*, 1995). Treatment with Dex in conjunction with 5-aza also showed no significant apoptosis of DMS 79 cells (Fig. 3.20). This was unexpected as qPCR performed with fresh 5-aza demonstrated massive GR re-expression in DMS 79 cells (Fig. 3.9), through which Dex could act. Furthermore, treatment of CORL47 SCLC cells with 5-aza and then Dex results in apoptosis (Kay *et al.*, 2011).

The lack of effect of the GR agonist on apoptosis suggests that the described GR-mediated apoptosis in DMS 79 cells is ligand-independent. Sommer *et al.* (2007) allude to this in their paper when they show that added Dex did not significantly affect cell death induced by retroviral GR over-expression. Ligand-independent effects of the GR are controversial; however several reports support the existence of ligand-independent effects of GR expression. In one study, over-expressed GR inhibited the activity of NF-κB, and in further work, a similar conclusion was reached, even when a mutated GR was expressed with disrupted nuclear localisation function (Mathieu *et al.*, 1999; Doucas *et al.*, 2000). Alternatively, it may be that the cells were analysed too late and were already in the process of cell death.

4.5.2. The effect of a GR agonist on HEK and DMS 79 cell death

Treatment with Dex alone caused significant death of the HEK cells (Fig. 3.19). A significant number of HEK cells exposed to Dex in combination with 5-aza, were also dead (Fig. 3.19). 5-Aza treatment alone did not result in cell death, implying that treatment with 5-aza enhanced cell death induced by Dex.

Significant cell death was observed in the DMS 79 cells in response to Dex exposure, as well as Dex in conjunction with 5-aza, but only when the cells were analysed by flow cyotmetry (Fig. 3.20a).

Hofmann *et al.* (1995) conducted a study on the growth inhibitory effects of Dex, mediated by the GR, in human lung cancer cell lines. DMS 79 and A549 cells were included. The greatest anti-proliferative effect was seen on the A549 cells, which express abundant GR. SCLC cell lines have comparatively lower amounts of GR and the growth of all SCLC cells was insensitive to Dex. High GR content is thus a prerequisite for growth inhibition induced by Dex (Hofmann *et al.*, 1995; Sommer *et al.*, 2007). This suggests that both HEK and DMS 79 cells should be unresponsive to the effects of Dex however, in this study, Dex induced cell death in both cell lines. This cell death may be due to an apoptotic effect of Dex on the cells. Analysis of the cells for apoptosis (section 4.5.1) did not reveal the presence of apoptotic cells; however this may be due to the fact that the cells had already undergone apoptosis and were already in the process of cell death. Alternatively, Dex has previously been shown to induce cell death in lymphoid leukaemia (Laane *et al.*, 2009) and insulin secreting cells (Ranta *et al.*, 2006).

4.6. The effect of a GR antagonist on HEK and DMS 79 cell death and apoptosis

Essentially all cancers are characterised by global hypomethylation, and gene-promoter-specific hypermethylation (Robertson, 2001; Baylin and Ohm, 2006). Many genes are silenced by promoter hypermethylation in cancer cells. Inhibition of DNA methylation by 5-aza results in a range of phenotypic changes, from suppressing the growth of tumour cells, which is most likely due to re-activation of growth-regulatory genes (other than the GR) silenced by *de novo* methylation, to inducing apoptosis (Bender *et al.*, 1998; Baylin and Ohm, 2006). 5-Aza produces global non-specific changes in DNA methylation (Christman, 2002; Karpf and Jones, 2002), thus it is not specific to the GR. Therefore, to determine whether apoptosis associated with 5-aza treatment was specifically due to demethylation and subsequent re-expression of the GR, cells were also treated with the GR antagonist, RU486. The HEK cells served as the control because they express very little GR, yet unlike the DMS 79 cells, do not undergo apoptosis when the GR is re-expressed. We have shown that, in control HEK cells, 5-aza treatment induces negligible cell death or apoptosis. However, these treatments induce significant cell death and apoptosis in the DMS 79 cells. The cells were treated with RU486 to

determine empirically whether these effects are due to re-expression of the GR. These experiments were conducted in parallel with those described in section 4.4 and used 0.5 µM 5-aza as this concentration was shown to induce massive re-expression of the GR (Fig. 3.9). Due to difficulties accessing the cytometer, the A549 and HEK cells were not analysed by flow cytometry. Because of additional problems with the fluorescent microscope, only the HEK cells could be analysed by microscopy.

4.6.1. The effect of a GR antagonist on apoptosis of HEK and DMS 79 cells

No significant apoptosis was seen in the HEK or DMS 79 cells treated with RU486 alone, or RU486 together with 0.5 µM 5-aza (Fig. 3.21 and Fig. 3.22). This was predicted for the HEK cells, as the cells do not undergo apoptosis when the GR is re-expressed (Kay *et al.*, 2011).

Although not significant, flow cytometric and microscopic analyses of the DMS 79 cells showed that only 0.5 µM 5-aza treatment induced greater apoptosis than the untreated control (Fig. 3.22). Further experiments using different concentrations of 5-aza and RU486, and different exposure periods, are required to tease out whether this trend is true.

Fewer apoptotic DMS 79 cells were present in the RU486 sample relative to the untreated control, with the least number of apoptotic cells in the sample treated with 5-aza in conjunction with RU486 (Fig. 3.22a). The microscopy data mirrors this trend of the flow cytometry data (Fig. 3.22b). This suggests that RU486 inhibits the apoptosis induced by 5-aza. In these experiments, a concentration of fresh 0.5 µM 5-aza was used as this concentration was shown to induce massive re-expression of the GR (Fig. 3.9), and it was hoped that lower concentrations of 5-aza may offset its potential toxicity. The trend in the data suggest that specific re-expression of the GR may be responsible for apoptotic induction. Our findings, although not significant, hint that endogenous re-expression of the GR leads to apoptosis.

This is in agreement with Sommer *et al.* (2007), who found that retroviral over-expression of the GR induced apoptosis in SCLC cells. *In vitro*, apoptosis was induced by GR over-expression via up-regulation of the pro-apoptotic genes, Bad and Bax. However *in vivo*, apoptosis caused by GR over-expression resulted from down-regulation of the anti-apoptotic genes, Bcl-2 and Bcl-xL (Sommer *et al.*, 2007; Sommer *et al.*, 2010). It is expected that apoptosis in the DMS 79 cells was induced by suppression of the pro-survival gene, Bcl-2 (Kay *et al.*, 2011).

4.6.2. The effect of a GR antagonist on HEK and DMS 79 cell death

The anti-Gc RU486 alone produced no effect on HEK cell death (Fig. 3.21). This is consistent with the study by Hofmann *et al.* (1995), who found that RU486 was virtually inactive when administered alone. However, the HEK cells underwent significant cell death in response to treatment with RU486 in combination with 5-aza (Fig. 3.21). This is strange as no significant effect on cell death was observed in the HEK cells treated with either RU486, or 5-aza alone. As our data have clearly demonstrated, the GR in HEK cells is not methylated, and the significant cell death observed in HEK cells may be due to excessive drug exposure or combined drug toxicity.

RU486 treatment alone and in combination with 5-aza induced significant cell death of the DMS 79 cells (Fig. 3.22a). This was only seen in the samples analysed by flow cytometry, perhaps because too few cells (300) were analysed using microscopy. These data are confusing as RU486 generally has a protective effect against cell death (Ghoumari *et al.*, 2003). These experiments need to be repeated with a variety of different 5-aza and RU486 concentrations and different exposure periods to dissect out the true effects.

4.7. Summary

The aim of this project was to determine whether re-expression of endogenous GR, by treatment with the DNMTi 5-aza, induces apoptosis of SCLC cells. This study found that treatment with 5-aza had no effect on A549 and HEK cell GRα mRNA expression, yet strangely affected GRα protein expression in these cells. Conversely, 5-aza treatment affected GRα mRNA expression in DMS 79 cells, but had no effect on GRα protein expression. In an attempt to understand these confounding data, cell viability assays were performed. 5-Aza had no effect on the viability of A549 cells and DMS 79 cells. Treatment with 5-aza had minimal effect on HEK cell viability. These data may be confounded by the use of possibly degraded 5-aza. qPCR using fresh 5-aza showed that treatment with 0.5 μM 5-aza lead to massive re-expression of GRα mRNA in DMS 79 cells. 5-Aza treatment leading to GR re-expression in DMS 79 cells has also been demonstrated very recently by others (Kay *et al.*, 2011).

Therefore, in SCLC cells, 5-aza treatment leads to GR re-expression. To determine whether this endogenous re-expression can induce apoptosis, flow cytometry and/or microscopy were performed. Overall, treatment with 5-aza induced negligible apoptosis and cell death of HEK

cells. These negligible effects were probably the result of the trauma involved in preparation for flow cytometry and microscopy, *viz.* the formation of single cell suspensions. In contrast, 5-aza treatment induced significant apoptosis and cell death of the DMS 79 cells subsequent to demethylation, consistent with the recent study by Kay *et al.* (2011).

The cells were then treated with Dex to establish whether Gc action enhanced apoptosis of SCLC cells. In HEK cells, neither Dex nor Dex and 5-aza together significantly affected apoptosis, but 5-aza treatment enhanced cell death induced by Dex. This was unexpected as HEK cells express very little unmethylated GR, and may be due to excessive drug exposure or combined drug toxicity. In the DMS 79 cells, 5-aza appeared to enhance cell death induced by Dex when analysed by flow cytometry; whereas microscopic analysis showed no significant effect on cell death. Analysis of insufficient cell numbers may be the reason for this trend not being observed with microscopy. Dex had no effect on apoptosis of DMS 79 cells treated with 5-aza. This suggests that the GR-mediated apoptosis seen is ligand-independent, or that Dex treatment did indeed accelerate apoptosis but that the cells were analysed at the wrong stage and had already committed to cell death.

To determine whether apoptosis was specifically due to re-expression of the GR, cells were exposed to the GR antagonist, RU486. 5-Aza stimulated HEK cell death in conjunction with RU486 treatment, but had negligible effects on apoptosis. The observed cell death may again have been due to combined drug toxicity or excessive drug exposure. For the DMS 79 cells, flow cytometric data showed that RU486 treatment, as well as RU486 in combination with 5-aza induced cell death. This may only have been demonstrated by flow cytometry, as possibly too few cells were examined by microscopy. Although not significant, in general, RU486 treatment appeared to inhibit apoptosis induced by 5-aza in the DMS 79 cells. This trend in the flow cytometry and microscopy data suggest that re-expression of the GR may be responsible for apoptotic induction.

Further experiments treating the cells with fresh 5-aza, and exposing them to different concentrations of RU486 and Dex, for different time periods, need to be conducted to definitively determine whether treatment with 5-aza results in endogenous GR re-expression, leading to apoptosis of the SCLC cells.

4.8. Conclusion

The poor survival rate for SCLC provides a motivation to better understand the mechanisms of carcinogenesis and apoptosis. The induction of apoptosis is a key molecular mechanism by which cytotoxic drugs kill tumour cells, therefore apoptosis is one of the most promising targets for lung cancer therapy (Motadi *et al.*, 2007).

The many epimutated TSGs in cancer clearly demonstrate that aberrant DNA methylation is a significant contributor to carcinogenesis. Sites of aberrant DNA methylation also constitute promising molecular markers for use in early cancer detection and in monitoring disease progression and treatment responses (Hopkins-Donaldson *et al.*, 2003). Unlike mutations, epigenetic marks are reversible and clinical trials with both DNMTis and HDAC inhibitors have shown promising results (Lyko and Brown, 2005). The development of agents that reverse epigenetic silencing in a gene-specific manner, while avoiding global effects, is essential for the improvement of cancer therapeutics.

While advances in the diagnosis and treatment of SCLC have been made in recent years, long term survival remains rare (Sommer *et al.*, 2010). The identification of a novel endogenous mechanism that specifically induces apoptosis of SCLC cells offers great promise for the development of targeted therapeutics for the treatment of this deadly disease.

4.9. Future prospects

Kay *et al.* (2011) determined that the GR in SCLC cell lines is silenced by methylation and that re-expression of the endogenous GR using a DNMTi induces apoptosis of the cells. Further studies will therefore investigate whether the GR is similarly methylated in biopsies from patients suffering from SCLC. The methylation profile of the GR promoter from SCLC biopsies will be compared to matched tissue controls and correlated with age, cancer stage, smoking status, recurrence, death rates and DNMT 1 expression levels.

To establish whether re-expression of the GR *in vivo* induces apoptosis, cells from SCLC biopsies will be cultured *ex vivo* and the ability of endogenous re-expression of the GR to induce apoptosis, determined. The effect of Dex will be examined to determine whether Gc treatment can accelerate apoptosis of the SCLC cells, and the GR antagonist RU486 will be used to establish whether apoptosis is specifically a result of endogenous GR re-expression.

Furthermore, a bystander effect has been observed in xenograft where normal SCLC cells neighbouring cells with restored GR expression also undergo apoptosis (Sommer *et al.*, 2010). It will be established whether apoptotic stimuli are transferred between SCLC cells *in vitro*, thereby inducing a bystander effect. Thus, silencing of the GR may contribute to SCLC progression. It is therefore proposed that the GR is a novel TSG for SCLC.

5. APPENDIX

A. MIQE checklist

MIQE is a set of guidelines that detail the minimum information required for assessing qPCR experiments. The guidelines focus on the reliability of results to help maintain the integrity of scientific literature, promote consistency between laboratories, and increase experimental transparency. By providing all relevant experimental conditions and assay characteristics, reviewers can assess the validity of the protocols used (Bustin *et al.*, 2009). The necessary information, specified by the MIQE guidelines, is presented below.

A.1. Experimental design

The GR was examined to evaluate the effect of 5-aza treatment on GR expression. The SCLC DMS 79 cells, Gc-resistant HEK, and NSCLC A549 cells were treated with either vehicle control, or 0.5 µM, 1 µM or 5 µM 5-aza. The HEK cell line served as a control, because like DMS 79 cells, HEK cells also demonstrate minimal GR expression. The GR promoter in these cells however, in contrast to the DMS 79 GR promoter, is not methylated. The A549 cells also served as a control, as they express abundant GR (which is not methylated), and GR expression is not affected by vehicle or 5-aza treatment. The effect of demethylation by 5-aza treatment was evaluated using qPCR analyses. RNA was extracted from cells cultured in a single 10 cm^3 dishes or T75 flasks for each treatment within a given experiment. RNA was only isolated from fully confluent dishes/flasks. cDNA was initially synthesised using the High Capacity RNA-to-cDNA Master Mix (Applied Biosystems), but this method was later replaced by the Tetro cDNA Synthesis Kit (Bioline), as the former was discontinued by the manufacturer. All qPCR analyses were performed by myself at the laboratory of my supervisor Dr P. Sommer in the School of Life Sciences, University of KwaZulu-Natal, Durban, South Africa.

A.2. Sample information

Stocks of all cell lines were frozen down from confluent T75 flasks. Cell stocks were stored in cryovials (Corning®) in 1.5 mL culture medium containing 10% dimethyl sulfoxide (DMSO). The cryovials were stored in liquid nitrogen at -196°C. As all cell lines were human, cells were cultured at a temperature of 37°C with 5% CO_2 in DMEM or RPMI 1640 medium supplemented

with 10% FBS Gold, and 2% 100x Penicillin-Streptomycin to a final concentration of 100 units/mL.

Total RNA was isolated from confluent 10 cm^3 dishes or T75 flasks of cells in culture. One 10 cm^3 dish or T75 flask was used per treatment. HEK and A549 cells were processed for RNA isolation by first aspirating all culture medium and then washing the cells once with 1x PBS solution. A volume of 1 mL Trypsin-EDTA solution was added to the cells which were incubated for 5 min to detach them from the bottom of the culture dish. The trpysin solution was inactivated by the addition of 1 mL culture medium.

For the DMS 79 cells, up to 15 mL medium, containing the cells, was transferred into 15 mL centrifuge tubes. The solution containing the suspended DMS 79, HEK or A549 cells was then centrifuged for 3 min at 2000 rpm. Supernatant was aspirated from the cell pellets. The cell pellets were then processed for RNA extraction.

A.3. Nucleic acid extraction

RNA was extracted using the RNeasy® Mini Kit, as detailed in section 2.2. of the Materials and Methods. RNA yield and concentration were quantified by NanoDrop spectrophotometry (ND1000) at a 260/280 absorbance ratio. The RNA was not DNase treated, as this degraded the RNA and interfered with gene amplification during qPCR. Instead, 'no RT' controls were included to assess contamination with genomic DNA. Genomic DNA contamination and RNA integrity were assessed by agarose/formaldehyde gel electrophoresis (see A.3.2. below). RNA samples were immediately aliquoted following quantification and stored at -80°C. RNA samples were only subjected to one freeze-thaw cycle.

A.3.1. RNA quantification

RNA was quantified by spectrophotometry using a NanoDrop ND1000 Spectrophotometer. RNA purity is shown Table 5.1, Table 5.2 and Table 5.3.

Table 5.1. Concentration of RNA isolated from DMS 79 cells. Following treatment of the DMS 79 cells with varying concentrations of 5-aza for 72 h, RNA was extracted from the cells using the RNeasy Mini Kit at P24 and P30. RNA concentration of each sample is shown.

Treatment	Biological repeat 1 Concentration (ng/µL)	Biological repeat 2 Concentration (ng/µL)
Control	402.8	323.7
0.5 µM	661.3	179.0
1 µM	881.9	801.6
5 µM	1083.8	594.2

Table 5.2. Concentration of RNA isolated from HEK cells. Following treatment of the HEK cells with varying concentrations of 5-aza for 72 h, RNA was extracted from the cells at P19 and P21 using the RNeasy Mini Kit. RNA concentration from each treatment is shown.

Treatment	Biological repeat 1 Concentration (ng/µL)	Biological repeat 2 Concentration (ng/µL)
Control	2465.9	2781.5
0.5 µM	607.0	2983.2
1 µM	232.4	2187.0
5 µM	2066.9	2202.1

Table 5.3. Concentration of RNA isolated from A549 cells. Following treatment of the A549 cells with varying concentrations of 5-aza for 72 h, RNA was extracted from the cells using the RNeasy Mini Kit. RNA concentration from each sample at P112 and P113 is shown.

Treatment	Biological repeat 1 Concentration (ng/µL)	Biological repeat 2 Concentration (ng/µL)
Control	3145.7	944.7
0.5 µM	2760.6	1995.3
1 µM	2998.3	2162.8
5 µM	1726.0	776.8

A.3.2. RNA gels

In accordance with the MIQE guidelines (Bustin *et al.*, 2009), the integrity of each RNA sample was validated before use in qPCR analyses. RNA samples (2 µg) were run on 1.5% agarose 2.2 M formaldehyde gels (see Appendix B.vi), with a 10 kb DNA MWM run in each gel. The gels

were imaged using a ChemiDoc™ XRS+ Imaging System with Image Lab™ software (Bio-Rad). The presence of two distinct, intact bands of 18 S rRNA and 28 S rRNA subunits were used to verify good quality RNA (see section 3.1 of the Results for RNA gel images).

A.4. Reverse transcription

Two different procedures were used to reverse transcribe RNA to cDNA. These procedures are described in section 2.3. of the Materials and Methods. The High Capacity RNA-to-cDNA Master Mix was the first method used, but this was later replaced by the Tetro cDNA Synthesis Kit.

For both reverse transcription procedures, a single cDNA synthesis reaction had a final volume of 20 µL. 1 µg Starting quantity of RNA was required for the High Capacity RNA-to-cDNA Master Mix kit, whereas 2 µg starting RNA was used for the Tetro cDNA Synthesis Kit. cDNA was diltuted with 20 µL nuclease-free water and aliquoted immediately to allow for only one thaw cycle for each qPCR run. cDNA was stored at -20°C until use.

The High Capacity RNA-to-cDNA Master Mix (Applied Biosystems), catalog number 4390777, was used for reverse transcription. The 5x Master Mix includes optimized concentrations of the components. The components of the 5x Master Mix include reverse transcriptase, recombinant RNase inhibitor protein, dNTPs, random primers, oligo(dT) primer and stabilizers, buffer, $MgCl_2$ and stabilizer.

The Tetro cDNA Synthesis Kit was also used for reverse transcription. The details of the reagents used are as follows (Table 5.4):

Table 5.4. Components and concentrations of reagents in the Tetro cDNA Synthesis Kit.

Reagent	Concentration
5x RT buffer	50 mM Tris-HCl (pH 8.6)
	40 mM KCl
	1 mM $MnSO_4$
	1 mM DTT
	0.5 mM [3H]TTP
Reverse transcriptase	200 u/µL
RNase inhibitor	10 u/µL
dNTP mix	10 mM total
Oligo $(dT)_{18}$ primer mix	200 µM

All reagents are part of the Tetro cDNA Synthesis Kit purchased from Bioline, catalog number BIO-65042, and were prepared using the DEPC-treated water provided in the kit. The inclusion of an RNase inhibitor protein reduced template degradation and increased the yield of the PCR product.

A.5. qPCR target gene and primer information

A summary of the qPCR target gene and primer information is presented in Table 2 of the Materials and Methods chapter. 100 µM primer stock solutions were stored at -20°C. Aliquots of 10 µM working solutions were used for qPCR reactions.

A.5.1. Blast specificity evaluation of primer set

The specificity of each primer set was evaluated by 'BLASTing' them against the entire *Homo sapien* genome in the NCBI database (www.ncbi.nlm.nih.gov) using the Primer BLAST tool (http://www.ncbi.nlm.nih.gov/tools/primer-blast/). The possible matches for each primer set, excluding the target sequence, were recorded and the data is available if required. The specificity of each primer set was confirmed by agarose gel electrophoresis of the PCR products (Fig. 5.1), as well as agarose gel electrophoresis of the qPCR products (see section A.7.1 of the Appendix).

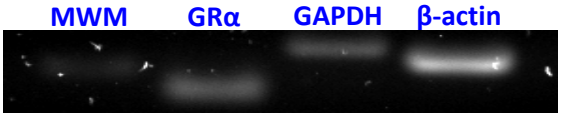

Figure 5.1. Validation of GRα, GAPDH and β-actin primer sets by agarose gel electrophoresis.

A.6. qPCR protocol

A.6.1. 5x HOT FIREPol® EvaGreen® qPCR Mix Plus (no ROX) protocol

The same protocol (Fig. 5.2) was used for all experimental runs that amplified target genes (Fig. 5.3) with 5x HOT FIREPol® EvaGreen® qPCR Mix Plus (no ROX) (Solis BioDyne). Each EvaGreen reaction consisted of 1 µL of diluted cDNA synthesised from 1 µg of RNA (the High Capacity RNA-to-cDNA Master Mix was used to synthesize cDNA used in EvaGreen reactions), 0.5 µL of the forward and reverse primer, 16 µL nuclease-free H_2O, and 2 µL 5x HOT FIREPol® EvaGreen® qPCR Mix Plus (no ROX), to a total standard reaction volume of 20 µL. 5x HOT FIREPol® EvaGreen® qPCR Mix Plus (no ROX) contains HOT FIREPol® DNA polymerase; 5x EvaGreen® qPCR buffer; 12.5 mM $MgCl_2$ (2.5 mM per 20 µL reaction); dNTPs; EvaGreen® dye; and NO ROX dye.

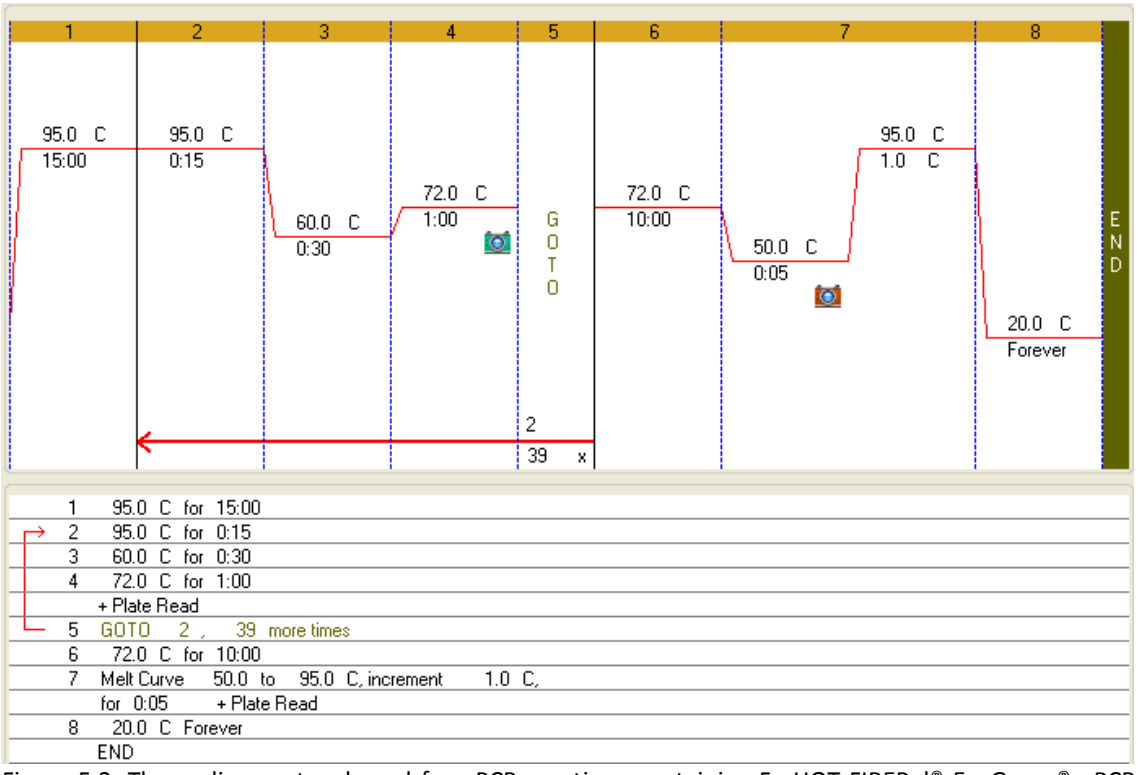

Figure 5.2. The cycling protocol used for qPCR reactions containing 5x HOT FIREPol® EvaGreen® qPCR Mix Plus (no ROX).

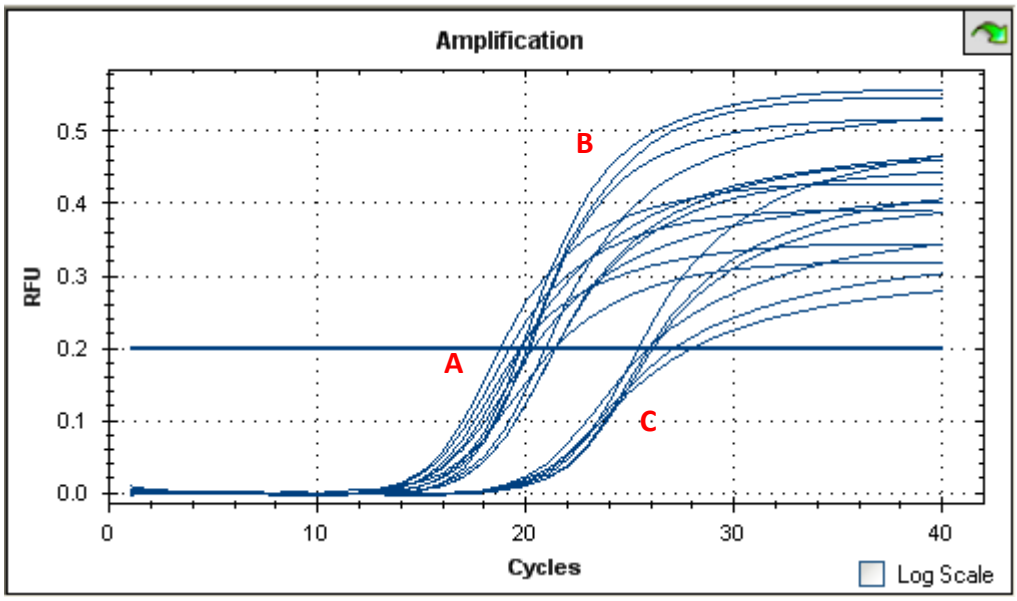

Figure 5.3. A representation of fluorescence curves amplified with 5x HOT FIREPol® EvaGreen® qPCR Mix Plus (no ROX) for A) GAPDH, B) β-actin and C) GRα.

A.6.2. SYBR® Green JumpStart™ *Taq* ReadyMix™ protocol

Similarly, the same protocol (Fig. 5.4) was used for all experimental runs that amplified target genes (Fig. 5.5) with SYBR® Green JumpStart™ *Taq* ReadyMix™ (Sigma®). Each SYBR Green reaction consisted of 1 µL of diluted cDNA synthesised from 2 µg of RNA (the Tetro cDNA Synthesis Kit was used to synthesize cDNA used in SYBR Green reactions), 0.5 µL of the forward and reverse primer, 10.5 µL nuclease-free H_2O, and 12.5 µL SYBR® Green JumpStart™ *Taq* ReadyMix™, to a total standard reaction volume of 25 µL. SYBR® Green JumpStart™ *Taq* ReadyMix™ contains 20 mM Tris-HCl at pH 8.3; 100 mM KCl; 7 mM $MgCl_2$; 0.4 mM of each dNTP (dATP, dCTP, dGTP and dTTP); stabilizers; 0.05 units/mL *Taq* DNA polymerase; JumpStart *Taq* antibody; and SYBR Green I.

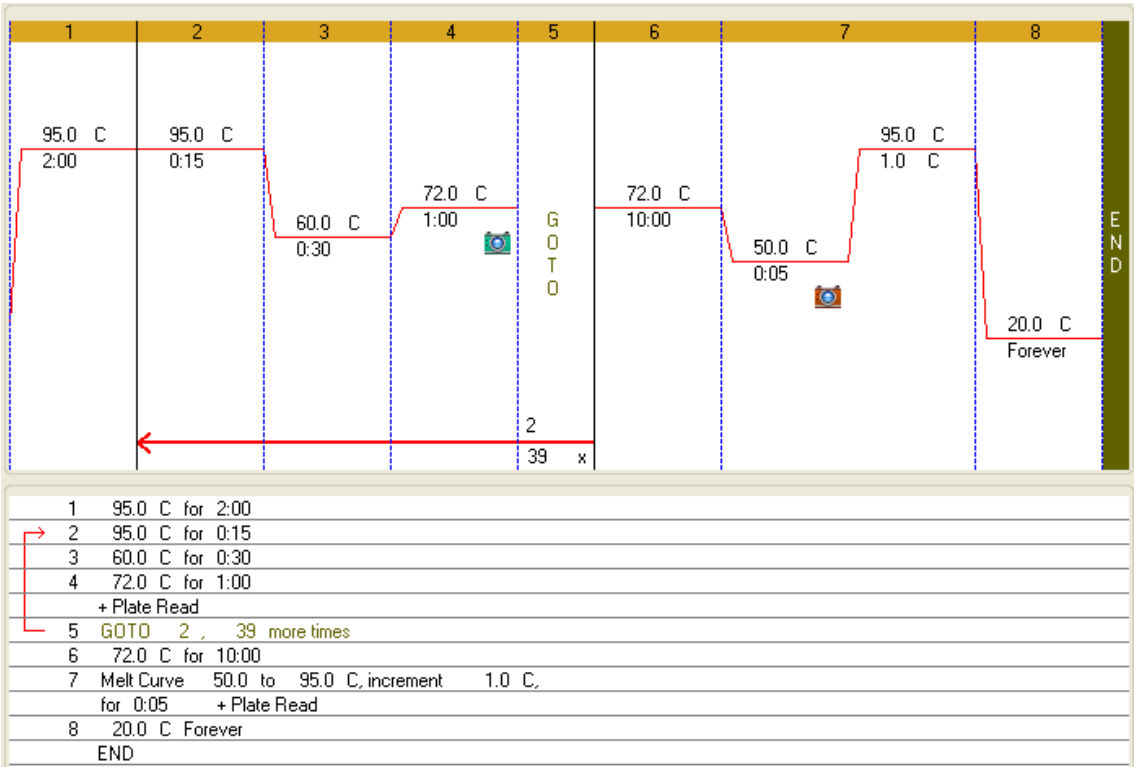

Figure 5.4. The cycling protocol used for qPCR reactions containing SYBR® Green JumpStart™ *Taq* ReadyMix™.

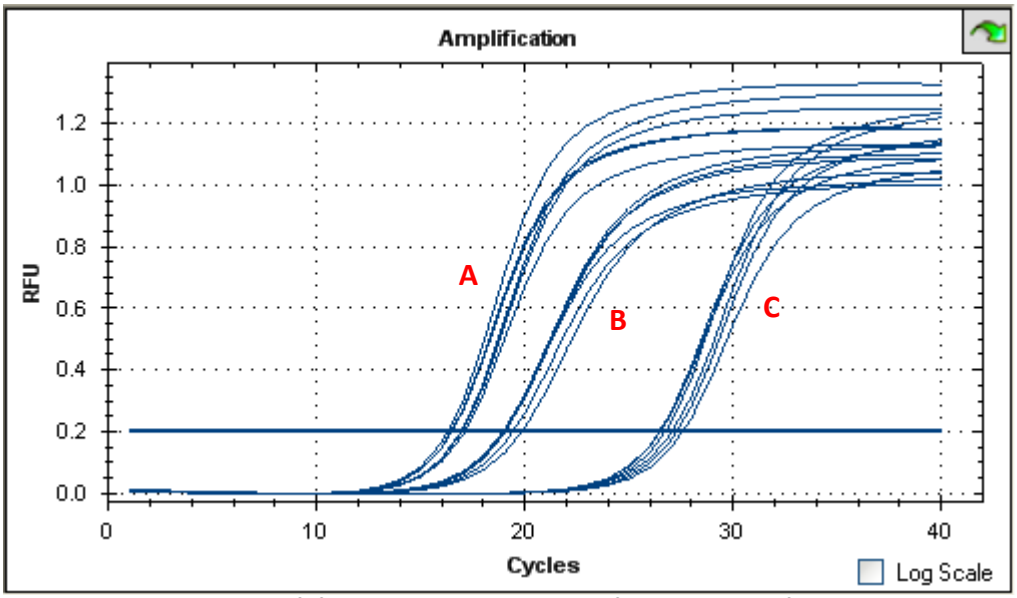

Figure 5.5. A representation of fluorescence curves amplified with SYBR® Green JumpStart™ *Taq* ReadyMix™ for A) GAPDH, B) β-actin and C) GRα.

qPCR plasticware consisted of 0.2 mL low profile white strip tubes (Bio-Rad), and optically clear flat cap strips (Bio-Rad). qPCR reactions were manually set up using the same set of Gilson Pipetman starter kit micropipettes (Gilson) with TipOne bevelled filter tips (Starlab) across all experiments and runs. All reagents were kept on ice and reactions were prepared on ice for the entire procedure. A MiniOpticon™ Real-Time PCR Detection System (Bio-Rad) was used for all qPCR runs. The CFX Manager™ Software version 2.1 (Bio-Rad) software package was used to define qPCR reaction parameters, and for the analyses of amplification readings. C_q readings were determined by using the single threshold setting on the CFX manager software. Fluorescence was read in the FAM channel and not the SYBR1 channel as a bug in the initial version of the software package prevented the use of the SYBR1 channel. The plate-type setting MJ white was used for all experimental runs. The baseline value for fluorescence readings was set to a standardised value of 0.2 RFU for all experimental runs (see Fig. 5.3 and Fig. 5.5).

A.7. qPCR validation

A.7.1. qPCR melt analysis verification

The melt curve analysis for each qPCR target and its verification by agarose gel electrophoresis are presented in the figures below (Fig. 5.6, Fig. 5.7 and Fig. 5.8). A single melting temperature was shown to correspond to a single product for each primer set. A 10 kb GeneRuler™ DNA Ladder Mix (Fermentas) was run as the MWM on each gel to confirm the size of the products.

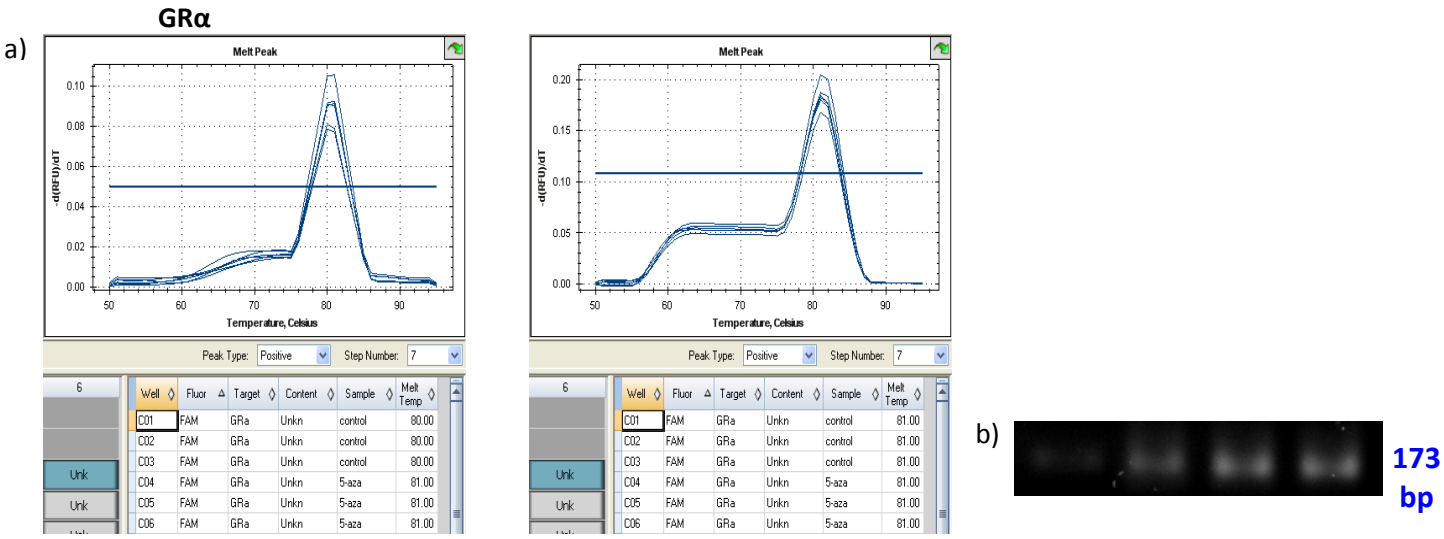

Figure 5.6. Melt curve analysis and gel verification of GRα primers. (a) GRα qPCR melting temperature at 81°C and (b) validation of GRα qPCR product by agarose gel electrophoresis.

GAPDH

a)

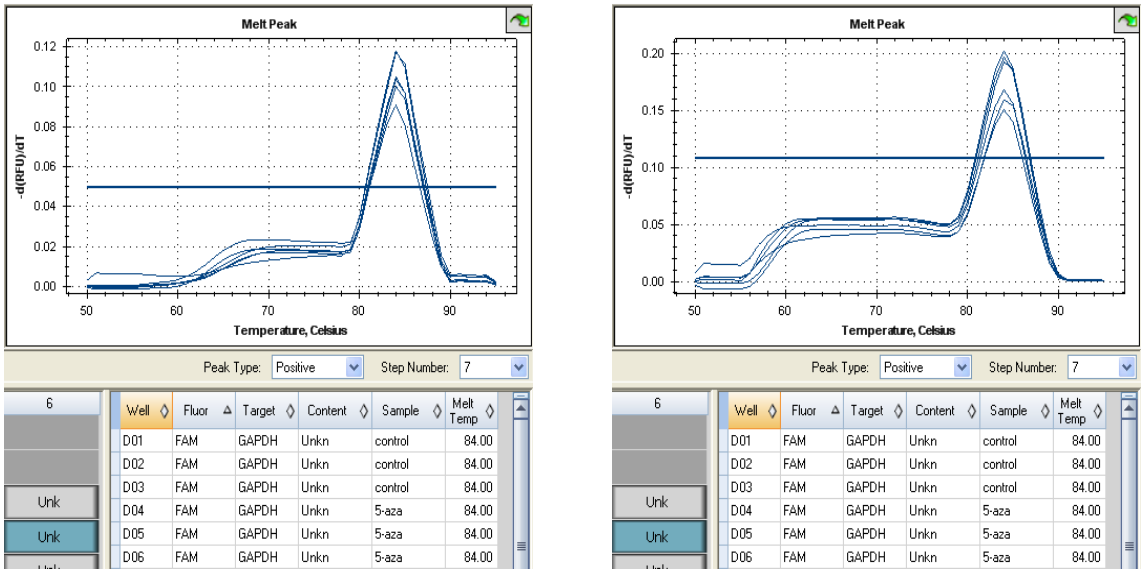

b)

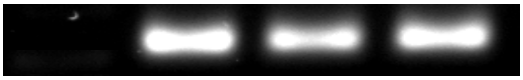

Figure 5.7. Melt curve analysis and gel verification of GAPDH primers. (a) GAPDH qPCR melting temperature at 84°C and (b) validation of GAPDH qPCR product by agarose gel electrophoresis.

β-actin

a)

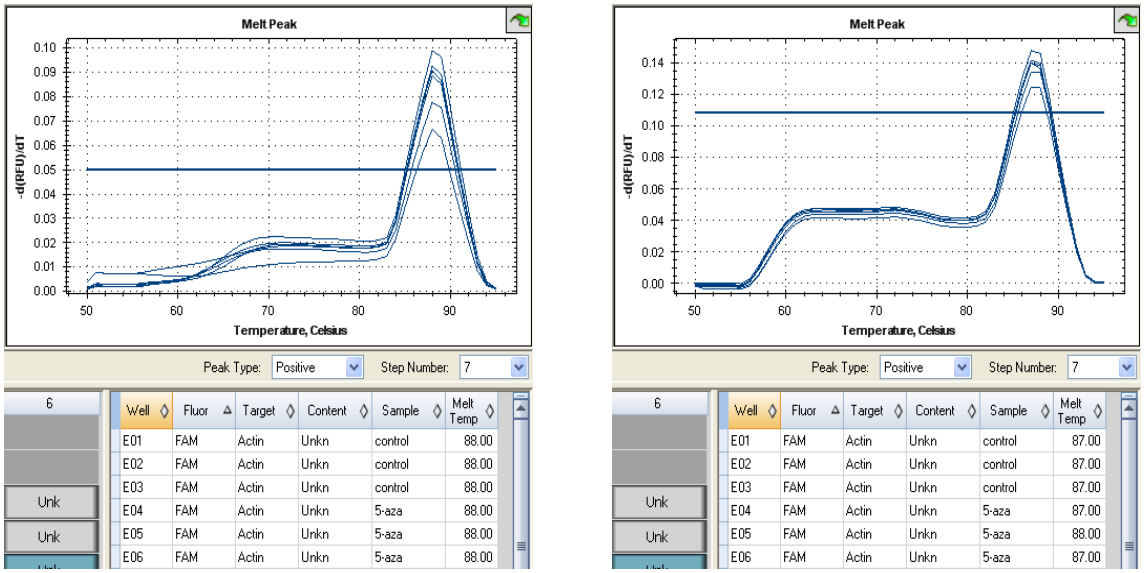

b)

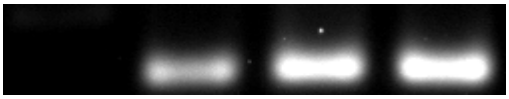

Figure 5.8. Melt curve analysis and gel verification of β-actin primers. (a) β-Actin qPCR melting temperature at 87/88°C and (b) validation of β-actin qPCR product by agarose gel electrophoresis.

A.7.2. Evaluation of qPCR reaction efficiency

For the $2^{-\Delta\Delta CT}$ method to be applicable, an $r^2 > 0.98$ and a reaction efficiency between 90% and 110% should be obtained. The reaction efficiency of the gene of interest (GRα) should be equal to that of the reference genes, GAPDH and β-actin (Livak and Schmittgen, 2001).

As discussed in section 2.5.4.2. of the Materials and Methods, the reaction efficiencies of each target gene were evaluated by qPCR analysis of serial 10x dilutions of template cDNA. Equal reaction efficiencies of the gene of interest and reference genes were denoted by a slope value close to zero in the linear analysis of average Cq vs. cDNA concentration. The relevant r^2 value and reaction efficiency for each target gene are presented below (Fig. 5.9).

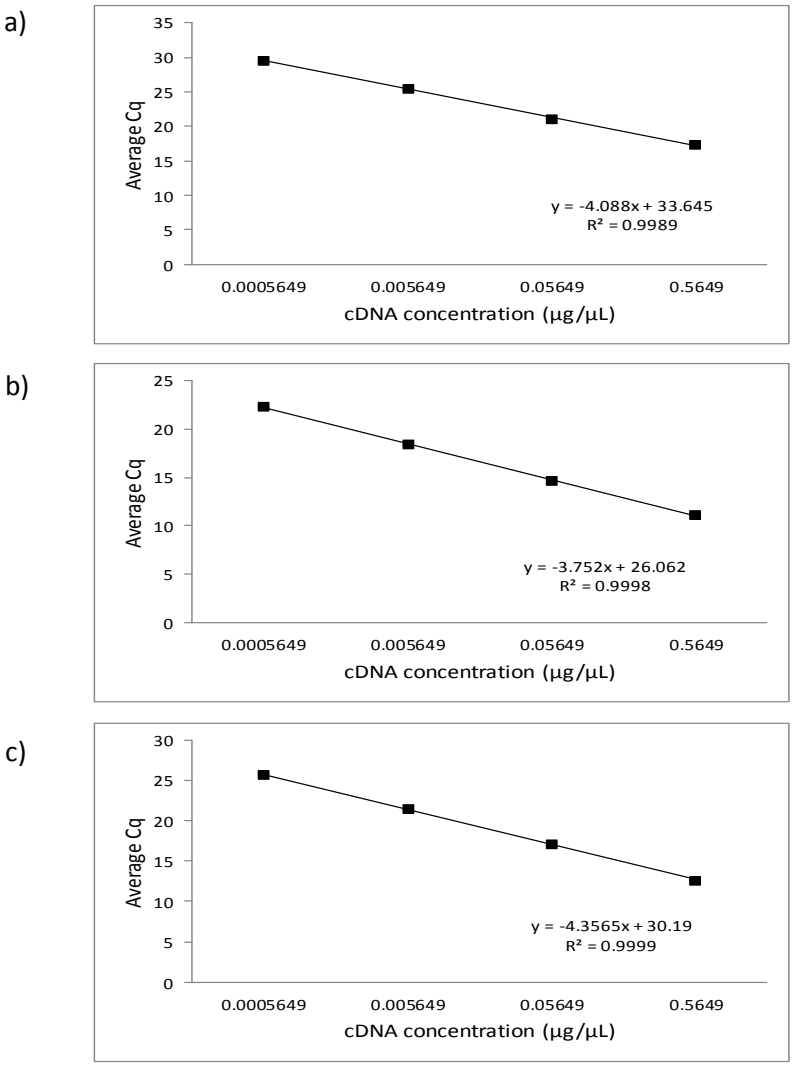

Figure 5.9. Linear analysis of (a) GRα ($r^2 = 0.9989$; reaction efficiency = 75.638%), (b) GAPDH ($r^2 = 0.9998$; reaction efficiency = 84.725%) and (c) β-actin ($r^2 = 0.9999$; reaction efficiency = 69.645%) qPCR reaction efficiencies.

A.8. Data analysis

CFX Manager™ Software version 2.1 (Bio-Rad) was used to analyse qPCR data. C_q values for each experiment were determined by fluorescence readings at the 0.2 RFU baseline. This baseline was standardised across all experimental runs, for both EvaGreen and SYBR Green reactions. Outliers or C_q values that did not meet the criteria were excluded from analyses. Criteria for the exclusion of reactions are shown in Fig. 5.11. The NTC and no-RT controls for each qPCR target were determined to either result in the formation of primer dimers, or have no product at all (see Fig. 5.13 and Fig. 5.15). Primer dimer formation is verified by a melt temperature lower than 80°C, and by agarose gel electrophoresis.

A.8.1. Justification for use of reference genes

Two reference genes were used for qPCR analyses. GAPDH and β-actin are both well-known reference genes that have been widely used in experimental research. Alt *et al.* (2010) conducted a study in which RT-PCR was performed using primers for GAPDH, β-actin and GRα. GRα levels remained stable whether analysed against GAPDH or β-actin. Therefore results obtained relative to GAPDH and/or β-actin are comparable. β-Actin was however ultimately identified as the more stable reference gene (Alt *et al.*, 2010).

A.8.2. The $2^{-\Delta\Delta CT}$ method

Reactions for each target gene in each treatment/control were repeated in triplicate in a single qPCR experimental run. The average C_q for each target in each treatment was then normalised against GAPDH and β-actin individually, as well as the geometric mean of the two reference genes (Vandesompele *et al.*, 2002) (see Fig. 5.10). The fold change values were calculated by use of the $2^{-\Delta\Delta CT}$ method, which uses the following equations:

Average C_q (gene of interest) – average C_q (reference gene) = ΔC_T

$\Delta\Delta C_T = \Delta C_T$ (treatment) – ΔC_T (control)

Thus, $\Delta\Delta C_T$ (control) = ΔC_T (control) – ΔC_T (control) = 0

Therefore $2^{-\Delta\Delta CT}$ of control = $2^0 = 1$ and for each treatment the fold change value = $2^{-(\Delta CT\ (treatment)\ -\ \Delta CT\ (control))}$

Example:

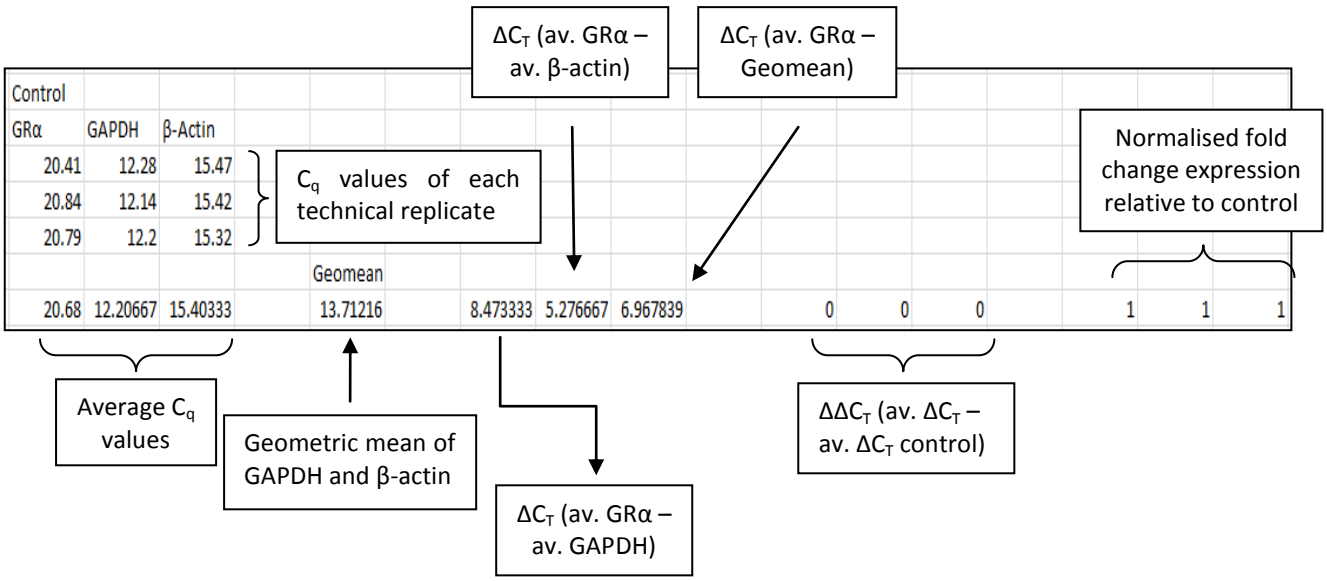

Figure 5.10. Example of the $2^{-\Delta\Delta CT}$ equations used to calculate fold change values.

A.8.3. Statistical analyses

The statistical significance of the relative fold change values for GRα expression of the treatments relative to the control were determined by one-way ANOVA. IBM SPSS Statistics Version 21 was the statistical analysis software package used. Two assumptions of the one-way ANOVA must be satisfied in order for the ANOVA results to be valid. The assumption of the ANOVA that the residuals from the analysis are normally distributed, was determined by the one-sample Kolmogorov-Smirnov test. The other assumption that the residuals must be homoscedastic, was tested with the Levene's test. The Bonferroni t-test was the multiple comparisons analysis performed to determine whether there were significant differences between the GRα expression of the control and the GRα expression of the treatments. $p < 0.05$ was considered statistically significant. Fold change values were presented as bar graphs along with the standard error of the mean fold change values (see Results section 3.2).

Description	Value	Use	Results	Exclude Wells
Negative control with a Cq less	38	☑		☐
NTC with a Cq less than	38	☑		☐
NRT with a Cq less than	38	☑		☐
Positive control with a Cq great	30	☑		☐
Unknown without a Cq	N/A	☑		☐
Standard without a Cq	N/A	☑		☐
Efficiency greater than	110.0	☑		
Efficiency less than	90.0	☑		
Std Curve R^2 less than	0.980	☑		
Replicate group Cq Std Dev gre	0.20	☑		☐

Figure 5.11. The parameters used to exclude reactions from $2^{-\Delta\Delta CT}$ analyses, as shown in the CFX Manager™ Software program.

A.8.4. NTC data

The relevant NTC data for GRα, GAPDH and β-actin are shown below. The GRα NTC quantitation data (Fig. 5.12) showed that NTC samples had C_q values > 10, whereas GAPDH and β-actin had C_q values > 21 and 30 respectively.

However the melt curve analyses for the GRα, GAPDH and β-actin NTC samples (Fig. 5.13) showed that no product was amplified by these primer sets. The melt curve analyses and NTC quantitation data thus suggest that there is no contamination present or that if there is, it cannot be amplified by the GRα, GAPDH and β-actin primer sets.

Well	Fluor	Target	Content	Sample	Cq	Cq Mean	Cq Std. Dev
C02	FAM	GR	Unkn	NTC	34.30	34.30	0.000
C03	FAM	GR	Unkn	NTC	27.80	27.80	0.000
C04	FAM	GR	Unkn	NTC	10.15	10.15	0.000
D02	FAM	GAPDH	Unkn	NTC	37.50	37.50	0.000
D03	FAM	GAPDH	Unkn	NTC	21.67	21.67	0.000
D04	FAM	GAPDH	Unkn	NTC	31.11	31.11	0.000
E02	FAM	Actin	Unkn	NTC	31.10	31.10	0.000
E03	FAM	Actin	Unkn	NTC	30.61	30.61	0.000
E04	FAM	Actin	Unkn	NTC	33.72	33.72	0.000

Figure 5.12. Quantitation data of GRα, GAPDH and β-actin NTC reactions.

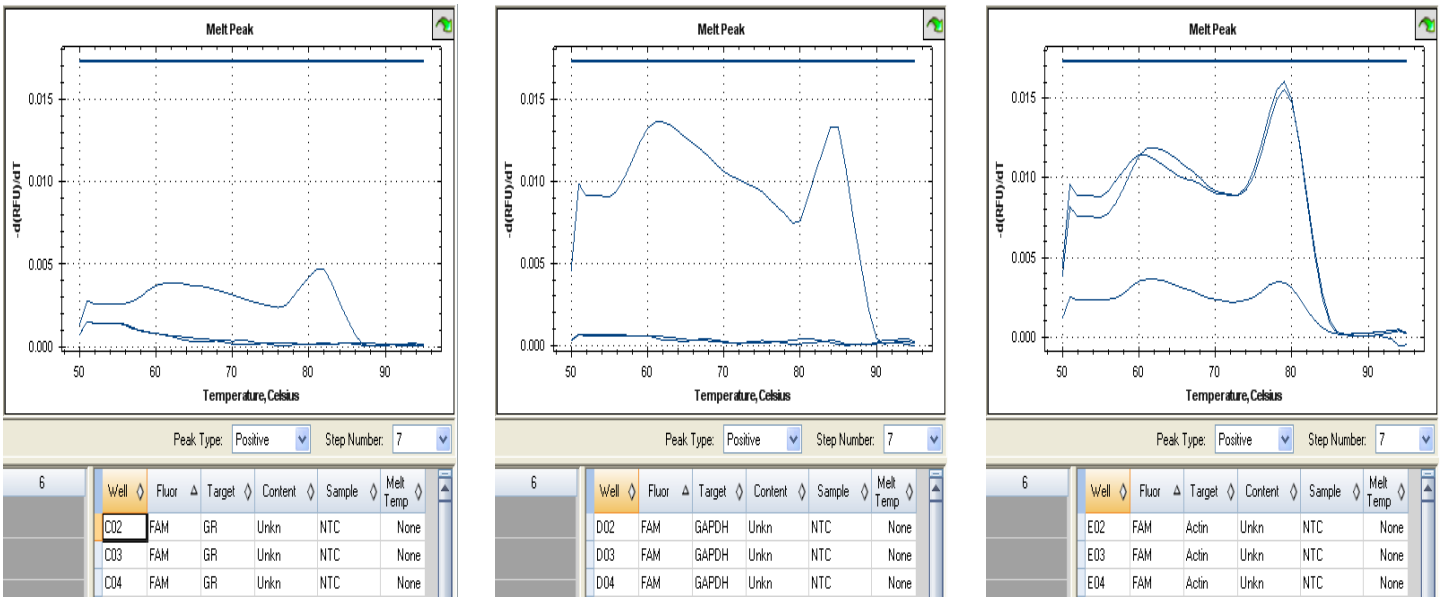

Figure 5.13. Melt curve analyses for GRα, GAPDH and β-actin NTC samples. Amplification of the NTC samples resulted in the formation of either primer dimers, or there was no amplification at all.

A.8.5. No-RT data

The relevant no-RT data for GRα, GAPDH and β-actin are shown below. The no-RT control quantitation data for GRα (Fig. 5.14) showed that no-RT samples had a either a C_q value > 36, or one that was not applicable. No-RT GAPDH samples had a C_q value > 35, or one that was not applicable, whereas β-actin no-RT samples had C_q values > 31 (Fig. 5.14). The melt curve analyses for the GRα, GAPDH and β-actin no-RTs (Fig. 5.15) also show either the formation of primer dimers or no amplification at all. The melt curve analyses and no-RT quantitation data thus suggest that there is no contamination with genomic DNA or that if there is, it cannot be amplified by the GRα, GAPDH and β-actin primer sets.

Well	Fluor	Target	Content	Sample	Cq	Cq Mean	Cq Std. Dev
C01	FAM	GR	Unkn	control	36.32	36.32	0.000
C02	FAM	GR	Unkn	control	N/A	0.00	0.000
C03	FAM	GAPDH	Unkn	control	N/A	0.00	0.000
C04	FAM	GAPDH	Unkn	control	39.43	39.43	0.000
C05	FAM	Actin	Unkn	control	32.65	32.65	0.000
C06	FAM	Actin	Unkn	control	32.01	32.01	0.000
D01	FAM	GR	Unkn	0.5 uM	N/A	0.00	0.000
D02	FAM	GR	Unkn	0.5 uM	N/A	0.00	0.000
D03	FAM	GAPDH	Unkn	0.5 uM	39.52	39.52	0.000
D04	FAM	GAPDH	Unkn	0.5 uM	38.46	38.46	0.000
D05	FAM	Actin	Unkn	0.5 uM	32.71	32.71	0.000
D06	FAM	Actin	Unkn	0.5 uM	33.43	33.43	0.000
E01	FAM	GR	Unkn	1 uM	N/A	0.00	0.000
E02	FAM	GR	Unkn	1 uM	N/A	0.00	0.000
E03	FAM	GAPDH	Unkn	1 uM	N/A	0.00	0.000
E04	FAM	GAPDH	Unkn	1 uM	39.43	39.43	0.000
E05	FAM	Actin	Unkn	1 uM	33.36	33.36	0.000
E06	FAM	Actin	Unkn	1 uM	34.40	34.40	0.000
F01	FAM	GR	Unkn	5 uM	39.72	39.72	0.000
F02	FAM	GR	Unkn	5 uM	N/A	0.00	0.000
F03	FAM	GAPDH	Unkn	5 uM	35.90	35.90	0.000
F04	FAM	GAPDH	Unkn	5 uM	36.95	36.95	0.000
F05	FAM	Actin	Unkn	5 uM	33.39	33.39	0.000
F06	FAM	Actin	Unkn	5 uM	31.41	31.41	0.000

Figure 5.14. Quantitation data of GRα, GAPDH and β-actin no-RT samples. C_q values were detected as > 36 or not applicable, indicating that there was no target gene amplification.

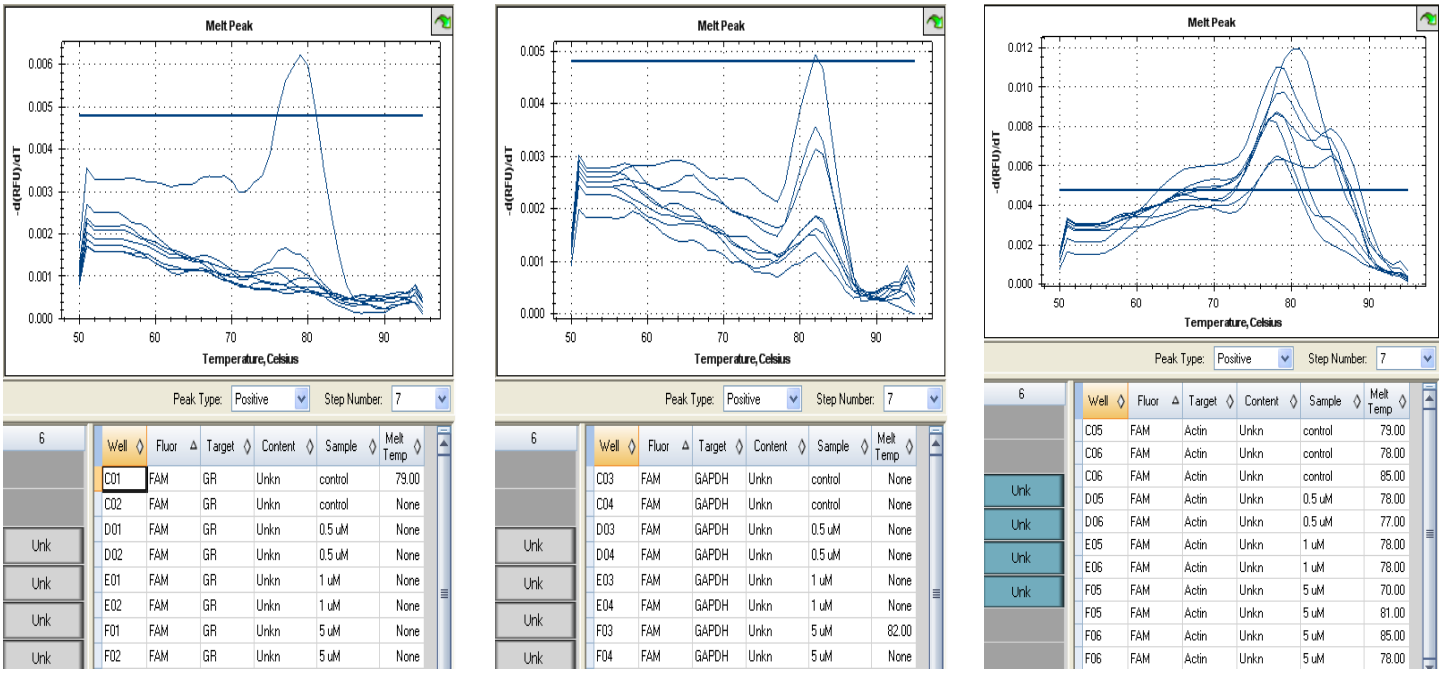

Figure 5.15. Melt curve analyses for GRα, GAPDH and β-actin no-RT samples across the various treatments. Amplification of the no-RT samples resulted in the formation of either primer dimers, or there was no amplification at all.

B. General recipes

i. 1x Trypsin-EDTA solution

Reagent	10 mL Volume
10x Trypsin	1 mL
Sodium EDTA	9 mL

1 part 10x Trypsin was diluted with 9 parts sodium EDTA.

ii. 5-Aza

Reagent	Volume
5-Aza	5 mg
Acetic acid	50 µL
Distilled water	50 µL

5-Aza was dissolved in 50% acetic acid and 50% distilled water. A 1:100 dilution was then made in the appropriate cell culture medium.

iii. Vehicle Control

Reagent	Volume (µL)
Acetic acid	0.5
Cell culture medium	99.5

Filter sterilized acetic acid was diluted in the appropriate cell culture medium.

iv. 1x PBS Buffer

Reagent	1 L Volume
NaCl (Merck)	8 g
KCl (Merck)	0.2 g
Na_2HPO_4 (Merck)	1.44 g
KH_2PO_4 (Merck)	0.24 g
Distilled water	800 mL

The components were dissolved in 800ml distilled H_2O and the pH adjusted to 7.4. The volume was adjusted to 1 L with additional distilled H_2O. The PBS was sterilized by autoclaving.

v. 70% Ethanol

Reagent	50 mL Volume (mL)
100% Ethanol	35
Distilled water	15

Distilled water was combined with 100% ethanol to yield a 70% volume.

vi. Agarose/formaldehyde RNA gel

DEPC treatments:

DEPC H_2O

Reagent	1 L Volume
DEPC (Sigma®)	100 µL
Di.H_2O	1 L

DEPC was added to the di.H_2O. The solution was incubated at 37°C for 2 h, then autoclaved and allowed to cool before use.

1 M NaOAc

Reagent	100 mL Volume
NaOAc (Sigma®)	8.203 g
DEPC	100 µL
Di.H_2O	100 mL

NaOAc was dissolved in 100 mL di.H_2O. DEPC was then added to the solution.

0.5 M EDTA

Reagent	80 mL Volume
EDTA (Merck)	18.6 g
DEPC	100 µL
Di.H_2O	100 mL

EDTA was dissolved in di.H_2O containing DEPC. The pH was adjusted to 8.0 by the addition of NaOH.

To make up ethidium bromide stock solution:

Reagent	1 mL Volume
Ethidium bromide	10 mg
Di.H_2O	1 mL

Ethidium bromide was dissolved in di.H_2O to make a 10 mg/mL stock solution.

Ethidium bromide working solution

The ethidium bromide stock solution was diluted 1:200 in di.H_2O to create a 0.05 mg/mL working solution.

DEPC ethidium bromide

Reagent	10 mL Volume
Ethidium bromide working solution	10 mL
DEPC	10 µL

Ethidium bromide was treated with DEPC.

10x MOPS buffer

Reagent	100 mL Volume
MOPS (Sigma®)	4.18 g
1 M NaOAc (DEPC-treated)	2 mL
0.5 M EDTA, pH 8 (DEPC-treated)	2 mL
DEPC H_2O	100 mL

MOPS was dissolved in DEPC H_2O. 1 M NaOAc and 0.5 M EDTA were added to the solution.

1.5% Agarose 2.2 M formaldehyde gel

Reagent	110 mL Volume
Agarose	1.5 g
DEPC H_2O	72 mL
DEPC-treated ethidium bromide	10 µL
10x MOPS buffer	10 mL
Deionized formaldehyde (Merck)	18 mL

Agarose was melted in DEPC H_2O and allowed to cool to 55°C. DEPC-treated ethidium bromide was added to the solution, followed by 10x MOPS buffer and deionized formaldehyde.

1x MOPS running buffer

10x MOPS buffer was diluted 1:10 to yield 1x MOPS buffer.

vii. TE buffer

To prepare 1 M Tris-base:

Reagent	100 mL Volume
Tris-base (Merck)	12.1 g
Distilled water	100 mL

Tris-base was dissolved in 70 mL distilled water. The pH of the solution was adjusted to pH 8.0 by the addition of HCl. The total solution volume was then made up to 100 mL with distilled water.

To prepare 0.5 M EDTA:

Reagent	100 mL Volume
EDTA	18.6 g
Distilled water	80 mL

EDTA was dissolved in distilled water. The pH was adjusted to 8.0 by the addition of NaOH. The solution was then made up to 100 mL with distilled water.

To make up TE buffer:

Reagent	1000 mL Volume (mL)
1 M Tris-base	10
0.5 M EDTA	2
Distilled water	990

1 M Tris-base and 0.5 M EDTA were diluted with distilled water.

viii. 1.5% Agarose gel

Reagent	40 mL Volume
Agarose	0.6 g
1x TBE running buffer	40 mL
0.5 µg/mL Ethidium bromide	2.5 µL

The agarose was melted in 1x TBE running buffer. The solution was allowed to cool before ethidium bromide was added.

To make up ethidium bromide solution:

The ethidium bromide stock solution was prepared as above in Appendix B.vi.

Ethidium bromide working solution

Reagent	100 mL Volume
Ethidium bromide	500 µL
1x TBE buffer	100 mL

The ethidium bromide stock solution was diluted 1:200 in 1x TBE buffer to create a 0.05 mg/mL working solution.

ix. 1x TBE running buffer

To make up 10x TBE running buffer:

Reagent	400 mL Volume
Tris-base	43.2 g
Boric acid (Merck)	22 g
EDTA	3.72 g
Distilled water	320 mL

Tris-base, boric acid and EDTA were dissolved in 320 mL distilled water.

To make up 1x TBE running buffer:

Reagent	1 L Volume
10x TBE running buffer	100 mL
Distilled water	900 mL

10x TBE running buffer was diluted with distilled water.

C. Immunoblot recipes

i. Reducing sample treatment buffer

Reagent	10 mL Volume
4x Stacking gel buffer (see Appendix D.iii)	2.5 mL
10% SDS stock solution (see Appendix D. ii)	4 mL
Glycerol	2 mL
2-Mercaptoethanol (Sigma®)	1 mL
Bromothymol blue (Sigma®)	0.1 g
Di.H_2O	0.5 mL

The stacking gel buffer, SDS solution, glycerol and 2-mercaptoethanol were mixed together. Approximately 0.1g bromothymol blue was added to the solution, or until the solution was dark blue/purple. The solution was then made up to 10 mL with d.H_2O.

ii. 10% SDS stock solution

Reagent	50 mL Volume
SDS (Calbiochem)	5.00 g
Di.H_2O	50 mL

SDS was dissolved in di.H_2O to create a 10% m/v solution.

To make a 1% SDS solution:

Reagent	50 mL Volume
10% SDS stock solution	5 mL
Di.H_2O	45 mL

10% SDS stock solution was diluted with di.H_2O to create a 1% solution.

iii. 13.5% SDS PAGE gel

Solutions	Resolving gel (13.5%)	Stacking gel (4%)
30% Bis-acrylamide solution (Bio-Rad)	3.375 mL	0.47 mL
4x Running gel buffer	1.875 mL	/
4x Stacking gel buffer	/	0.875 mL
Di.H_2O	2.099 mL	2.15 mL
10% SDS	75 µL	35 µL
15% APS initiator	37.5 µL	17.5 µL
TEMED (Sigma®)	3.75 µL	7.5 µL

To make 4x running gel buffer:

Reagent	50 mL Volume
Tris-HCl (Calbiochem)	9.09 g
Di.H_2O	50 mL

Tris-HCl was dissolved in 50 mL di.H_2O and pH titrated to 8.8 with NaOH.

To make 4x stacking gel buffer:

Reagent	50 mL Volume
Tris-HCl	3.00 g
Di.H_2O	50 mL

Tris-HCl was dissolved in 50 mL di.H_2O and pH titrated to 6.8 with NaOH.

To make a 15% ammonium persulfate (APS) initiator solution:

Reagent	500 µL Volume
Ammonium persulfate	0.033 g
Di.H_2O	500 µL

Ammonium persulfate was dissolved in di.H_2O to create a 15% m/v solution.

iv. 1x Electrode Buffer

Reagent	1000 mL Volume
Tris-HCl	3.0 g
Glycine (Sigma®)	14.4 g
SDS	10 mL
Di.H_2O	990 mL

Tris-HCl and glycine were dissolved in 800 mL di.H_2O. SDS was then added to the solution. The pH was adjusted to 8.3, and the volume was adjusted to 1 L with additional di.H_2O.

v. Protein Transfer Buffer

Reagent	1000 mL Volume
Tris-base	3.03 g
Glycine	14.4 g
Methanol (Merck)	200 mL
SDS	1 g
Di.H_2O	600 mL

Tris-base, glycine and SDS were made up to 600 mL with di.H_2O. Methanol was then added and the solution pH titrated to 8.3. The volume was adjusted to 1 L with additional di.H_2O.

vi. Tris-Buffered Saline-Tween

Reagent	1000 mL Volume
NaCl	8 g
KCl	0.2 g
Tris-base	3 g
Tween 20	1 mL
Di.H_2O	800 mL

NaCl, KCl and Tris-base were dissolved in 800 mL di.H_2O. The solution was pH titrated to 7.5. The volume was adjusted to 1 L with additional di.H_2O and tween was added.

vii. 6% Skim milk blocking buffer solution

Reagent	50 mL Volume
Skim milk powder (Sigma®)	3 g
Di.H_2O	50 mL

The skim milk powder solution was made up to 50 mL with di.H_2O.

D. Recipes for flow cytometry and microscopy

i. Camptothecin

Reagent	Volume
Camptothecin	8.7 mg
DMSO	870 µL

Camptothecin was dissolved in DMSO at a concentration of 10 mg/mL. The solution was heated at 95°C for 10 min to completely dissolve the product. A 1:100 dilution was made in the appropriate cell culture medium.

ii. 1x Annexin V Binding Buffer

1 part 10x Annexin V Binding Buffer (0.1 M HEPES/NaOH (pH 7.4), 1.4 M NaCl, 25 mM $CaCl_2$; provided in the FITC Apoptosis Detection Kit) was diluted with 9 parts autoclaved distilled water.

iii. Dexamethasone

5 mg Dex was dissolved in 5 mL ethanol to make a concentration of 1 mg/mL. The Dex solution was then diluted 1:100 in the appropriate cell culture medium.

iv. RU486

50 mg RU486 was dissolved in 1 mL ethanol to yield a concentration of 50 mg/mL. A 1:100 dilution was then made in the appropriate cell culture medium.

v. DAPI

A 1:50 dilution of DAPI was made by diluting 1 part DAPI in 49 parts 1x PBS.

vi. Mowiol mountant

Reagent	100 mL Volume
Mowiol 40-88 (Sigma®)	8 g
0.2 M Tris buffer (pH 8.5)	40 mL
Distilled H_2O	25 mL
Glycerol (Merck)	25 mL
DABCO (Sigma®)	1 g

The Tris buffer and distilled H_2O were added to a beaker which was placed on a magnetic stirrer and heated to 60 °C. The mowiol was then added to the solution and the beaker was covered in foil. The mowiol was allowed to dissolve for several hours to form a viscous solution. The glycerol and DABCO were then added to the mixture which was again heated to 60 °C and stirred until the reagents had dissolved. The mixture was stirred for several hours to form a homogenous solution. The mountant was then aliquoted and stored in the dark at -20°C. The mountant was brought to room temperature 5 - 10 min before use and once mounted, slides were stored at 4 °C.

E. Flow cytometry quadrant dot plots

i. Quadrant dot plots of HEK cells

a)

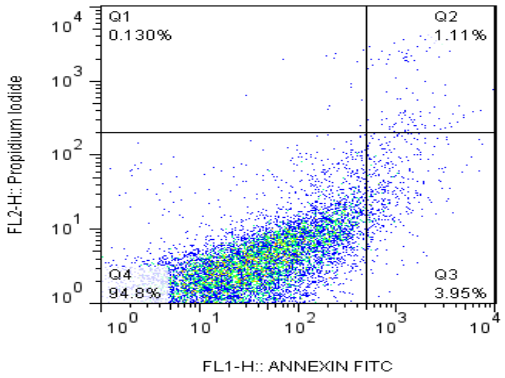

b)

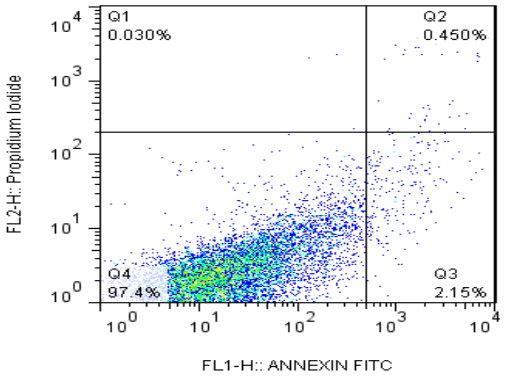

c)

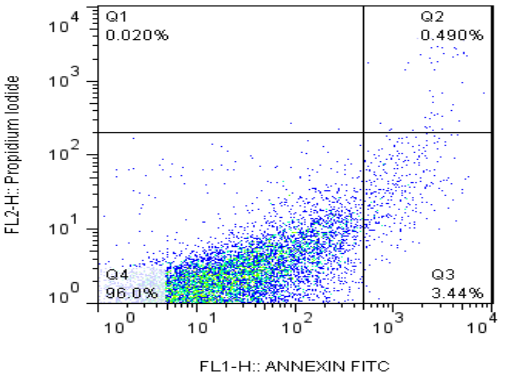

d)

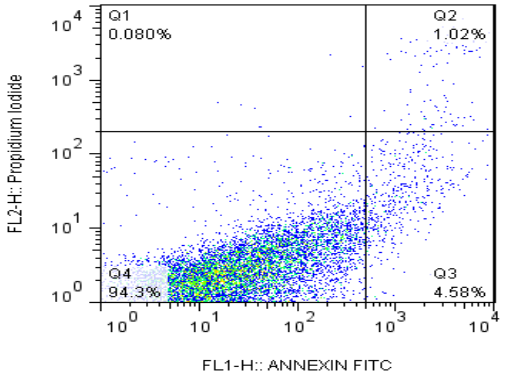

e)

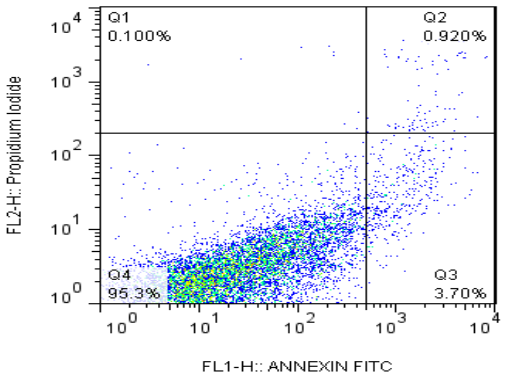

Figure 5.16. Treatment with 5-aza resulted in negligible cell death and apoptosis in HEK cells. The HEK cell line was treated with various concentrations of 5-aza for 72 h. There was an untreated control. Cells were then analysed by flow cytometry for viability by PI, and apoptosis by FITC Annexin V. The percentage of PI and FITC Annexin V positive cells were established in the cells subsequent to treatment with (a) no treatment, (b) vehicle, (c) 0.5 µM, (d) 1 µM, and (e) 5 µM 5-aza.

ii. Quadrant dot plots of DMS 79 cells

a)

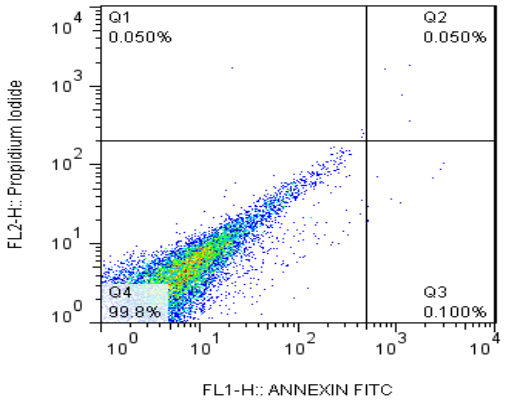

b)

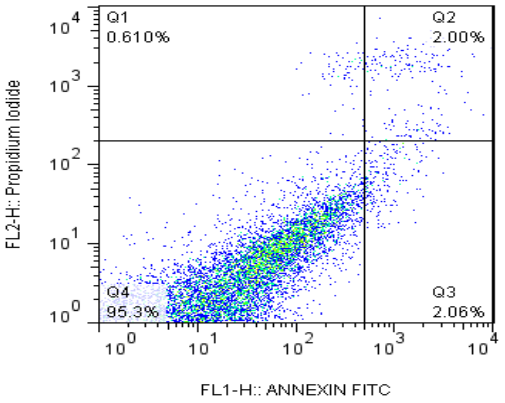

c)

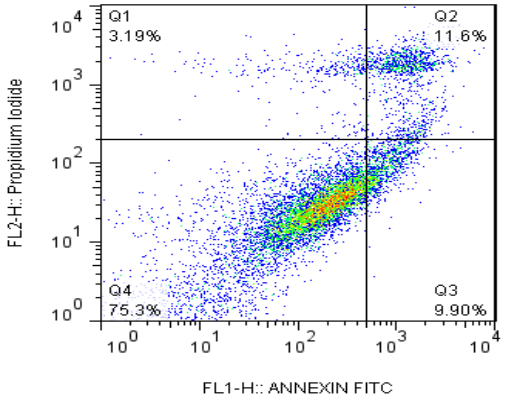

d)

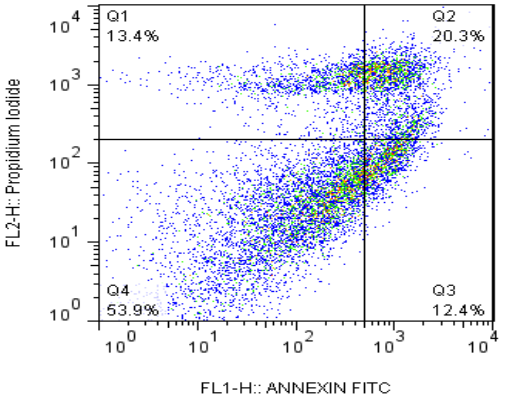

e)

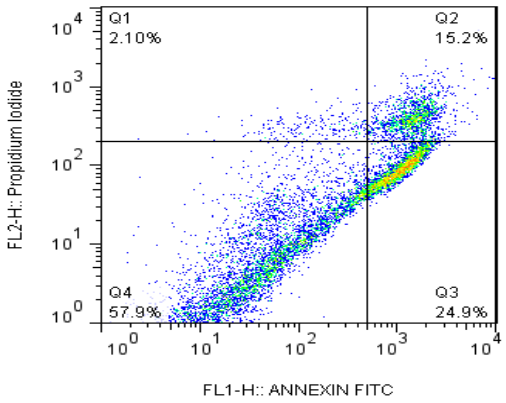

Figure 5.17. Treatment with 5-aza resulted in negligible cell death and apoptosis in DMS 79 cells. The DMS 79 cell line was treated with various concentrations of 5-aza for 72 h. There was an untreated control. Cells were then analysed by flow cytometry for viability by PI, and apoptosis by FITC Annexin V. The percentage of PI and FITC Annexin V positive cells were established in the cells subsequent to treatment with (a) no treatment, (b) vehicle, (c) 0.5 µM, (d) 1 µM, and (e) 5 µM 5-aza.

F. Microscopy images

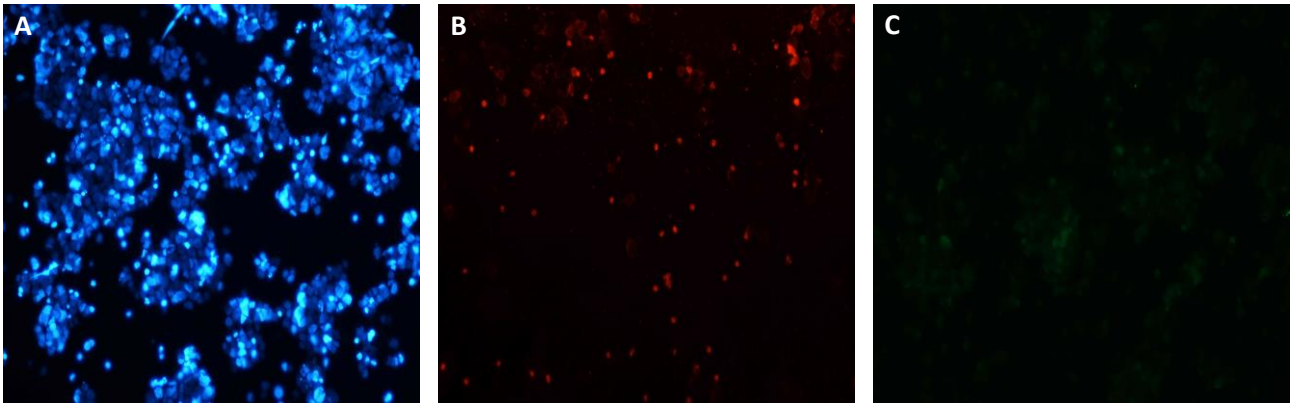

Figure 5.18. Representative microscopy images of DMS 79 and HEK cells. The HEK and DMS 79 cell lines were treated with either vehicle control, 0.5 µM, 1 µM or 5 µM 5-aza; 0.5 µM 5-aza and Dex or RU486; or untreated for 72 h. Cells were then analysed by microscopy for viability by PI, and apoptosis by FITC Annexin V and DAPI. The percentage of PI, FITC Annexin V, and DAPI positive cells with condensed chromatin were established in the cells subsequent to treatment. DMS 79 cells stained with (A) DAPI, (B) PI and (C) FITC Annexin V are presented (X200).

6. LITERATURE CITED

Bai, W., Rowan, B.G., Allgood, V.E., O'Malley, B.W., Weigel, N.L. 1997. Differential phosphorylation of chicken progesterone receptor in hormone-dependent and ligand-independent activation. The Journal of Biological Chemistry 272: 10457-10463.

Baylin, S.B., Futscher, B.W., Gore, S.D. 2004. Understanding DNA methylation and epigenetic gene silencing in cancer. Current Therapeutics 1: 1-25.

Baylin, S.B., Jones, P.A. 2011. A decade of exploring the cancer epigenome — biological and translational implications. Nature Reviews Cancer 11: 726-734.

Bello, B., Fadahun, O., Kielkowski, D., Nelson, G. 2011. Trends in lung cancer mortality in South Africa: 1995-2006. BioMed Central Public Health 11: 1-5.

Bender, C.M., Pao, M.M., Jones, P.A. 1998. Inhibition of DNA methylation by 5-aza-2'-deoxycytidine suppresses the growth of human tumor cell lines. Cancer Research 58: 95-101.

Brueckner, B., Kuck, D., and Lyko, F. 2007. DNA methyltransferase inhibitors for cancer therapy. Cancer Journal 13: 17-22.

Bustin, S.A., Benes, V., Garson, J.A., Hellemans, J., Huggett, J., Kubista, M., Mueller, R., Nolan, T., Pfaffl, M.W., Shipley, G.L., Vandesompele, J., Wittwer, C.T. 2009. The MIQE guidelines: Minimum Information for Publication of Quantitative Real-Time PCR Experiments. Clinical Chemistry 55: 611-622.

Christman, J.K. 2002. 5-Azacytidine and 5-aza-2'-deoxycytidine as inhibitors of DNA methylation: mechanistic studies and their implications for cancer therapy. Oncogene 21: 5483-5495.

Cole, T.J., Blendy, J.A., Monaghan, A.P., Krieglstein, K., Schmid, W., Aguzzi, A., Fantuzzi, G., Hummler, E., Unsicker, K., Schütz, G. 1995. Targeted disruption of the glucocorticoid receptor gene blocks adrenergic chromaffin cell development and severely retards lung maturation. Genes & Development 9: 1608-1621.

Deaton, A.M., Bird, A. 2011. CpG islands and the regulation of transcription. Genes & Development 25: 1010-1022.

Doucas, V., Shi, Y., Miyamoto, S., West, A., Verma, I., Evans, R.M. 2000. Cytoplasmic catalytic subunit of protein kinase A mediates cross-repression by NF-kappa B and the glucocorticoid receptor. Proceedings of the National Academy of Sciences of the United States of America 97: 11893-11898.

Duma, D., Jewell, C.M., Cidlowski, J.A. 2006. Multiple glucocorticoid receptor isoforms and mechanisms of post-translational modification. The Journal of Steroid Biochemistry and Molecular Biology 102: 11-21.

Esteller, M. 2007. Epigenetic gene silencing in cancer: the DNA hypermethylome. Human Molecular Genetics 16: R50-R59.

Ganong, W.F. 2005. The adrenal medulla and adrenal cortex. Review of Medical Physiology, 22nd Edition, Lange Medical Books/McGraw-Hill, United States of America, p. 374.

Geutjes, E.J., Bajpe, P.K., Bernards, R. 2012. Targeting the epigenome for treatment of cancer. Oncogene 31: 3827-3844.

Ghoumari, A.M., Dusart, I., El-Etr, M., Tronche, F., Sotelo, C., Schumacher, M., Baulieu, E.-E. 2003. Mifepristone (RU486) protects Purkinje cells from cell death in organotypic slice cultures of postnatal rat and mouse cerebellum. Proceedings of the National Academy of Sciences 100: 7953-7958.

Herr, I., Gassler, N., Friess, H., Büchler, M.W. 2007. Regulation of differential pro- and anti-apoptotic signaling by glucocorticoids. Apoptosis 12: 271-291.

Herr, I., Ucur, E., Herzer, K., Okouoyo, S., Ridder, R., Krammer, P.H., von Knebel Doeberitz, M., Debatin, K.-M. 2003. Glucocorticoid cotreatment induces apoptosis resistance toward cancer therapy in carcinomas. Cancer Research 63: 3112-3120.

Hertzberg, R.P., Caranfa, M.J., Hecht, S.M. 1989. On the mechanism of topoisomerase I inhibition by camptothecin: evidence for binding to an enzyme-DNA complex. Biochemistry 28: 4629-4638.

Hofmann, J., Kaiser, U., Maasberg, M., Havemann, K. 1995. Glucocorticoid receptors and growth inhibitory effects of dexamethasone in human lung cancer cell lines. European Journal of Cancer 31A: 2053-2058.

Hopkins-Donaldson, S., Ziegler, A., Kurtz, S., Bigosch, C., Kandioler, D., Ludwig, C., Zangemeister-Wittke, U., Stahel, R. 2003. Silencing of death receptor and caspase-8 expression in small cell lung carcinoma cell lines and tumors by DNA methylation. Cell Death and Differentiation 10: 356-364.

Hsu, H.-S., Chen, T.-P., Hung, C.-H., Wen, C.-K., Lin, R.-K., Lee, H.-C., Wang, Y.-C. 2007. Characterization of a multiple epigenetic marker panel for lung cancer detection and risk assessment in plasma. Cancer 110: 2019-2026.

Jackman, D.M., Johnson, B.E. 2005. Small-cell lung cancer. Lancet 366: 1385-1396.

Karpf, A.R., Jones, D.A. 2002. Reactivating the expression of methylation silenced genes in human cancer. Oncogene 21: 5496-5503.

Kay, P., Schlossmacher, G., Matthews, L., Sommer, P., Singh, D., White, A., Ray, D. 2011. Loss of glucocorticoid receptor expression by DNA methylation prevents glucocorticoid induced apoptosis in human small cell lung cancer cells. Plos One 6.

Kerr, J.F.R., Winterford, C.M., Harmon, B.V. 1994. Apoptosis – its significance in cancer and cancer therapy. Cancer 73: 2013-2026.

Kim, J. S., Kim, H., Shim, Y.M., Han, J., Park, J., Kim, D.-H. 2004. Aberrant methylation of the FHIT gene in chronic smokers with early stage squamous cell carcinoma of the lung. Carcinogenesis 25: 2165-2171.

Laane, E., Pokrovskaja Tamm, K., Buentke, E., Ito, K., Khahariza, P., Oscarsson, J., Corcoran, M., Björklund, A.-C., Hultenby, K., Lundin, J., Heyman, M., Söderhäll, S., Mazur, J., Porwit, A., Pandolfi, P.P., Zhivotovsky, B., Panaretakis, T., Grandér, D. 2009. Cell death induced by dexamethasone in lymphoid leukemia is mediated through initiation of autophagy. Cell Death and Differentiation 16: 1018-1029.

Lin, R.K., Hsieh, Y.S., Lin, P., Hsu, H.S., Chen, C.Y., Tang, Y.A., Lee, C.F., Wang, Y.C. 2010. The tobacco-specific carcinogen NNK induces DNA methyltransferase 1 accumulation and tumor suppressor gene hypermethylation in mice and lung cancer patients. Journal of Clinical Investigation 120: 521-532.

Liu, Z.J., Peng, W.C., Yang, X., Huang, J.F., Zhang, X.B., Zhang, Y., Maekawa, M. 2003. Relative mRNA expression of the lactate dehydrogenase A and B subunits as determined by simultaneous amplification and single strand conformation polymorphism - relation with subunit enzyme activity. Journal of Chromatography B-Analytical Technologies in the Biomedical and Life Sciences 793: 405-412.

Livak, K.J., Schmittgen, T.D. 2001. Analysis of relative gene expression data using real-time quantitative PCR and the 2(T)(-Delta Delta C) method. Methods 25: 402-408.

Lu, N.Z., Collins, J.B., Grissom, S.F., Cidlowski, J.A. 2007. Selective regulation of bone cell apoptosis by translational isoforms of the glucocorticoid receptor. Molecular and Cellular Biology 27: 7143-7160.

Lyko, F., Brown, R. 2005. DNA methyltransferase inhibitors and the development of epigenetic cancer therapies. Journal of the National Cancer Institute 97: 1498-1506.

Mathieu, M., Gougat, C., Jaffuel, D., Danielsen, M., Godard, P., Bousquet, J., Demoly, P. 1999. The glucocorticoid receptor gene as a candidate for gene therapy in asthma. Gene Therapy 6: 245-252.

Mitsuuchi, Y., Testa, J.R. 2002. Cytogenetics and molecular genetics of lung cancer. American Journal of Medical Genetics 115: 183-188.

Motadi, L.R., Misso, N.L., Dlamini, Z., Bhoola, K.D. 2007. Molecular genetics and mechanisms of apoptosis in carcinomas of the lung and pleura: Therapeutic targets. International Immunopharmacology 7: 1934-1947.

Nam, D.K., Lee, S., Zhou, G.L., Cao, X.H., Wang, C., Clark, T., Chen, J.J., Rowley, J.D., and Wang, S.M. 2002. Oligo(dT) primer generates a high frequency of truncated cDNAs through internal poly(A) priming during reverse transcription. Proceedings of the National Academy of Sciences of the United States of America 99: 6152-6156.

Nephew, K.P., Huang, T.H. 2003. Epigenetic gene silencing in cancer initiation and progression. Cancer Letters 190: 125-133.

Nojima, D., Nakajima, K., Li, L.C., Franks, J., Ribeiro-Filho, L., Ishii, N., Dahiya, R. 2001. CpG methylation of promoter region inactivates E-cadherin gene in renal cell carcinoma. Molecular Carcinogenesis 32: 19-27.

Panani, A.D., Roussos, C. 2006. Cytogenetic and molecular aspects of lung cancer. Cancer Letters 239: 1-9.

Pariante, C.M., Miller, A.H. 2001. Glucocorticoid receptors in major depression: relevance to pathophysiology and treatment. Biological Psychiatry 49: 391-404.

Parkin, D.M. 2001. Global cancer statistics in the year 2000. The Lancet Oncology 2: 533-543.

Ranta, F., Avram, D., Berchtold, S., Düfer, M., Drews, G., Lang, F., Ullrich, S. 2006. Dexamethasone induces cell death in insulin-secreting cells, an effect reversed by exendin-4. Diabetes 55: 1380-1390.

Ray, D.W., Littlewood, A.C., Clark, A.J.L., Davis, J.R.E., White, A. 1994. Human small cell lung cancer cell lines expressing the proopiomelanocortin gene have aberrant glucocorticoid receptor function. Journal of Clinical Investigation 93: 1625-1630.

Ray, D.W., Davis, J.R.E., White, A. Clark, A.J.L. 1996. Glucocorticoid receptor structure and function in glucocorticoid-resistant small cell lung carcinoma cells. Cancer Research 56: 3276-3280.

Risch, A., Plass, C. 2008. Lung cancer epigenetics and genetics. International Journal of Cancer 123: 1-7.

Robertson, K.D. 2001. DNA methylation, methyltransferases, and cancer. Oncogene 20: 3139-3155.

Rom, W.N., Hay, J.G., Lee, T.C., Jiang, Y., Tchou-Wong, K.M. 2002. Molecular and genetic aspects of lung cancer. American Journal of Respiratory and Critical Care Medicine 161: 1355-1367.

Schlossmacher, G., Stevens, A., White, A. 2011. Glucocorticoid receptor-mediated apoptosis: mechanisms of resistance in cancer cells. Journal of Endocrinology 211: 17-25.

Schmidt, S., Rainer, J., Ploner, C., Presul, E., Riml, S., Kofler, R. 2004. Glucocorticoid-induced apoptosis and glucocorticoid resistance: molecular mechanisms and clinical relevance. Cell Death and Differentiation 11: S45-S55.

Sommer, P., Le Rouzic, P., Gillingham, H., Berry, A., Kayahara, M., Huynh, T., White, A., Ray, D.W. 2007. Glucocorticoid receptor overexpression exerts an antisurvival effect on human small cell lung cancer cells. Oncogene 26: 7111-7121.

Sommer, P., Cowen, R.L., Berry, A., Cookson, A., Telfer, B.A., Williams, K.J., Stratford, I.J., Kay, P., White, A., Ray, D.W. 2010. Glucocorticoid receptor over-expression promotes human small cell lung cancer apoptosis *in vivo* and thereby slows tumour growth. Endocrine-Related Cancer 17: 203-213.

Stresemann, C., Lyko, F. 2008. Modes of action of the DNA methyltransferase inhibitors azacytidine and decitabine. International Journal of Cancer 123: 8-13.

Tessema, M., Willink, R., Do, K., Yu, Y.Y., Yu, W., Machida, E.O., Brock, M., Van Neste, L., Stidley, C.A., Baylin, S.B., Belinsky, S.A. 2008. Promoter methylation of genes in and around the candidate lung cancer susceptibility locus *6q23-25*. Cancer Research 68: 1707-1714.

Ting, A.H., McGarvey, K.M., Baylin, S.B. 2006. The cancer epigenome – components and functional correlates. Genes & Development 20: 3215-3231.

Turek-Plewa, J., Jagodziński, P.P. 2005. The role of mammalian DNA methyltransferases in the regulation of gene expression. Cellular & Molecular Biology Letters 10: 631-647.

Turner, J.D., Pelascini, L.P.L., Macedo, J.A., Muller, C.P. 2008. Highly individual methylation patterns of alternative glucocorticoid receptor promoters suggest individualized epigenetic regulatory mechanisms. Nucleic Acids Research 36: 7207-7218.

Turney, M.K., Kovacs, W.J. 2001. Function of a truncated glucocorticoid receptor form at a negative glucocorticoid response element in the proopiomelanocortin gene. Journal of Molecular Endocrinology 26: 43-49.

Tycko, B. 2000. Epigenetic gene silencing in cancer. Journal of Clinical Investigation 105: 401-407.

Vaissière, T., Hung, R.J., Zaridze, D., Moukeria, A., Cuenin, C., Fasolo, V., Ferro, G., Paliwal, A., Hainaut, P., Brennan, P., Tost, J., Boffetta, P., Herceg, Z. 2009. Quantitative analysis of DNA methylation profiles in lung cancer identifies aberrant DNA methylation of specific genes and its association with gender and cancer risk factors. Cancer Research 69: 243-252.

Vandesompele, J., De Preter, K., Pattyn, F., Poppe, B., Van Roy, N., De Paepe, A., Speleman, F. 2002. Accurate normalization of real-time quantitative RT-PCR data by geometric averaging of multiple internal control genes. Genome Biology 3: 1-12.

Virmani, A., Rathi, A., Sugio, K., Sathyanarayana, U.G., Toyooka, S., Kischel, F.C., Tonk, V., Padar, A., Takahashi, T., Roth, J.A., Euhus, D.M., Minna, J.D., Gazdar, A.F. 2003. Aberrant methylation of TMS1 in small cell, non small cell lung cancer and breast cancer. International Journal of Cancer 106: 198-204.

Waters, C.E., Stevens, A., White, A., Ray, D.W. 2004. Analysis of co-factor function in a glucocorticoid-resistant small cell carcinoma cell line. Journal of Endocrinology 183: 375-383.

Weigel, N.L., Zhang, Y. 1998. Ligand-independent activation of steroid hormone receptors. Journal of Molecular Medicine 76: 469-479.

Worm, J., Guldberg, P. 2002. DNA methylation: an epigenetic pathway to cancer and a promising target for anticancer therapy. Journal of Oral Pathology & Medicine 31: 443-449.

Young, B., Lowe, J.S., Stevens, A., Heath, J.W. 2006. Respiratory system. In: Wheater's Functional Histology: A Text and Colour Atlas, 5th Edition, Churchill Livingstone Elsevier, China, p. 246.

Yuan, B., Jefferson, A.M., Popescu, N.C., Reynolds, S.H. 2004. Aberrant gene expression in human non small cell lung carcinoma cells exposed to demethylating agent 5-aza-2'-deoxycytidine. Neoplasia 6: 412-419.

Zhou, J., Cidlowski, J.A. 2005. The human glucocorticoid receptor: one gene, multiple proteins and diverse responses. Steroids 70: 407-417.